EFFECT OF STRESS ON ULTRASONIC WAVE VELOCITIES IN ROCK SALT

Thesis for the Degree of Ph. D.

MICHIGAN STATE UNIVERSITY

Othman M. Abu-Gheida

1964

This is to certify that the

thesis entitled

Effect of Stress On Ultrasonic Wave Velocities In Rock Salt

presented by

Othman M. Abu-Gheida

has been accepted towards fulfillment
of the requirements for

Ph.D. degree in Mechanics

Lawrence E. Malvern

Major professor
Lawrence E. Malvern

Date July 17, 1964

O-169

ROOM USE ONLY

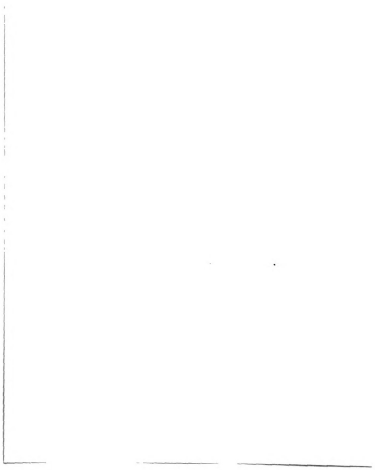

ABSTRACT

EFFECT OF STRESS ON ULTRASONIC WAVE VELOCITIES IN ROCK SALT

by Othman M. Abu-Gheida

The main objective of this investigation was to investigate the possible use of ultrasonic wave techniques for studying stresses in an undisturbed continuous medium. Present stress analysis methods employing strain gages or photoelastic and stress coat techniques cannot be readily used to analyze underground stress conditions. Recent tests by many investigators revealed that the velocity of ultrasonic waves propagating in rocks changed with changes in hydrostatic pressure. No mathematical explanation has been given for this change in rocks.

Theoretical expressions for the wave velocities in an initially isotropic solid, subjected to homogeneous stresses similar to underground conditions, were developed in the present investigation. The theoretical development considered the superposition of small strains, due to waves, onto finite strains due to static stresses. The relevant elastic constants which determine the wave velocities were calculated in terms of the static stresses, Lamé's constants and the third-order elastic constants of

the finite theory of elasticity. Seven functions of the three third-order elastic constants were derived. Four of these functions were measured in rock salt.

Preliminary investigations on uniaxially stressed salt and steel specimens were conducted to determine the changes that occurred in the velocity and attenuation of longitudinal waves, propagating in the lateral and axial directions.

The basic information derived from the preliminary tests was used in designing tests to determine the third-order elastic constants of rock salt. Longitudinal and shear wave velocities were measured in rock salt specimens subjected to hydrostatic compression. Similar measurements were made along the direction of uniaxial strain in tri-axially stressed specimens.

The results revealed that the changes in velocity at high pressure are reproducible. This indicated an agreement with the theoretical predictions. Consequently, the third-order elastic constants of rock salt were determined from the changes in velocity at high pressures.

It was concluded that the theoretical and experimental results of this investigation might have possibilities of being used to study stress conditions in underground salt formations. Other possible geophysical applications are also discussed.

EFFECT OF STRESS ON ULTRASONIC WAVE VELOCITIES IN ROCK SALT

By

Othman M. Abu-Gheida

A THESIS

Submitted to
Michigan State University
in partial fulfillment of the requirements
for the degree of

DOCTOR OF PHILOSOPHY

IN MECHANICS

Department of Metallurgy, Mechanics and Materials Science

1964

ACKNOWLEDGEMENTS

The author wishes to acknowledge the National Science Foundation for providing financial assistance which made this investigation possible and Dr. S. Serata, thesis advisor and Project Director, for providing supervision and guidance throughout this challenging investigation and for assisting in the preparation of this manuscript.

The author is also indebted to the members of his guidance committee for their continuing interest and support. Dr. L. Malvern, professor of Applied Mechanics and major professor, edited and provided invaluable suggestions in the theoretical analysis. Dr. T. Triffet, professor of Applied Mechanics, offered encouragement and supervision. Dr. R. H. Wasserman, Professor of Mathematics, for serving as minor professor.

Others who were helpful in conducting this investigation were Dr. C. Tatro, former MSU professor of Applied Mechanics, who helped in the preliminary experimental investigation, and Dr. A. Chowdiah and Messrs. A. Dahir and S. Sakurai, who offered laboratory help whenever asked.

Appreciation is also extended to the author's wife, Betty, for editing the manuscript.

TABLE OF CONTENTS

LIST OF TABLES

LIST OF FIGURES

LIST OF APPENDICES

NOTATION

A^o	Unstressed, unstrained state of an isotropic body.
A'	State of finite strain
A	State of finite plus infinitesimal strain
x_i^o	Coordinates in state A^o
x_i'	Coordinates in state A'
x_i	Coordinates in state A
J_1	Jacobian matrix of the transformation $x_i^o \rightarrow x_i'$
J_2	Jacobian matrix of the transformation $x_i' \rightarrow x_i$
$J = J_2\ J_1$	Jacobian matrix of the transformation $x_i^o \rightarrow x_i$
U_i^o	Particle displacements from state A^o to A'
$u_i = u,\ v,\ w$	Particle displacements from state A' to A
$B_{ij} = \frac{\partial U_i^o}{\partial x_j^o}$	
$b_{ij} = \frac{\partial u_i}{\partial x_j'}$	
ϵ_{ij}	Strain, or infinitesimal strain from state A' to A
η	Strain, or finite strain from state A^o to A
σ_{ij}	Stress, or total stress in state A

S_{ij}	Increment of stress from state A' to A
E_3	Identity square matrix of dimension 3
C_{ij}	Second-order elastic moduli
C'_{ij}	Effective elastic moduli
C_{ijr}	Third-order elastic constants
ℓ, m, n	Third-order elastic constants
V_{kij}	Velocity; 1st subscript refers to type of wave, s for shear and L for longitudinal, 2nd subscript refers to direction of particle motion, 3rd subscript refers to direction of propagation.
V_{kj}	Velocity; 1st subscript refers to type of wave, 2nd subscript refers to type of stress, h for hydrostatic and t for triaxial stress with uniaxial strain
E	Young's modulus
ν	Poisson's ratio
K	Bulk modulus
ρ	Density
P	Hydrostatic Pressure
α	Linear hydrostatic strain
e	Uniaxial strain
kcs	Kilocycles per second
mcs	Megacycles per second
μ in/in	Micro-inches per inch

I. INTRODUCTION

The use of ultrasonic pulse techniques to study stress waves in solids advanced after World War II when fast pulsed circuits were developed. During the past decade, extensive literature has been published on the use of ultrasonic propagation methods for studying dynamic elastic moduli, propagation velocity and internal friction in unstressed solids. Most of the investigations were restricted to single crystals and unstressed specimens.

The factor of stress was recently introduced in some experiments to study dislocations,[27] residual stresses,[58] changes in elastic moduli and propagation characteristics in single crystals,[39] polycrystalline metals[30] and rocks.[13] Such studies are still in the early stages of development due to limited available data and absence of well defined theories.

To date, characteristic changes in velocity versus hydrostatic pressure in rocks have been interpreted as due to pore closure at low pressure,[14] and to undetermined intrinsic changes at high pressures.[53] A study of the basic principles involved in wave propagation is required to explain the intrinsic changes in velocity.

With the growing use of radioactive materials, there is an increased demand for safe and economic disposal of

radioactive wastes. Recently, rock salt cavities have been suggested for this purpose.[66] Serata[60] concluded that knowledge of the existing underground stress field was needed for the structural design of such cavities.

The objectives of the present research were to investigate the possibility of using ultrasonic-wave methods to study stress conditions in underground salt formations and to determine the third-order elastic constants of rock salt.

The theoretical development included a derivation of wave velocities in an initially isotropic material when subjected to homogeneous deformations due to hydrostatic pressure or to triaxial stress with uniaxial strain.

Preliminary tests were conducted on uniaxially stressed steel and salt specimens to determine the sensitivity of the ultrasonic pulse method for measuring relative attenuation and absolute velocity at different stress levels.

The results of these tests were used to design a more sensitive circuit for measuring the changes in velocity with an accuracy of 0.05%. This circuit was used to measure changes in longitudinal and shear wave velocities in rock salt due to hydrostatic pressure and to triaxial stress with uniaxial strain. The maximum axial and lateral stresses in the triaxial tests were 13,800 and 11,000 psi respectively. The maximum hydrostatic pressure was 9,000 psi. The dynamic elastic moduli and the third-order elastic constants of rock salt were determined from the collected data.

II. LITERATURE REVIEW

2.1 Mechanical Properties of Rock Salt

The ultimate and safe disposal of radioactive waste has become one of the important problems of this age.[60] The feasibility of using underground salt cavities for this purpose has initiated extensive exploratory research on the geophysical, radiological and economic aspects of using rock salt cavities for reactor waste disposal. In 1955 the cumulative results of this research led the Committee on Waste Disposal of the Division of Earth Sciences, National Academy of Science, to endorse the disposal of radioactive waste in salt cavities as a most promising and practical solution.[66]

In 1959, Serata[60] developed design principles for the disposal of reactor fuel waste in underground salt cavities. To arrive at his results, he conducted an experimental and theoretical investigation of the chemical, radiological, thermal and structural factors which affect the salt cavity. Of these factors, he found that the structural stability of the cavity is of prime importance. Consequently, Serata[61,62] and later Morrison,[45] Raman[51] and Chowdiah[20] studied the mechanical properties of rock salt such as strength, Young's modulus, creep behavior, etc.

A summary of the results obtained by the above investigators which are related to this investigation will be presented below. For a summary and an account of previous investigations that were done on rock salt the reader is referred to Serata.[60]

Uniaxial Compression

Serata[60] analyzed the results obtained from uniaxial compression tests on rock salt. He suggested that the wide variations observed in the shape of the stress strain curve, yield strength, Young's modulus (E) and Poisson's ratio (ν) were due to the variation of certain factors in the testing procedure. Of these factors, he analyzed the following:

1. Use of a friction reducer on the loading surface of the salt.
2. Ratio of height to cross sectional area of the salt.
3. Method of measuring the strain by use of strain gages or dial gages.

The results obtained by Serata indicated the following:

1. The friction developed on the loading surface of the salt increased the yield strength through the formation of a triaxial stress zone in the central region of the specimen. This effect became more pronounced when the ratio of cross sectional area to the height was increased, Figs. 2.1 and 2.2.

2. The specimen size effect could be eliminated by the use of a friction reducer.
3. The mechanical properties obtained after eliminating the end friction were as follows:
   (a) Mean maximum stress was 2,300 psi with a standard deviation of 200 psi.
   (b) Mean value of E was 0.14 million psi with a standard deviation of 0.03 million psi.
   (c) Poisson's ratio was more than 0.5 for stress beyond 3,000 psi.

Chowdiah[20] used the friction reduction technique developed by Serata. The results he obtained from the uni-axial compression of 5 inch cubic specimens, indicated the following:

1. The stress strain curve did not exhibit any linearity and as such the conventional methods of calculating E and ν could not be adapted.
2. The average value of E as calculated from the slope of a straight line connecting two points on the stress strain curve (chord modulus) was as follows:

Stress range	E (SR-4 Gages)	E (Dial Gages)
psi	Million psi	Million psi
0 to 1,000	1.408	0.4559
1,000 to 2,000	0.1913	0.1757

3. The value of ν, when dial gages were used, varied linearly from 0 to 0.5 as the stress increased from 0 to 1,500 psi, and increased very slightly for

higher stresses. The value of ν when SR-4 gages were used was consistently higher than the values obtained from dial gages.

The high values of ν, 0.5 and above, were explained as due either to errors in the measurement or to brittle fracture between the crystal grains resulting in a volume increase of the specimen.

Biaxial Compression

Chowdiah[20] used strain gages, dial gages and photo-stress technique to determine the behavior of rock salt due to biaxial compression. Five inch cubic specimens were subjected to vertical and lateral stresses of equal or different magnitudes. His results indicated the following:

1. Rock salt in a biaxial state of stress fails by plastic flow.
2. Yielding begins when the octahedral shear stress reaches a value of 1,885 psi. The octahedral shear stress is defined by:

$$\tau_o = \frac{1}{3}\left[(\sigma_1-\sigma_2)^2 + (\sigma_2-\sigma_3)^2 + (\sigma_3-\sigma_1)^2\right]^{\frac{1}{2}}$$

where:

τ_o = octahedral shear stress

$\sigma_1, \sigma_2, \sigma_3$ = principal stresses

For condition of equal lateral and vertical stresses

$$\sigma_1 = \sigma_2 = \sigma$$

$$\sigma_3 = 0$$

this equation reduces to:

$$\tau_o = \frac{\sqrt{2}}{3}\,\sigma$$

Triaxial Compression

Handin[26] studied the triaxial behavior of cylindrical salt specimens subjected to a confining liquid pressure and compressed in the third direction. His results indicated that rock salt exhibits an increased ductility and plastic behavior with an increase in confining pressure. A specimen, at 1,200 atmosphere confining pressure, was shortened 75% before fracture.

Serata[61] used the experimental results of Handin to plot Mohr's envelope for rock salt. Mohr's envelope is represented by the line A B C D E, Fig. 2.3. This envelope is tangent to Mohr's circles for a number of triaxial tests in a large range of the mean principal stress. Serata suggested that the envelope could be considered to be composed of three portions:

1. A B corresponds to brittle behavior and can be best described by the Coulomb-Mohr theory of triaxial failure in the form:

$$\tau = \tau_c + \theta\,\sigma \qquad (2.2)$$

where:

τ = shear stress on the plane of failure

θ = coefficient of internal friction of the material

σ = normal stress on the plane of failure

τ_c = the constant part of the shear strength which depends on the material.

2. B D represents a transition state.

3. The horizontal line D E represents a plastic behavior which could be explained by the octahedral shear strength theory of failure in the form of Eq. 2.1.

$$\tau_o = \frac{1}{3}\left[(\sigma_1-\sigma_2)^2 + (\sigma_2-\sigma_3)^2 + (\sigma_3-\sigma_1)^2\right]^{\frac{1}{2}} = \text{const.} = k_o$$

when $\sigma_1 = \sigma_2 = \sigma_3$ this condition reduces to

$$\tau_o = \frac{\sqrt{2}}{3}(\sigma_2-\sigma_3) = k_o$$

If the octahedral shearing strength of salt is defined by k_o,

$$k_o = \frac{\sqrt{2}}{3}(\sigma_2-\sigma_3) \qquad (2.3)$$

then the maximum shearing stress corresponding to the line D E will be:

$$\tau_{max.} = \frac{\sigma_2-\sigma_3}{2} = \frac{3}{2\sqrt{2}}\,k_o \qquad (2.4)$$

By an extension of Mohr's envelope method, a theory of underground stress field was developed by Serata[61] and investigated by Serata,[61] Morrison[45] and Raman.[51] This theory predicted that the underground stress field is elastic at small depths and abruptly changes to plastic at a certain depth depending upon the material. This behavior was represented by Mohr's envelope FDE, Fig. 2.3. FD represents the elastic state and DE the plastic state. The theory and the results are given below:

The relation between the principal stresses and strains is:

$$\epsilon_x = \frac{1}{E}\,[\sigma_x - \nu(\sigma_y + \sigma_z)]$$

$$\epsilon_y = \frac{1}{E}\,[\sigma_y - \nu(\sigma_z + \sigma_x)] \qquad (2.5)$$

$$\epsilon_z = \frac{1}{E}\,[\sigma_z - \nu(\sigma_x + \sigma_y)]$$

where:

compressive stress and strain are considered to be positive.

ϵ_x, ϵ_y = strains in horizontal directions

ϵ_z = strain in vertical direction

σ_x, σ_y = stresses in horizontal directions

σ_z = stress in vertical direction

E = Young's modulus

ν = Poisson's ratio

The underground stress condition is essentially a triaxial stress state with uniaxial strain. The horizontal strains ϵ_x, ϵ_y are zero since no lateral strain is possible when the medium extends to infinity. The vertical stress is equal to the overburden pressure. The lateral stresses are equal and are developed due to the restriction of lateral deformation. Substituting these conditions in Eq. 2.5 leads to:

$$\sigma_L = \frac{\nu}{1-\nu}\,\sigma_z \qquad (2.6)$$

where:

$$\sigma_x = \sigma_y = \sigma_L$$

This equation represents the relationship between the lateral and vertical pressures at small depths. Eq. (2.6) remains valid for increasing depths until the octahedral shearing stress τ_o reaches the value of the octahedral shearing strength k_o. At this point there is a sharp transition from elastic to plastic behavior and the relation between σ_L and σ_z could be derived from the yield condition:

$$\tau_o = k_o = \frac{1}{3} [(\sigma_x-\sigma_y)^2 + (\sigma_y-\sigma_z)^2 + (\sigma_z-\sigma_x)^2]^{\frac{1}{2}} \qquad (2.7)$$

when $\sigma_x = \sigma_y = \sigma_L$, this equation reduces to:

$$\sigma_L = \sigma_z \pm \frac{3}{2} k_o \qquad (2.8)$$

Using Eqs. 2.6 and 2.8, Serata's transition theory was represented in a plot of σ_L vs. σ_z (Fig. 2.4). Line AB represents an elastic state with a slope defined by $\frac{\nu}{1-\nu}$. Point B is a transition point. Line BC represents a plastic condition with a slope of unity. Line CD represents elastic unloading and DE plastic unloading. AE is equal to the residual lateral stress after a complete cycle.

This transition theory was experimentally investigated using different rocks[51] and salt.[45] A uniaxial state of strain was created by applying axial loads to cylindrical rock specimens which were tightly fitted in thick-walled steel cylinders. Lateral stresses were calculated from the measured strains in SR-4 gages on the outer surface of the steel cylinders. For the tests on rock salt the steel

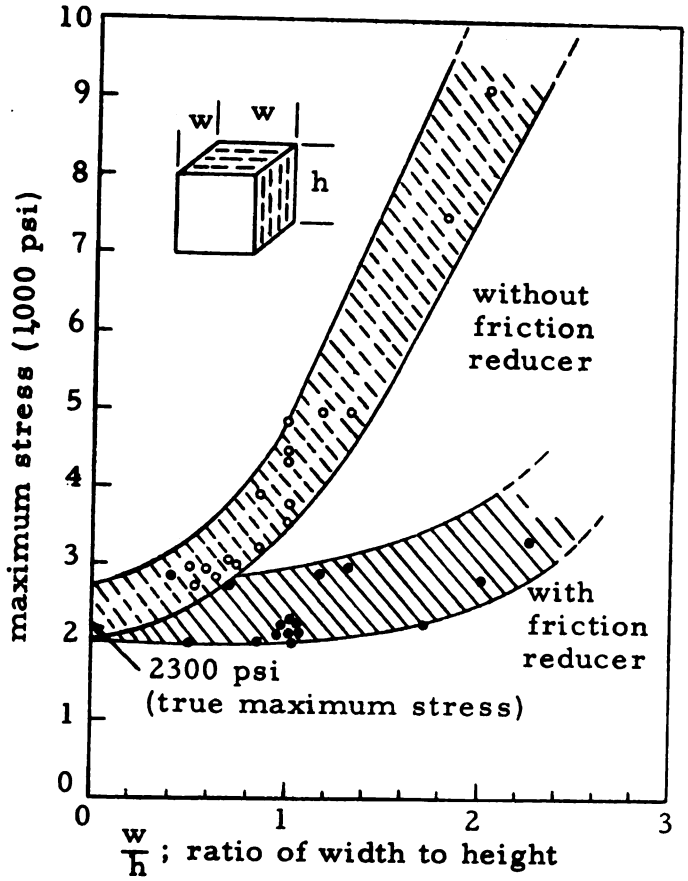

Fig. 2.1. Effect of dimension and end friction on maximum stress. (Serata)

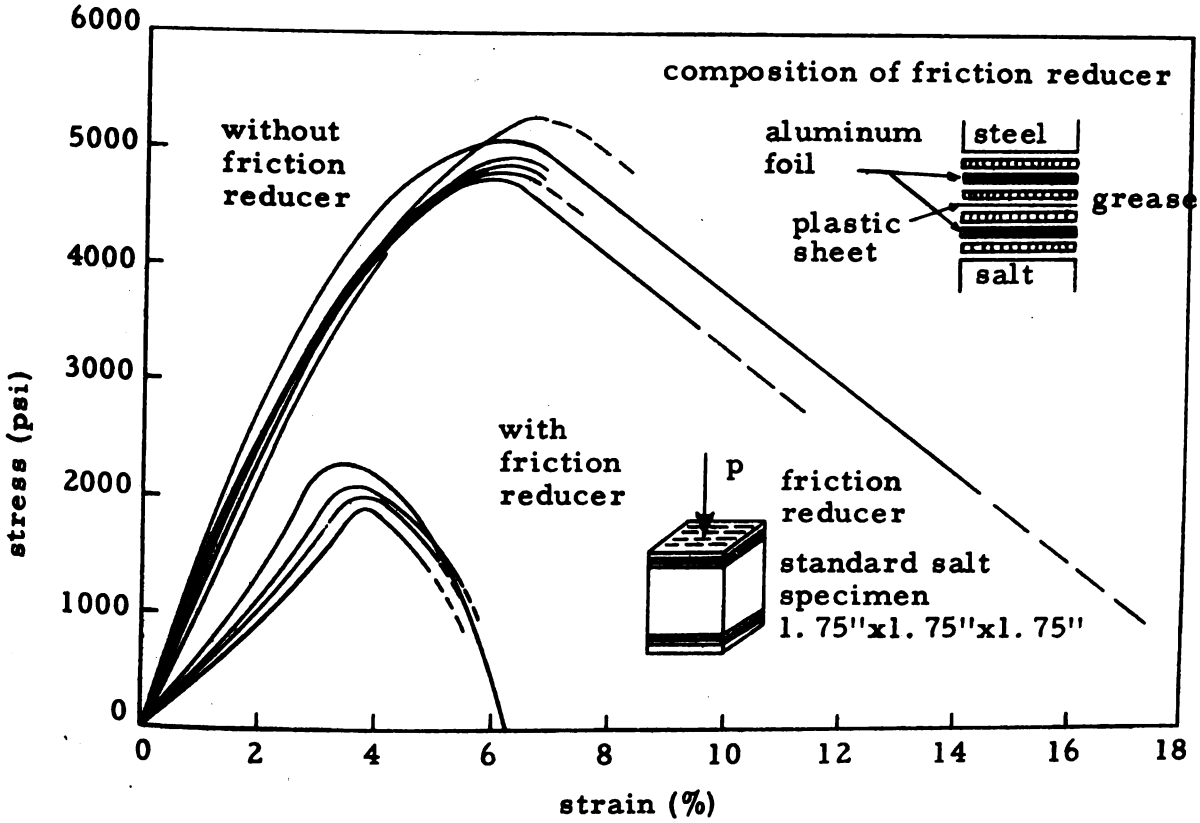

Fig. 2.2. Effect of end friction reducer on stress-strain relation. (Serata)

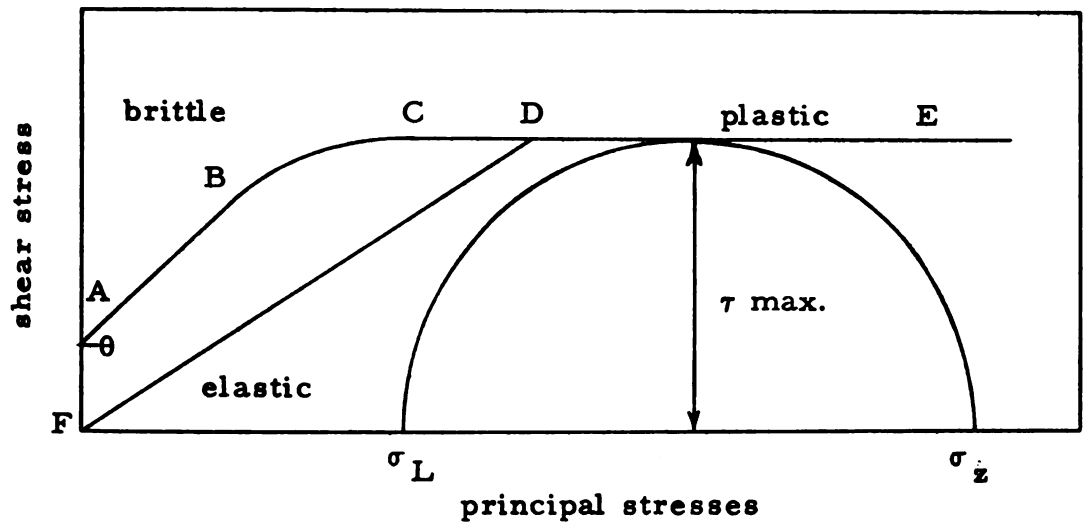

Fig. 2.3. Mohr's envelope representing stresses in a triaxial stress state. (Serata)

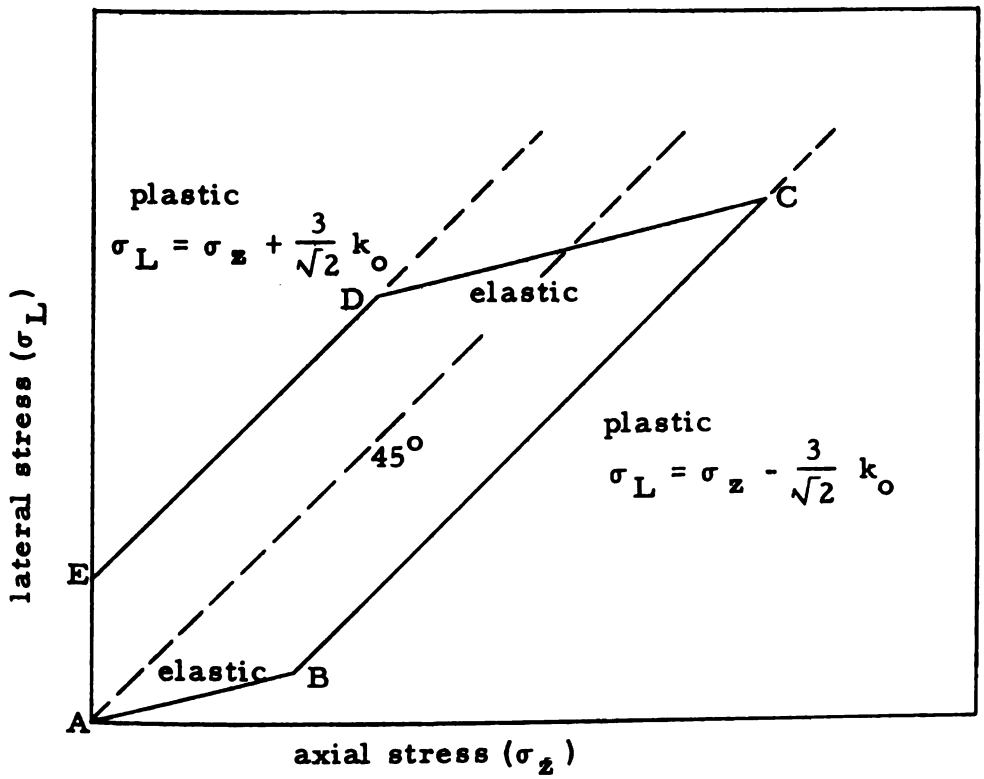

Fig. 2.4. Serata's transition theory.

cylinders had an inside diameter of 3.25 inches, an outside diameter of 4 inches and a height of 3.25 inches. A friction reducer consisting of a plastic sheet coated with a grease-graphite mixture was applied to all sides of the salt to prevent the development of shear stresses.

The experimental results obtained from the tests on rock salt showed remarkable agreement with the theory as outlined by Serata. The value of ν, obtained from line AB, was 0.17 and k_o 1,750 psi. Fig. 5.9 shows a typical plot of σ_L vs. σ_z as obtained by the present author during this investigation.

2.2. Theory of Stress Waves in Solids

2.2.1. Hooke's Law

A generalization of Hooke's linear law may be stated as: Each of the six components of stress is at any point a linear function of the six components of strain. This may be expressed as:

$$\begin{bmatrix} \sigma_{xx} \\ \sigma_{yy} \\ \sigma_{zz} \\ \sigma_{yz} \\ \sigma_{zx} \\ \sigma_{xy} \end{bmatrix} = \begin{bmatrix} C_{11} & C_{12} & C_{13} & C_{14} & C_{15} & C_{16} \\ C_{21} & C_{22} & C_{23} & C_{24} & C_{25} & C_{26} \\ C_{31} & C_{32} & C_{33} & C_{34} & C_{35} & C_{36} \\ C_{41} & C_{42} & C_{43} & C_{44} & C_{45} & C_{46} \\ C_{51} & C_{52} & C_{53} & C_{54} & C_{55} & C_{56} \\ C_{61} & C_{62} & C_{63} & C_{64} & C_{65} & C_{66} \end{bmatrix} \begin{bmatrix} \epsilon_{xx} \\ \epsilon_{yy} \\ \epsilon_{zz} \\ \gamma_{yz} \\ \gamma_{zx} \\ \gamma_{xy} \end{bmatrix} \qquad (2.9)$$

where:

σ_{xx}, σ_{yy}, σ_{zz} -- normal stresses

σ_{yx}, σ_{zx}, σ_{xy} -- sheer stresses

C_{11}, C_{12}, ... C_{ij} -- elastic constants of the material

ϵ_{xx}, ϵ_{yy}, ϵ_{zz} -- normal strains

γ_{xy}, γ_{yz}, γ_{zx} -- are two times the shear strains

It may be shown[40] that the matrix C_{ij} is symmetric i.e., $C_{ij} = C_{ji}$. For a completely aeolotropic (non symmetrical, non isotropic) material, the elastic constants C_{ij} reduce to twenty-one constants. Where the material has axes or planes of symmetry, relations may be established between the elastic constants. For a cubic crystal there are only three independent constants, and the C_{ij} matrix becomes:

$$\begin{bmatrix} C_{11} & C_{12} & C_{12} & 0 & 0 & 0 \\ C_{12} & C_{11} & C_{12} & 0 & 0 & 0 \\ C_{12} & C_{12} & C_{11} & 0 & 0 & 0 \\ 0 & 0 & 0 & C_{44} & 0 & 0 \\ 0 & 0 & 0 & 0 & C_{44} & 0 \\ 0 & 0 & 0 & 0 & 0 & C_{44} \end{bmatrix}$$

For an isotropic solid,

$$C_{11} = C_{12} + 2\,C_{44}$$

$$C_{12} = \lambda$$

$$C_{44} = \mu$$

where λ and μ are called Lamé's constants.

The matrix can be written as:

$$\begin{bmatrix} \lambda + 2\mu & \lambda & \lambda & 0 & 0 & 0 \\ \lambda & \lambda + 2\mu & \lambda & 0 & 0 & 0 \\ \lambda & \lambda & \lambda + 2\mu & 0 & 0 & 0 \\ 0 & 0 & 0 & \mu & 0 & 0 \\ 0 & 0 & 0 & 0 & \mu & 0 \\ 0 & 0 & 0 & 0 & 0 & \mu \end{bmatrix}$$

The generalized Hooke's law (Eq. 2.9) for an isotropic solid in the elastic state may now be written as:

$$\begin{aligned} \sigma_{xx} &= \lambda \Delta + 2\mu \epsilon_{xx} & \sigma_{xy} &= \mu \gamma_{xy} = \mu \left(\frac{\partial u}{\partial y} + \frac{\partial v}{\partial x}\right) \\ \sigma_{yy} &= \lambda \Delta + 2\mu \epsilon_{yy} & \sigma_{xz} &= \mu \gamma_{xz} = \mu \left(\frac{\partial u}{\partial z} + \frac{\partial w}{\partial x}\right) \\ \sigma_{zz} &= \lambda \Delta + 2\mu \epsilon_{zz} & \sigma_{yz} &= \mu \gamma_{yz} = \mu \left(\frac{\partial v}{\partial z} + \frac{\partial w}{\partial y}\right) \end{aligned} \qquad (2.10)$$

where:

u, v, w = displacement components in x, y, z directions.

$$\Delta = \epsilon_{xx} + \epsilon_{yy} + \epsilon_{zz}$$

$$= \frac{\partial u}{\partial x} + \frac{\partial v}{\partial y} + \frac{\partial w}{\partial z} = \text{dilatation} = \text{change in volume per unit volume}$$

Lamé's constants can be expressed in terms of E, ν, G, and K.

where:

E = Young's modulus

ν = Poisson's ratio

K = Bulk modulus $= \dfrac{P}{|\Delta|} = \dfrac{\text{Applied hydrostatic pressure}}{\text{Change in volume}}$

G = Shear modulus $= \mu$

The relations are:

$$E = \frac{\mu\ (3\lambda + 2\mu)}{\lambda + \mu}$$

$$\nu = \frac{\lambda}{2\ (\lambda + \mu)}$$

$$K = \lambda + \frac{2\mu}{3} \qquad (2.11)$$

$$\mu = G = \frac{E}{2\ (1 + \nu)}$$

2.2.2 Wave Velocities in an Infinite Linear Elastic Isotropic Medium

The equations of motion for an isotropic linear elastic medium are:

$$\rho \frac{\partial^2 u}{\partial t^2} = \rho\ddot{u} = \rho X + \frac{\partial \sigma_{xx}}{\partial x} + \frac{\partial \sigma_{xy}}{\partial y} + \frac{\partial \sigma_{xz}}{\partial z}$$

$$\rho\ddot{v} = \rho Y + \frac{\partial \sigma_{yx}}{\partial x} + \frac{\partial \sigma_{yy}}{\partial y} + \frac{\partial \sigma_{yz}}{\partial z} \qquad (2.12)$$

$$\rho\ddot{w} = \rho Z + \frac{\partial \sigma_{zx}}{\partial x} + \frac{\partial \sigma_{zy}}{\partial y} + \frac{\partial \sigma_{zz}}{\partial z}$$

where:

X, Y, Z are body forces in x, y, z directions

ρ = density

Substituting for the stresses in Eq. (2.10), and neglecting the body forces X, Y, Z, in Eq. (2.12) yields:

$$\rho\ddot{u} = (\lambda + \mu)\ \frac{\partial \Delta}{\partial x} + \mu \nabla^2 u \qquad (2.13a)$$

$$\rho\ddot{v} = (\lambda + \mu)\ \frac{\partial \Delta}{\partial y} + \mu \nabla^2 v \qquad (2.13b)$$

$$\rho\ddot{w} = (\lambda + \mu)\ \frac{\partial \Delta}{\partial z} + \mu \nabla^2 w \qquad (2.13c)$$

where:

$$\nabla^2 = \left(\frac{\partial^2}{\partial x^2} + \frac{\partial^2}{\partial y^2} + \frac{\partial^2}{\partial z^2}\right)$$

These equations may be shown to correspond to the propagation of two types of waves through a medium.[36,41]

Differentiating (2.13a) with respect to x, (2.13b) with respect to y and (2.13c) with respect to z, and adding the three equations yields:

$$\rho \frac{\partial^2 \Delta}{\partial t^2} = (\lambda + 2\mu)\ \nabla^2 \Delta \qquad (2.14)$$

This is a wave equation[36,41] which shows that the dilatation Δ is propagated through the medium with a velocity (V_L) equal to:

$$V_L = \sqrt{\frac{\lambda + 2\mu}{\rho}} \qquad (2.15)$$

On the other hand, Δ can be eliminated by differentiating (2.13b) with respect to z, (2.13c) with respect to y and subtracting the results. The resulting equation is:

$$\rho \frac{\partial^2}{\partial t^2} \left(\frac{\partial w}{\partial y} - \frac{\partial v}{\partial z}\right) = \mu \nabla^2 \left(\frac{\partial w}{\partial y} - \frac{\partial v}{\partial z}\right)$$

or,

$$\rho \frac{\partial^2 \bar{w}_{yz}}{\partial t^2} = \mu \nabla^2 \bar{w}_{yz} \qquad (2.16)$$

where:

$\bar{w}_{yz}$ is the rotation around the x axis.

This is another form of the wave equation and shows that the rotation $\bar{w}_{yz}$ is propagated with a velocity V_s:

$$V_s = \sqrt{\frac{\mu}{\rho}} \tag{2.17}$$

Similar soultions for the rotation about the y and z axes may be obtained.

For a plane wave with a single particle displacement component v, independent of x and z, Eq. (2.14) can be put into the form:

$$\rho \frac{\partial^2 v}{\partial t^2} = (\lambda + 2\mu) \frac{\partial^2 v}{\partial y^2} \; ; \; u = w = 0 \tag{2.18}$$

It can be verified by direct differentiation and substitution that this equation describes a wave of the type,[41]

$$V = V_o \cos \omega \left(t - \frac{y}{V_L}\right) \tag{2.19}$$

where:

ω = angular frequency,

which travels with the velocity V_L of Eq. (2.15) and has a particle displacement v in the same direction as the wave propagation y. This type of wave is called a longitudinal plane wave, and may be designated as:

$$V_{Lyy}$$

where:

the first subscript, L, indicates a longitudinal wave,

the second subscript, y, indicates the direction of particle displacement, and

the third subscript, y, indicates the direction of wave propagation.

By similar procedure, it may be shown that two other plane waves, V_{Lxx}, V_{Lzz}, could be propagated in an isotropic medium with the same velocity V_L.

For a plane wave, with a single particle displacement v independent of x and y, Eq. (2.16) can be put into the form:

$$\rho \frac{\partial^2 v}{\partial t^2} = \mu \frac{\partial^2 v}{\partial z^2} \quad ; \quad u = w = 0 \tag{2.20}$$

This equation describes a wave of the type,

$$V = V_o \cos \omega \left(t - \frac{z}{V_s}\right) \tag{2.21}$$

which travels with the velocity V_s of Eq. (2.17) and has a particle displacement v perpendicular to the direction of propagation z. This type of wave is called a transverse or shear wave, and may be designated as V_{syz}. Similar solutions can be obtained for V_{sxz}, V_{sxy}, V_{syx}, V_{szx} and V_{szy}.

2.2.3. Rayleigh Surface Waves

In an unbounded isotropic elastic solid only longitudinal and shear waves can be propagated. However, when there is a bounding surface, elastic surface waves may also occur. These waves are similar to gravitational surface waves in liquids and were first investigated by Lord Rayleigh in 1887, who showed that their effect decreases rapidly with depth, and that their velocity of propagation is smaller than that of shear waves.[36]

Kolsky[36] gave a discussion of these waves and showed that,

If

$$R = \frac{V_n}{V_s} ,$$

where:

V_n = velocity of Rayleigh wave,

V_s = velocity of shear wave,

then R is found to satisfy the equation,

$$R^8 - 8\,R^4 + (24 - 16\,A^2)\,R^2 + (16\,A^2 - 16) = 0 \quad (2.22)$$

where:

$$A = \frac{1 - 2\nu}{2 - 2\nu}$$

ν = Poisson's ratio.

Equation (2.22) shows that R depends on Poisson's ratio. For $\nu = \frac{1}{4}$; R = 0.9194; for ν = 0.5, R = 0.9554, for steel ν = 0.29, and R = 0.9258.

2.2.4. Longitudinal Waves in Elastic Rods

There are three types of vibrations which occur in rods. They are classified as longitudinal, torsional and flexural.[36] The following discussion will be limited to longitudinal waves.

An approximate solution for the longitudinal wave velocity in an elastic rod can be obtained by assuming that plane transverse sections of the bar remain plane during the passage of the stress wave.[36] Consider a small section, RS, of the bar with a cross-sectional area, A, as shown below:

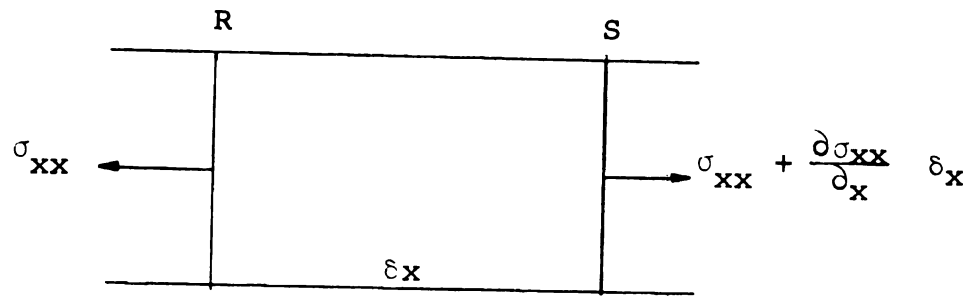

Newton's second law of motion yields:

$$\rho A \delta_x \frac{\partial^2 u}{\partial t^2} = A \frac{\partial \sigma_{xx}}{\partial x} \delta_x$$

where:

A = area of cross section

u = particle displacement

or,

$$\rho \frac{\partial^2 u}{\partial t^2} = \frac{\partial \sigma_{xx}}{\partial x}$$

But,

$$E = \frac{\sigma_{xx}}{\frac{\partial u}{\partial x}}$$

Therefore,

$$\frac{\partial^2 u}{\partial t^2} = \frac{\partial}{\partial x} \left[E \frac{\partial u}{\partial x} \right] = E \frac{\partial^2 u}{\partial x^2} \quad . \tag{2.23}$$

This is another form of the wave equation; its solution may be written as:[36]

$$u = f (V_R t - x) + F (V_R t + x) \tag{2.24}$$

where:

$$V_R = \sqrt{\frac{E}{\rho}} = \text{propagation velocity in rods,} \tag{2.25}$$

and F, f are arbitrary functions depending on the initial

conditions; f corresponds to a wave traveling in the direction of increasing x while F corresponds to a wave in the opposite direction.

For a wave traveling in the decreasing x direction,

$$u = F\ (V_R t + x). \tag{2.26}$$

Differentiating Eq. (2.26) with respect to t yields,

$$\frac{\partial u}{\partial t} = V_R F'\ (V_R t + x).$$

Here F' denotes differentiation with respect to the argument $(V_R t + x)$. Thus:

$$\frac{\partial u}{\partial t} = V_R \frac{\partial u}{\partial x} \qquad \text{But, } \frac{\partial u}{\partial x} = \frac{\sigma_{xx}}{E}$$

$$\sigma_{xx} = \left(\frac{E}{V_R}\right) \frac{\partial u}{\partial t} = \rho V_R \frac{\partial u}{\partial t}$$

$$\sigma_{xx} = \rho V_R \frac{\partial u}{\partial t} \tag{2.27}$$

This equation shows that there is a linear relation between the stresses at any point and the particle velocity.

When a wave reaches the end of a bar it will be reflected. The nature of the reflected wave depends on the boundary conditions at the end. It may be shown that[36] for a free end (no stress) the reflected wave will be opposite in sign to the original wave. Thus, a compression pulse will be reflected as tension. Applying the condition that the displacement is zero at the end of the bar, leads to the conclusion that the reflected wave is of the same sign as the incident pulse.

2.2.5. Limitations of the Rod Velocity Equation

In deriving Eq. (2.25) it was assumed that plane transverse sections remain plane. However, there is a lateral expansion and contraction in the rod that results in a non-uniform distribution of stress in the sections. This causes the sections to be distorted. This effect was first investigated by Pochhammer[50] in 1876. An account of Pochhammer's treatment is given by Love,[40] Kolsky[36] and Mason.[41] An exact solution is given for cylindrical bars whose length is much greater than their diameter. The equation derived is valid for wave lengths which are much longer than the diameter. They lead to the result that harmonic waves cannot be propagated in bars at a velocity larger than V_R.

2.2.6. Elastic Waves in Finite Cylinders

Kolsky[36] pointed out that "exact solutions have not been obtained for vibration of cylinders of finite length." The Pochhammer treatment leads to the result that no energy can be propagated in a bar at a velocity larger than V_R. However, Kolsky, Silaeva,[64] Tu and his colleagues,[70] have stated that a bar could be assumed to be an infinite medium, when the ratio of the bar radius to the wave length is large. This statement is especially important when elastic wave velocities are measured by ultrasonic pulse methods using rock specimens of small dimensions. In such experiments it is desirable, in many cases, to

measure V_L directly so that the velocities measured can be compared to velocities observed in nature.

The following experimental results may be considered as design criteria for the selection of specimen dimensions and frequencies to be used to measure V_L in small specimens.

Tu and his colleagues[70] measured the velocity of longitudinal pulses, with different carrier frequencies, in metal bars using quartz and barium titanate transducers. Their results are presented in Figure 2.5. V_g in the figure indicates the group velocity. This is the velocity with which the energy is transmitted in the bar[41] and is equal to the measured pulse velocity.[70] They indicated that their results agree with the theoretical calculation of Pochhammer for values of $\frac{a}{L}$ less than 0.8, where a is the bar radius and L is the wave length. At large $\frac{a}{L}$ the group velocity becomes equal to V_L.

Silaeva and Shamina[64] used ultrasonic pulse methods to measure distribution of elastic waves in cylindrical brass rods of different radii. Their results are presented in Figure 2.6. This figure shows the regions in which V_L and V_R are detected easily, depending upon the relative dimensions of the specimen. The relative dimensions of the specimen are presented by the ratios of the length (x) (distance between transducers) and radius (a), to the wave length (L).

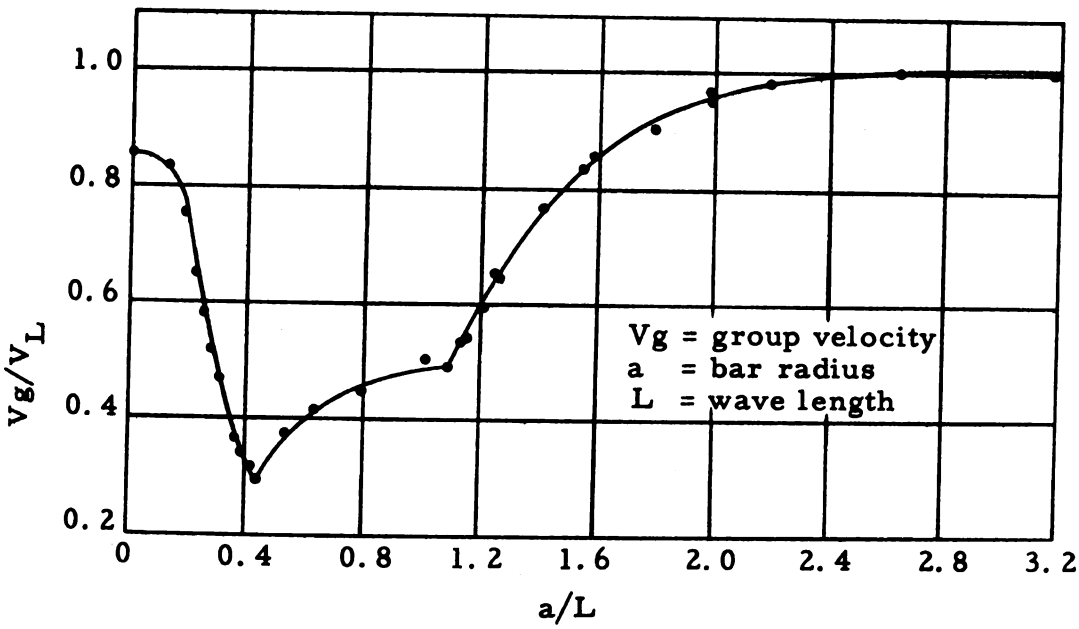

Fig. 2.5. Relative velocity as a function of the radius-wave length ratio. (Tu)

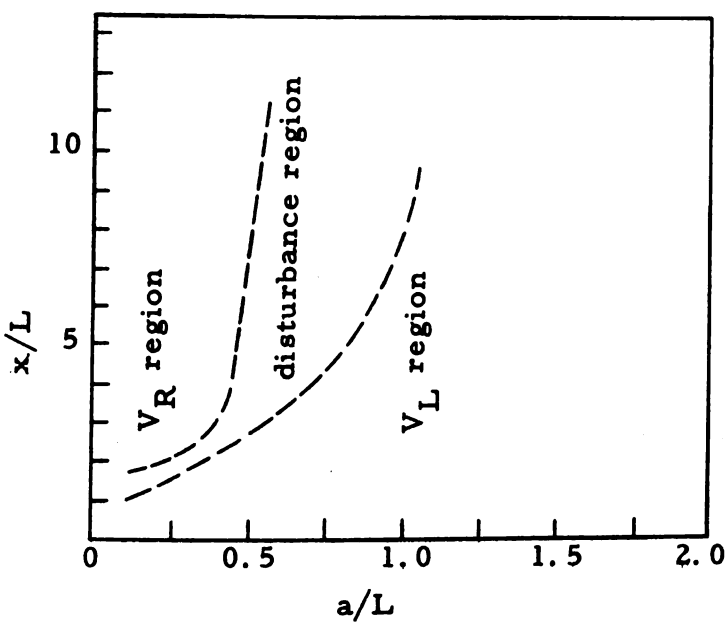

Fig. 2.6. Regions of observation along the profile of x/L for longitudinal waves propagated with velocities V_L and V_R in relation to a/L. (Silaeva and Shamina)

Figure 2.6 may be interpreted to state that the velocity measured by ultrasonic methods in rods will be V_R or V_L depending upon the ratio of $\frac{a}{L}$ as well as the length of the specimen. For small ratios of $\frac{a}{L}$, the measured velocity will be V_L for short specimens, and V_R for longer specimens. As the ratio $\frac{a}{L}$ increases, the length of the specimen for which V_L is observed becomes longer.

2.2.7. Determination of Elatic Moduli from Wave Velocities

In general, the elastic moduli (C_{ij}, Eq. 2.9)) of a solid are determined by measuring the velocities of longitudinal and shear waves in different directions. The types of waves and directions to be chosen depend upon the number of independent elastic moduli of the material.

For an isotropic solid, the elastic moduli λ and μ are determined by measuring V_L and V_s in any direction. The value of V_R, if known, provides an additional check.

$$V_L = \sqrt{\frac{\lambda + 2\mu}{\rho}} = \sqrt{\frac{E(1-\nu)}{\rho\,(1+\nu)(1-2\nu)}}$$

$$V_s = \sqrt{\frac{\mu}{\rho}} = \sqrt{\frac{G}{\rho}}$$

$$V_R = \sqrt{\frac{E}{\rho}}$$

Thus:

$$\mu = \rho V_s^2$$

$$\lambda = \rho V_L^2 - 2\mu \qquad (2.28)$$

$$\nu = \frac{1}{2} - \frac{V_s^2}{2 (V_L^2 - V_s^2)}$$

Additional relations are shown in Table 2.1.

For a cubic crystal the elastic constants C_{11}, C_{12} and C_{44} can be calculated from the measurement of longitudinal and shear wave velocities in a (110) crystal.* If the velocities are measured in the [110]direction, then:[39]

$$\frac{C_{11} + C_{12} + 2 C_{44}}{2} = \rho V_1^2$$

$$\frac{C_{11} - C_{12}}{2} = \rho V_2^2 \qquad (2.29)$$

$$C_{44} = \rho V_3^2$$

where:

V_1 = Velocity of longitudinal wave,

V_2 = Velocity of shear wave having a particle motion in the $[1\bar{1}0]$ direction,

V_3 = Velocity of shear wave having a particle motion in the [001] direction.

Additional checks are furnished from the measurement of longitudinal and shear wave velocities in a (100) crystal,

---

*The notation (110)or [110]refers to standard Miller indices of crystals. The ( ) means plane, the [ ] refers to direction.[35]

Table 2.1. Connecting identies for elastic constants of isotropic bodies (Birch). K = bulk modulus; E = Young's modulus; μ = shear modulus; β = compressibility = $1/K$; λ = Lamé's constant; ν = Poisson's ratio; ρ = density; $R_1 = V_L/V_s$.

K	$\rho V_R^2 = E$	λ	ν	ρV_L^2	$\lambda V_s^2 = \mu$
$\lambda+2\mu/3$	$\mu\,\frac{3\lambda+2\mu}{\lambda+\mu}$	...	$\frac{\lambda}{2(\lambda+\mu)}$	$\lambda+2\mu$	...
...	$9K\,\frac{K-\lambda}{3K-\lambda}$	...	$\frac{\lambda}{3K-\lambda}$	$3K-2\lambda$	$3(K-\lambda)/2$
...	$\frac{9K\mu}{3K+\mu}$	$K-2\mu/3$	$\frac{3K-2\mu}{2(3K+\mu)}$	$K+4\mu/3$	...
$\frac{E\mu}{3(3\mu-E)}$	...	$\mu\,\frac{E-2\mu}{3\mu-E}$	$E/(2\mu)-1$	$\mu\,\frac{4\mu-E}{3\mu-E}$	...
...	...	$3K\,\frac{3K-E}{9K-E}$	$\frac{3K-E}{6K}$	$3K\,\frac{3K+E}{9K-E}$	$\frac{3KE}{9K-E}$
$\lambda\,\frac{1+\nu}{3\nu}$	$\lambda\,\frac{(1+\nu)(1-2\nu)}{\nu}$	...	...	$\lambda\,\frac{1-\nu}{\nu}$	$\lambda\,\frac{1-2\nu}{2\nu}$
$\mu\,\frac{2(1+\nu)}{3(1-2\nu)}$	$2\mu(1+\nu)$	$\mu\,\frac{2\nu}{1-2\nu}$	...	$\mu\,\frac{2-2\nu}{1-2\nu}$	...
...	$3K(1-2\nu)$	$3K\,\frac{\nu}{1+\nu}$	...	$3K\,\frac{1-\nu}{1+\nu}$	$3K\,\frac{1-2\nu}{2+2\nu}$
$\frac{E}{3(1-2\nu)}$	...	$\frac{E\nu}{(1+\nu)(1-2\nu)}$	...	$\frac{E(1-\nu)}{(1+\nu)(1-2\nu)}$	$\frac{E}{2+2\nu}$
$\rho(V_L^2 - \frac{4}{3}V_s^2)$	...	$\rho(V_L^2 - 2V_s^2)$	$\frac{(R_1^2-2)}{2(R_1^2-1)}$	...	...

$$C_{11} = \rho V_4^2$$

$$C_{44} = \rho V_5^2 \qquad (2.30)$$

where:

V_4 = Velocity of longitudinal wave in [100] direction,

V_5 = Velocity of shear wave propagating in [100] direction.

2.3. Ultrasonic Techniques for the Measurement of Elastic Wave Velocities and Attenuation in Solids

2.3.1. Ultrasonic Test Components

The basic components of an ultrasonic test system are:

1. Electrical signal generator and indicator,
2. Transmitting and receiving transducers,
3. specimen and couplant.

1. Electrical signal generator and indicator:

The function of the signal generator is to provide an electrical signal in the form of a pulse or harmonic wave. This pulse is applied to the transmitting transducer.

The electrical indicator is usually the CRO screen of an oscilloscope. Its function is to display the signal from the receiving transducer.

2. Transmitting and receiving transducers:

The transducers used in ultrasonic testing can be best described by the term "high frequency electromechanical

transducers" i.e., elements that have the ability to transform high frequency electrical energy into high frequency mechanical energy and vice versa. The transmitting transducer vibrates when an electrical pulse is applied to it. These mechanical vibrations are transmitted to the specimen through a couplant. When the receiving transducer "feels" the vibrations in the specimen it vibrates and produces electrical signals which are displayed on the oscilloscope.

A conductive material such as silver paint is needed on the two opposite faces of both transducers, for connection to the electrical system.

Transducers are made from piezoelectric materials, such as quartz crystals, or from polarized ferroelectric ceramics such as barium titanate. A description of the properties of these materials and their electrical and acoustic constants, can be found in any of the standard books on this subject.[17,13,41] For the purpose of this investigation, it is sufficient to note the following:

Quartz piezoelectric transducers can be cut in various orientations, to generate the type of wave desired. An X-cut is used to generate longitudinal waves; a Y-cut is used to generate shear waves.

A ferroelectric ceramic is polarized by applying a large electrical field, usually at a temperature above the Curie point, and cooling the ceramic with the field applied. After cooling, the ceramic acts like a piezoelectric crystal.

The three most common transducers are quartz, barium titanate and lithium sulfate.[43] Quartz transducers have the advantage of being stable over a wide temperature range and the disadvantage of being the least efficient transmitters. Barium titanate transducers have the advantage of being the most efficient transmitters and the disadvantages of low Curie point and a tendency to age. Lithium sulfate transducers are the most efficient receivers. However, their use is limited because lithium sulfate is soluble in water.

The frequency of a transducer varies inversely, with its thickness. However, the relation is not linear and depends on the type of transducer, X or Y cut, and on the material from which it is made.

3. Specimen and Couplant:

The surface of the specimen to which a transducer is applied must be smooth to minimize the loss of acoustic energy due to reflection and refraction at the interface. A thin layer of a couplant is applied between the transducer and the specimen. The couplant serves as a means by which the acoustical energy is transferred between the transducers and the specimen. For longitudinal waves, a thin film of grease or oil serves this purpose. For shear transducers the couplant should possess the ability to transfer shear waves. Satisfactory results can be achieved by using Phenyl Salicylate or regular sealing wax. These materials

are applied to the heated surfaces of the transducer and the specimen to be joined. The transducer and the specimen are then clamped together and allowed to cool.

2.3.2. Ultrasonic Test Methods

Several methods have been used to measure the velocities and attenuation of ultrasonic waves in solids. The most favored method is the pulse method in which a short train of high frequency waves are propagated in the specimen. The frequency of the waves is equal to the vibration frequency of the transmitting transducer. When a rectangular voltage pulse is used, the transducer is assumed to vibrate at its natural frequency which depends on its thickness. However, a transducer can be driven to vibrate over a wide frequency range by using a pulse which consists of a short train of harmonic waves. The efficiency of the transducer is best when driven at a frequency which is equal to its natural frequency.

Pulse Echo Method (Figure 2.7)

This method uses only one transducer which acts as both a transmitter and receiver. The original pulse is reflected back and forth between two opposite parallel faces of the specimen. Both velocity and attenuation can be measured from the received signal. Velocity is determined by measuring the time delay between two echoes. Attenuation is measured from the relative amplitude of successive echoes.

Through Transmission (Figure 2.8)

In coarse grained materials, such as rock, the echo method cannot be used because of scattering and loss of acoustic energy both in the specimen and on the reflecting surface. In such materials, two transducers are used on the opposite faces of the specimen. The velocity is determined by measuring the delay time in the specimen. Relative attenuation can be determined by comparing the amplitude of the signals received from specimens of different lengths.

2.4. Experimental Results on the Effect of Stresses on Ultrasonic Wave Velocities and Attenuation in Solids*

During the past two decades, ultrasonic waves have assumed an increasingly important role as an industrial and research tool to study the physical properties of matter. In industry, ultrasonic inspectroscopes and thickness gauges are used to determine the integrity and dimensions of metal castings or other solids.[41] In research ultrasonic waves, and their variations with temperature, stress and frequency are used to study the composition of materials, elastic moduli, mechanisms of internal friction, atomic structure, imperfections in a crystal lattice and "even the interaction of lattice vibrations with free electrons and phonons."[41]

---

*The term "ultrasonic waves" refers to periodic disturbances in a medium above the audible range, i.e., above 20,000 cycles per second.

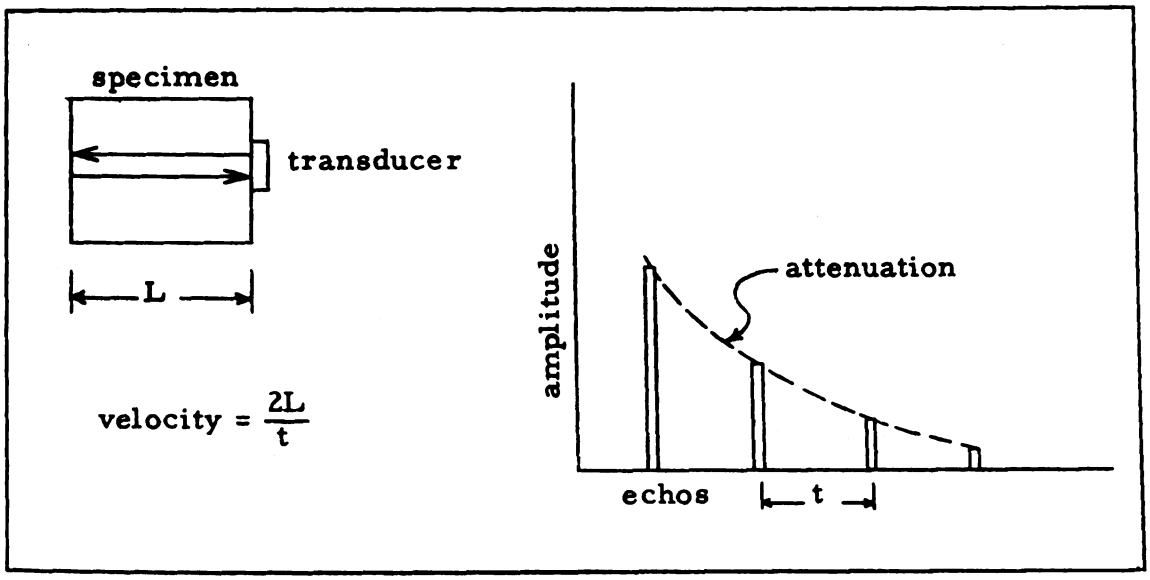

Fig. 2.7. The pulse-echo method.

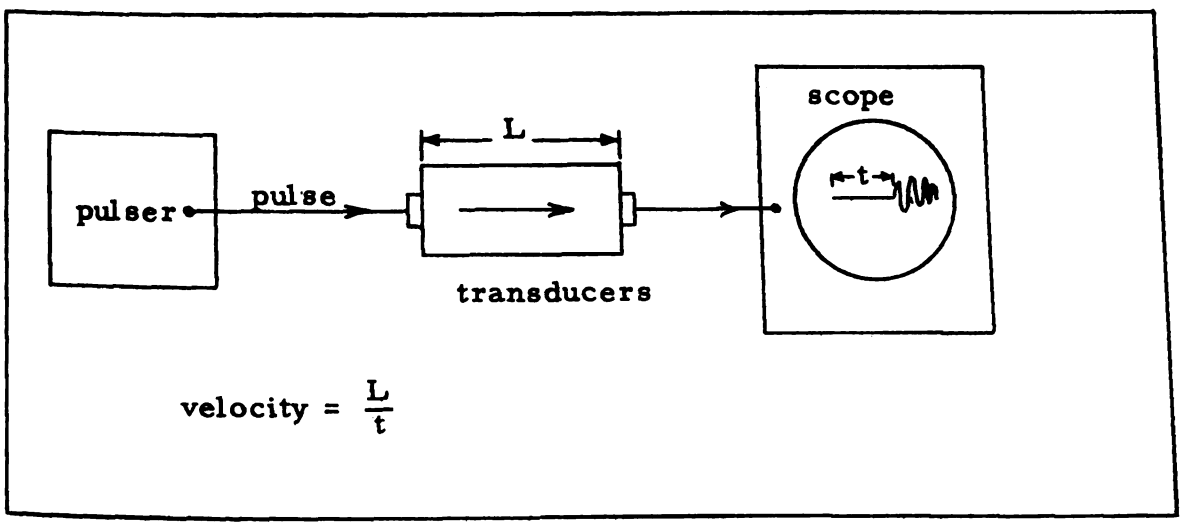

Fig. 2.8. Through transmission method.

The purpose of this section is to review the use of ultrasonic methods to measure the changes of elastic moduli and attenuation in solids, with special emphasis on rocks. Comprehensive bibliographies and discussion of additional uses can be found in any of the standard books on this subject.[18,31,41]

2.4.1. Single Crystals

Experimental results of the dependence of the elastic constants of single crystals on pressure, are aimed at investigating the atomic structure of crystals. Measured changes in the elastic constants are compared with theoretical changes that can be computed from Fuch's theoretical calculation of the cohesive energy contributions.[59,75] For example, the compressibility, β, for a cubic crystal can be expressed as[59]

$$\frac{1}{\beta} = \frac{1}{3}\,(C_{11} + 2\,C_{12}) = 2\,\frac{\delta\Phi}{\left(\frac{\delta V}{V}\right)^2} \qquad (2.31)$$

where:

$\delta\Phi$ = change in elastic energy per unit volume,

$\frac{\delta V}{V}$ = relative change in volume.

From quantum-mechanical considerations $\frac{\delta V}{V}$ is expressed in terms of the change in the radius of a sphere having the same volume as the atomic cell. (Φ) is expressed in terms of the cohesive energy per atom of the crystal.[59] The compressibility, β, at zero absolute temperature can then be expressed as:[59]

$$\frac{1}{\beta} = \frac{1}{12\ \pi\ r}\ \frac{\partial^2 \epsilon(r)}{\partial r^2} \qquad (2.32)$$

where:

r = radius of a sphere having the same volume as the atomic cell when $\epsilon(r)$ is minimum.

$\epsilon(r)$ = cohesive energy per atom

Lazarus[39] made the first ultrasonic measurements of the changes of elastic constants with pressure. He measured the changes in the elastic constants of NaCl, KCl, CuZn, Cu and Al with pressures up to 10 kilobars.* The elastic constants were calculated from the measured velocities of equations (2.29) and (2.30). The results for KCl and NaCl are presented in Figures 2.9 and 2.10. Lazarus pointed out that the increase in anisotrophy, C_{44} compared to $\frac{1}{2}(C_{11} - C_{12})$, of NaCl and KCl with pressure agrees with Zener's[75] predictions which are based on Fuch's calculations concerning the effect of short range exchange between closed-shell ions on shear moduli.

Daniels and Smith[21] reported similar measurements on Cu, Ag and Au. The values found for the pressure derivatives of the elastic constants were as follows:

	Cu	Ag	Au
$\frac{d\beta}{dP}$	5.59	6.18	6.43
$\frac{dC}{dP}$	2.35	2.31	1.79
$\frac{dC'}{dP}$	0.580	0.639	0.438

*1 bar = 10^6 dynes/cm^2 = 1.01972 kg/cm^2 ≈ 14 psi.

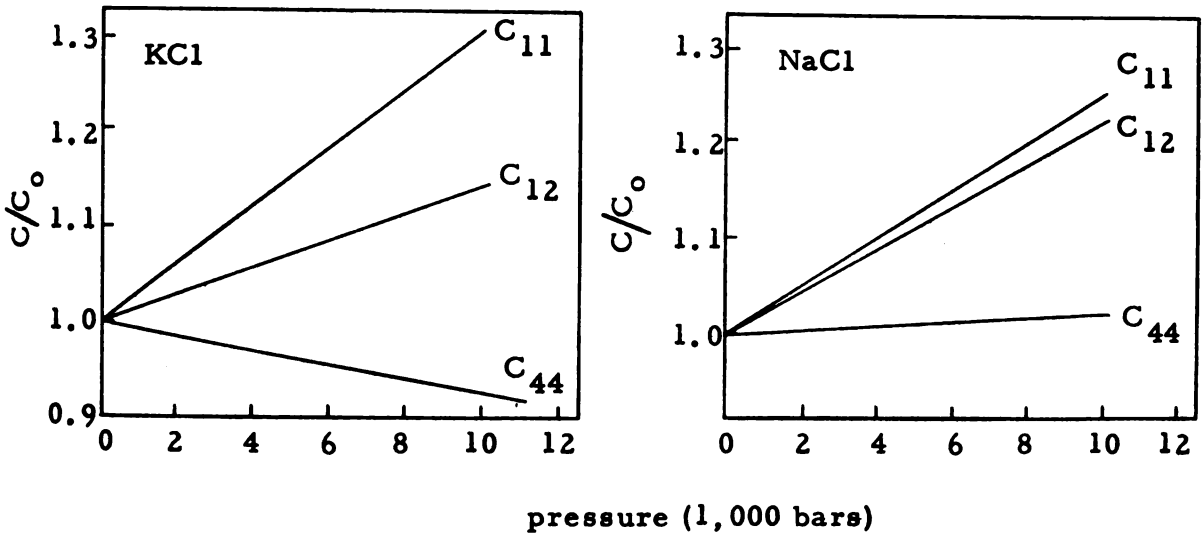

Fig. 2.9 Variation of the adiabatic elastic constants of KCl and NaCl with pressure. (Lazarus)

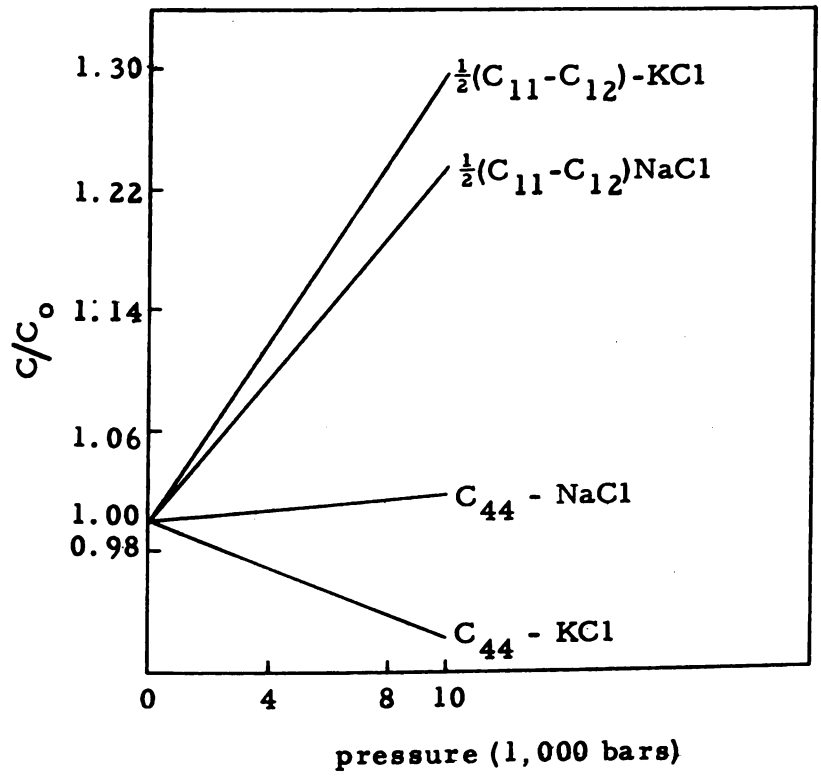

Fig. 2.10 Variation of the shear moduli of KCl and NaCl with pressure. (Lazarus)

where:

$$\beta = \frac{C_{11} + 2C_{12}}{3}$$

$$C = C_{44}$$

$$C' = \frac{C_{11} - C_{12}}{2}$$

The main conclusion of the authors was that the conventional assumption that short-range repulsions are considered to act along lines joining nearest neighbor atoms and depend only on the distance between them, does not account for the shear constants and their pressure derivatives in Cu, Ag and Au.

2.4.2. Polycrystalline Metals

While extensive literature has been published about the effect of stresses on ultrasonic wave velocities in single crystals, very little work has been done with polycrystalline metals. A summary of this work follows:

Bergman and Shahbender[5] measured the velocity changes of ultrasonic waves propagating in transverse direction to the applied stress in (4 x 4 x 20 inch) aluminum columns under uniaxial compressive stress. The ultrasonic modes considered were longitudinal waves, shear waves with particle motion along the direction of applied stress, and shear waves with particle motion transverse to the direction of applied stress. The authors used a through transmission method (Section 2.3.2). X and Y-cut quartz crystals were used. All transducers were driven at 4 mcs. A similar set of transducers was placed on an unstressed specimen to provide a

delay line and a comparison circuit for more accurate measurement of velocity changes.

The results obtained are presented in Figures 2.11-2.13. Figure 2.11 shows the load-strain curve. Figure 2.12 represents the experimental values of Poisson's ratio as measured by strain gages. Figure 2.13 represents velocity changes as functions of the load.

The authors concluded the following:

1. The relevant elastic constant governing the velocity of the longitudinal wave is independent of the applied stress. The observed changes in velocity may be accounted for by changes in density alone, using the following equation:

$$\frac{\Delta V_L}{V_L} = \epsilon_\ell \left(\frac{1}{2} - \nu\right) \tag{2.33}$$

where:

$\frac{\Delta V_L}{V_L}$ = fractional change in velocity

ϵ_ℓ = longitudinal strain at a given load

ν = Poisson's ratio at the same load

2. Changes in shear wave velocities cannot be accounted for by changes in density alone. This implies a change in the relevant elastic constant governing the propagation of shear waves. The authors gave the following equation:

$$\frac{\Delta C}{C} \approx 2 \left[-\epsilon_\ell \left(\frac{1}{2} - \nu\right) + \frac{\Delta V_s}{V_s}\right] \tag{2.34}$$

where:

$\frac{\Delta C}{C}$ = fractional change in relevant elastic constant of shear waves

ϵ_ℓ = longitudinal strain

$\frac{\Delta V_s}{V_s}$ = fractional change in shear velocity

A discussion of the above results will be given in Section 5.8.

The velocity difference between horizontally and vertically polarized shear waves initiated further exploratory investigations by Rollins,[58] Benson and Realson[4] and Benson,[3] to determine if this difference could be used to measure static or residual stresses.

The experimental arrangement used by Rollins is shown in Figure 2.14. Two 5 mcs shear transducers, A and B, were cemented to the side of the specimen. The particle motion of A was parallel to the direction of loading. The particle motion of B was perpendicular to the direction of loading. The two transducers were electrically connected in parallel so that each sent out a pulse of acoustic energy at the same instant. If the two shear waves travel at the same speed their echoes should return to the transducers at the same time. The received signals from the transducers would then be in phase and reinforce each other. However, when the two waves travel with different velocities the echoes will not return at the same time and received signals from the transducers will be out of phase.

Since the two transducers are connected in parallel, the receiver detects the sum of the two signals. When the phase difference is 180^{o} the sum of the two signals will be zero.

Figure 2.14 shows a schematic diagram of the echo pattern in aluminum. The first zero echo occurs when the phase difference is 180^{o}; the second when the phase difference is 540^{o}. Rollins observed that the first echo arrives at an earlier time when the stress is increased. He suggested that this might be a possible method of measuring residual stresses.

Rollins,[58] Benson and Realson[4] and Benson[3] were able to obtain similar results using only one shear transmitter with its particle motion oriented at 45^{o} to the direction of loading. In this case, "The ultrasonic wave train can be thought of as having two components"[4] of equal amplitude, one with particle motion along the axis of loading and the other with particle motion perpendicular to the direction of loading. When a load is applied to the specimen the two components travel with different velocities, just as the two separate shear waves did in the earlier example. "The different velocities of the components produce a rotation of their resultant which is completely analogous to the rotation of polarized light going through a double refracting medium."[58]

When the two components are 180^{o} out of phase the resultant of the two has rotated 90^{o} in space. When this

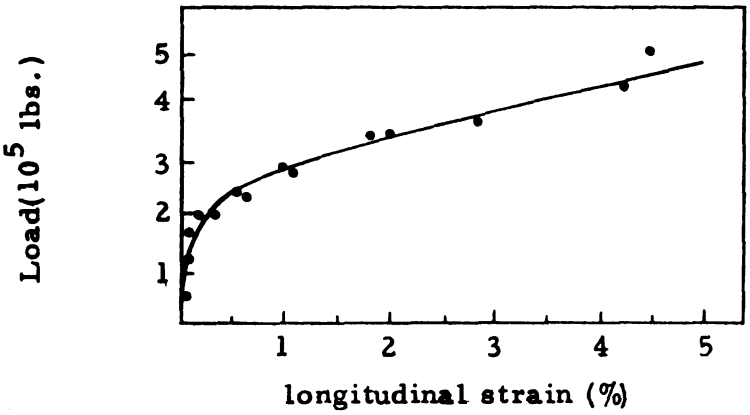

Fig. 2.11 Load-strain characteristics for the columns. (Bergman)

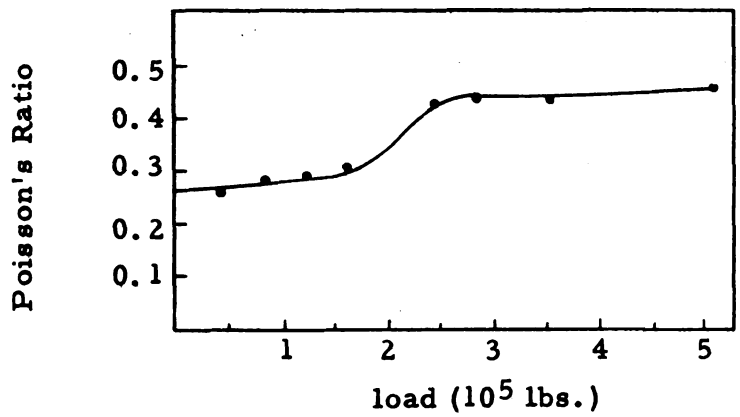

Fig. 2.12 Experimental values of Poisson's ratio at different load level. (Bergmen)

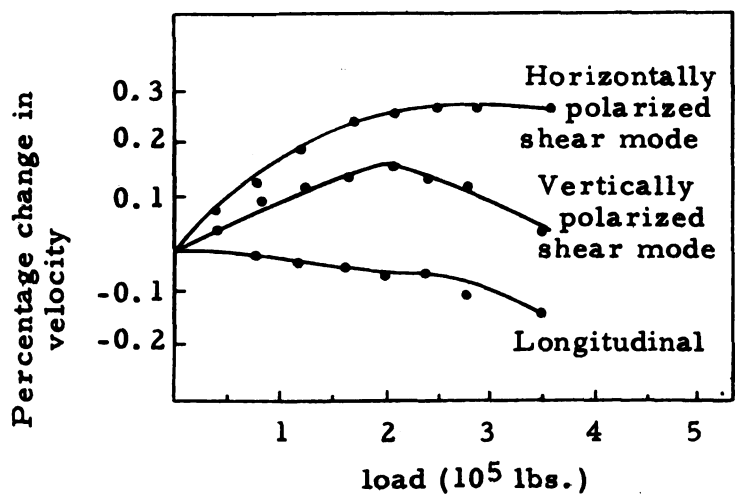

Fig. 2.13 Measured changes in the propagation velocities as functions of applied load. (Bergman)

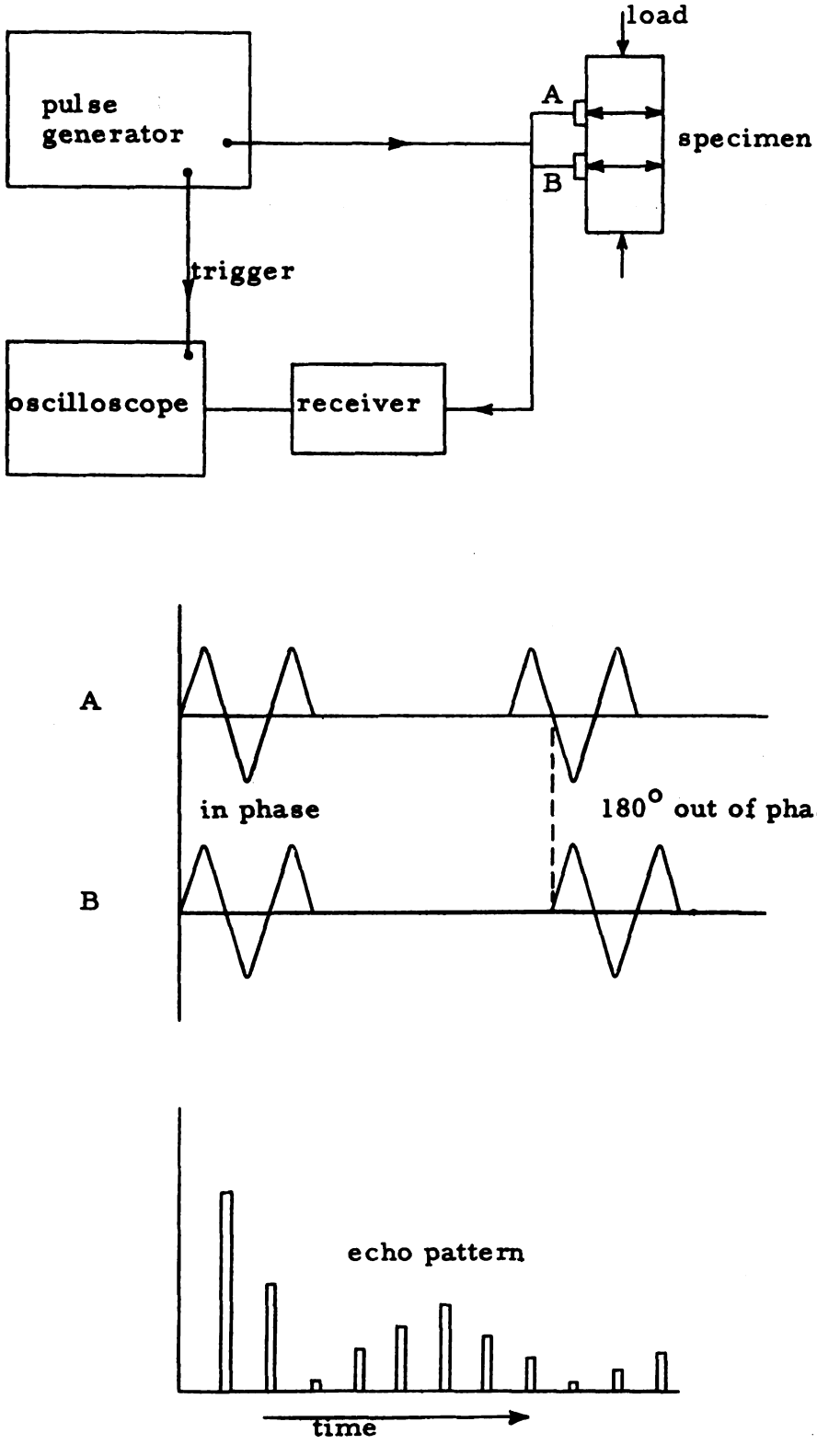

Fig. 2.14. Schematic diagram of Rollins experiment.

resultant wave train arrives at a receiving transducer which is oriented in the same direction as the transmitter it will produce no electrical signal because the receiving transducer is insensitive to vibration in that direction. Rollins used the echo method in which the transmitter served as a receiver. Benson and Realson used a through transmission method in which a shear transducer of the same orientation as the transmitter was placed on the opposite side of the specimen.

2.4.3. Rocks

Ultrasonic pulse methods have been used by many investigators to study factors affecting wave velocities in small specimens of rock. Birch[13] measured the velocity of longitudinal waves in 250 types of rocks with pressures up to 10 kilobars. Hughes[32,33] and his colleagues measured the variation of wave velocities due to pressure and temperature. Wyllie and his colleagues[73] studied the effect of porosity and water content. Tocher[67] studied the effect of uniaxial stress. Similar studies were made by scientists in the USSR[72] and India.[2] Rock salt was not studied by any of the above investigators. The only available literature on rock salt comes from seismic measurements of Project Cowboy.[48] The results obtained by the above authors indicated that the influence of pressure, temperature and water content on wave velocities followed a certain general behavior common to most rocks. A summary of this

general behavior is presented below. For the results obtained for a particular type of rock, the reader is referred to the original articles or to an excellent review paper by Rinehart.[53]

1. The velocity of longitudinal waves increases with an increase in hydrostatic pressure. At low pressures, up to 500 bars, the velocity increases by 10 to 30 percent of its original value. At very high pressures, above 1,000 or 2,000 bars, the velocity increases very slowly. Birch[14] suggested that the rapid increase of velocity at low pressures is due to closure of pore spaces and cracks among the rock grains. Rinehart[53] stated that the slow increase of velocity at high pressures has not been explained.
2. Velocities measured with decreasing pressures are higher than velocities measured with increasing pressures. Hughes[32] suggested that this is due to the fact that pores or cracks remain closed when the pressure is released.
3. Frequency has little effect on velocity. At low frequencies, 40 to 4,500 cps, the velocity variation does not exceed 2%.[14] At higher frequencies, 50 kcs to 3 mcs, velocity is independent of frequency.[14]
4. Velocities measured in three perpendicular directions in unstressed specimens do not differ by more than 2 or 3 percent.[2,14] A few rocks show a variation up to 15%.[14]

5. The principal factors determining longitudinal velocity in rocks are density and mean atomic weight. Velocity is approximately a linear function of density for rocks which have a common atomic weight.[14]
6. Velocity decreases with an increase in temperature. Temperature tends to cancel out the pressure affect when both are applied simultaneously.
7. Velocity decreases with an increase in porosity and water content.
8. The dynamic elastic moduli of rocks are higher than the static moduli which are obtained from uniaxial stress tests. The difference between the static and dynamic values of Young's modulus varies between 0 and 300 percent depending upon the type of rock. For dense rocks, with a high value of static E (7×10^6 psi), the difference is less than 40% while for rocks having low values of static E (2×10^6 psi), the difference is more than 100%.
9. When uniaxial pressure is applied to rocks, the longitudinal velocity in the direction of compression increases in a manner similar to that observed in hydrostatic compression. Velocity in a direction perpendicular to the compression, increases at a lower rate. The difference between the two velocities reaches 10% at fracture.[67]

10. Rock salt. The wave velocities and elastic moduli of rock salt in situ were measured by Nicholls and his colleagues[48] in connection with the U.S. Atomic Energy Commission, Project Cowboy.

The values obtained were as follows:

V_L = 14,350 ± 100 ft/sec. = 4,370 ± 30 meters/sec.

V_S = 8,380 ± 100 ft/sec. = 2,550 ± 30 meters/sec.

$E = 5.09 \times 10^6$ psi

$G = \mu = 2.05 \times 10^6$ psi

$\lambda = 1.91 \times 10^6$ psi

$K = 3.28 \times 10^6$ psi

$\nu = 0.241$

$\lambda/\mu = 0.931$

The dynamic breaking strength of rock salt was also investigated by the above authors using 30 to 50 inch cores of salt. Small charges were exploded at the end of the core. Strain gages attached at various distances from the end, were used to measure the peak compressive strains at the point of failure.

The dynamic compressive breaking strength was calculated from the peak values of compressive strains and the known value of dynamic E.

The data obtained are given as follows:

Length of core inches	Charge weight lbs.	Length crushed inches	Peak compressive strain micro - in/in	Dynamic compressive breaking strength psi
31.6	0.1	9.6	3700	18,800
31.9	0.05	8.9	6700	34,100
39.2	0.15	10.2	7100	36,200
48.4	0.4	13.9	7500	38,200
	Average		6250	31,800

Static tests were made for comparison and the authors pointed out that the dynamic compressive strength was 7 times the static value.

2.4.4. Attenuation

The term "attenuation" as used in this investigation refers to the dissipation of acoustic energy in a medium. Attenuation in solids is due to many factors of which the following are most important.

1. Internal Friction: The most direct method of defining internal friction is by the ratio:[36]

$$\frac{\Delta W}{W}$$

where:

ΔW = energy dissipated into heat while taking a specimen through a stress cycle.

W = maximum strain energy in the cycle.

For liquids and gases internal friction is due to viscosity and thermal conduction. These effects can be

treated analytically. In solids the behavior is found to be much more complex and to vary considerably with the nature of the solid. Kolsky[36] pointed out that there is at present no satisfactory theory of internal friction in solids.

2. Scattering: Scattering is the loss of acoustic energy due to reflections and refractions at the grain boundaries. This factor becomes very important when the wave length is compatible with the grain size.

3. Beam spreading: The beam spreading phenomena may be briefly explained by the following:

   An X cut crystal mounted on one side of a specimen will produce a plane wave pattern which extends some distance into the sample and a spherical wave pattern through the rest of the sample. In the plane wave region there is essentially a very small amount of reflection from the sides of the specimen. In the spherical wave region there is reflection from the sides of the specimen which results in loss of energy and phase interference which produces erroneous attenuation readings. Therefore, reliable attenuation measurements should be taken in the plane wave region.

Mason[41] analyzed the beam spreading problem and demonstrated that the plane and spherical regions can be represented by the figure below:

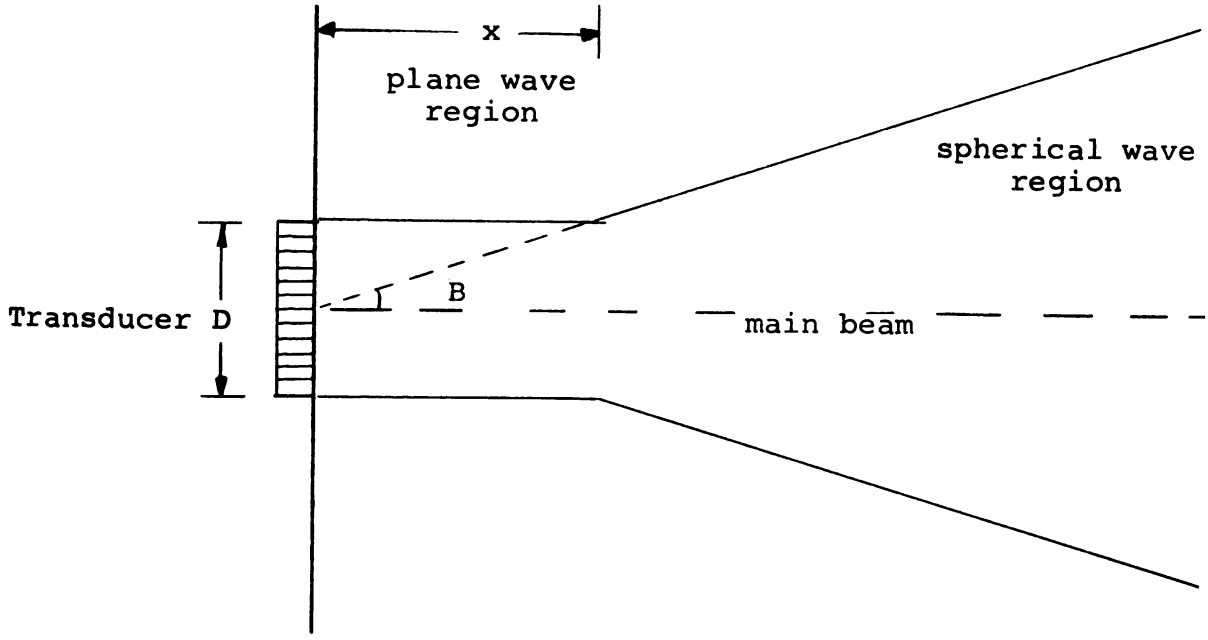

where:

$$\sin B = \frac{1.22\ L}{D}$$

L = wave length

D = diameter of transducer

$$\frac{D}{2x} = \tan B$$

Hikata and his colleagues[27] used the pulse echo method to measure the changes in attenuation in an aluminum specimen under tension. Their results indicated that attenuation increases with increasing stress in a manner similar to the stress-strain curve. A sudden jump discontinuity in the attenuation curve was observed near the yield stress region of the aluminum. The authors interpreted their results by using the theory of dislocation damping. This theory assumes that the dislocation loops are free to vibrate in a manner similar to a stretched

string. As the external stress is increased the dislocations break away from the weak impurity pinning points and the loop length becomes larger and thus absorbs more of the acoustic energy and leads to larger attenuations.

Auberger and Rinehart[1] used the through transmission method (Section 2.3.2) to measure the relative attenuation of rocks in a frequency range of 250 kcs to 1 mcs. Attenuation was computed from the amplitude of the first signals received for two specimens of different length.

$$\alpha = \frac{20 \log_{10} \frac{A_1}{A_2}}{L_2 - L_1}$$

where:

α = attenuation in decibels/unit length

A = amplitude of 1st signal received

L = length of specimen

$L_2 > L_1$, $A_1 > A_2$

For the rocks tested, a peak attenuation was observed at a frequency which corresponded to the resonance frequency of the largest grains of the rocks. This frequency is defined as:

$$\frac{V_L}{2L}$$

where:

V_L = velocity of longitudinal wave

L = maximum macroscopic size of the grains.

III. THE INFLUENCE OF HIGH STATIC STRESSES ON ELASTIC WAVE VELOCITIES

3.1. Previous Work

Elastic wave velocities in a medium are derived from the constitutive equations and the basic principles of conservation of mass and balance of momenta. The wave velocity V can be expressed as:

$$V = \sqrt{\frac{C}{\rho}} \tag{3.1}$$

C = relevant elastic constant

ρ = density

The relevant elastic constant C depends on the type of wave, direction of propagation, temperature and the material properties of the medium. Stress produces a change in temperature, density, material properties, and structural symmetry. The change in ρ can be determined from the principle of conservation of mass,

$$\rho_o \, d \, V_o = \rho_1 \, d \, V_1$$

where:

ρ = density

d V = unit volume

To find the changes in C it is necessary to examine the constitutive equations, stress-strain relationships, in which C appears. These equations are derived from energy considerations. For isothermal processes it is assumed that the work done on a medium, by the stresses applied to it, is stored in the form of strain energy and that the density of this energy is a function of the strain components.

In the classical theory of elasticity the strains are assumed to be infinitesimal and the strain energy function is expressed up to the 2^{nd} power of the strain components. Each component of stress is then the derivative of the strain energy with respect to the corresponding strain component. When the strains are measured from a state of zero stress, the strain energy and the stresses are expressed as:

$$\Phi = \frac{1}{2} C_{ij} \epsilon_i \epsilon_j \tag{3.2}$$

$$\sigma_i = \frac{\partial \Phi}{\partial \epsilon_i} = C_{ij} \epsilon_j \tag{3.3}$$

where:

Φ = strain energy/unit volume

$i,j = 1, 2, \ldots 6$

repetition of a suffic implies summation with respect to that suffix.

σ_i = six components of stress

ϵ_i = six components of strain

C_{ij} = 2^{nd} order elastic constants

C_{ij} are called 2^{nd} order elastic constants because they are multiplied by 2^{nd} powers of strain in the strain energy function (Φ).

Equation (3.3) is the well known Hooke's Law. For an isotropic material this equation reduces to Eq. (2.10) with only two independent elastic constants λ and μ. In this case the elastic wave velocities for an infinite medium are:

$$V_L = \sqrt{\frac{\lambda + 2\mu}{\rho}} \tag{3.4}$$

$$V_s = \sqrt{\frac{\mu}{\rho}} \tag{3.5}$$

where:

V_L = longitudinal wave velocity

V_s = shear wave velocity

When the strains are measured from a stressed state, Eqs. (3.2) and (3.3) become:

$$\Phi = \sigma_i^o \epsilon_i + \frac{1}{2} C'_{ij} \epsilon_i \epsilon_j \tag{3.6}$$

$$\sigma_i = \sigma_i^o + C'_{ij} \epsilon_j \tag{3.7}$$

where:

σ_i^o = initial stresses

In this case the C'_{ij} depend on the state from which the strain ϵ is measured, i.e., they depend on the initial stresses σ_i^o. For an isotropic material under hydrostatic pressure P, the C'_{ij} reduces to two indepdent constants λ' and μ'. Brillouin[16] used the infinitesimal strain theory, Eqs. (3.6) and (3.7), and derived the following expressions for λ' and μ':

$$\lambda' = \lambda + P$$

$$\mu' = \mu - P$$

The wave velocities V_L and V_s are then:

$$V'_L = \sqrt{\frac{\lambda' + 2\mu'}{\rho'}} = \sqrt{\frac{\lambda + 2\mu - P}{\rho'}} \tag{3.8}$$

$$V'_s = \sqrt{\frac{\mu'}{\rho'}} = \sqrt{\frac{\mu - P}{\rho'}} \tag{3.9}$$

where:

ρ' = density in the stressed state

These results were later rejected by Biot[10] and Birch[12] because they are contrary to experimental data and lead to the result that at sufficiently high pressures the velocities will be zero.

A more accurate derivation of the changes in the relevant elastic constants, C, was derived from the finite theory of elasticity by expanding the strain energy function Φ, Eq. (3.6), to include higher powers of strain.

3.1.1. Finite Theory of Elasticity

In the finite theory of elasticity the assumption of infinitesimal strains is removed and the strain energy function is expanded to include higher powers of strain. Thus, the energy stored in the body in its stressed state is:

$$\Phi = \frac{1}{2} C_{ij}\eta_i \eta_j + C_{ijr} \eta_i \eta_j \eta_r + \text{higher order terms} \tag{3.10}$$

where:

η_i = finite strain

C_{ijr} are called 3rd order elastic constants because they are multiplied by 3rd powers of strain.

The 3rd order constant C_{ijr} form a 36 x 6 matrix. Bhagavantam[6] has shown that for a body with no structural symmetry there are only 56 independent C_{ijr}. For cubic cyrstals the number of independent C_{ijr} is 6 and for isotropic bodies only 3. The stress is given by:

$$\sigma_i = C_{ij}\ \eta_j + C_{imn}\ \eta_m\ \eta_n + \text{higher order terms} \tag{3.11}$$

Thus, stresses are not linear functions of the strains. This is why the finite theory of elasticity is also called a non-linear theory of elasticity.

Another consequence of the finite theory is that the final coordinates of a point are not interchangeable with the original coordinates as is assumed in the infinitesimal theory. This is because the strains are large. Thus, in the finite theory, stresses and strains can be expressed in terms of either the initial or the final coordinates. The choice of coordinates would depend on the type of problem and the given boundary values. The initial coordinates are called "Lagrangian Coordinates" and the final coordinates are called "Eurlerian Coordinates."

The formulation of the finite theory of elasticity in a completely general tensor notation is given by Murnaghan,[46] Eringen,[23] Brillouin[16] and Green and Zerna.[25] Murnaghan[47] also gave the formulation using matrix notation. Biot[9] and Rivlin[54,55] discussed some of the fundamental concepts of the theory using rectangular cartesian coordinates.

3.1.2. Small Elastic Deformations Superposed on Finite Elastic Deformations

Green, Rivlin and Shield[24] developed a general theory for small elastic deformations superposed on known finite deformations. Their theory was later specialized by Rivlin and Hayes,[56] Truesdall[69] and Toupin and Bernstein[68] to the case where the small elastic deformations are due to wave motion in a material originally subjected to pure homogeneous deformations. The theory is developed by the above authors in general tensor notation and without assuming any special form for the strain energy function. Their treatment does not explicitly bring out the third-order elastic constants.

Bhagavantam[8] used Murnaghan's theory of finite strain to derive the "effective elastic constants" of cubic crystals under hydrostatic compression. The "effective elastic constants" are defined as the constants relating additional stresses to the additional infinitesimal strains. Bhagavantam assumed that:

$$\Phi_1 = \Phi_2 - \Phi_3 \tag{3.12}$$

where:

Φ_1 = strain energy of the infinitesimal strains

Φ_2 = strain energy of the infinitesimal strains plus the finite strains considered as a single composite finite state of strain

Φ_3 = strain energy of the initial finite strain

The effective elastic constants appear in Φ_1. The original 2nd and 3rd order elastic constants appear in

ϕ_2 and ϕ_3. The effective elastic constants are then derived by equating the coefficients of the infinitesimal strains appearing in both sides of the equation. The results are as follows:

$$C'_{11} = C_{11} + \eta\,(2C_{11} + 2C_{12} + 6C_{111} + 4C_{112})$$

$$C'_{12} = C_{12} + \eta\,(C_{123} + 4C_{112} - C_{11} - C_{12}) \qquad (3.12)$$

$$C'_{44} = C_{44} + \eta\,(C_{44} + C_{11} + 2C_{12} + \frac{C_{144}}{2} + C_{155})$$

Birch[11] obtained similar results for C'_{11} but slightly different expressions for C'_{12} and C'_{44} by equating stresses instead of energies. He assumed that:

$$T_1 = T_2 - P$$

where:

T_1 = stresses due to infinitesimal strains

T_2 = stresses due to infinitesimal plus the finite strains

P = hydrostatic pressure

3.1.3. Determination of the Third-Order Elastic Constants From Wave Velocities

Examination of the formulas in (3.12) indicates that certain functions of the third-order elastic constants can be calculated when the effective elastic constants are measured from wave velocities in the stressed state. The second-order elastic constants can be calculated from wave velocities at zero stress. Hydrostatic strain can be measured for any pressure. However, there are only three

equations for five unknown third-order elastic constants. Thus, an explicit solution cannot be obtained.

Hughes and Kelly[30] were the first to obtain a sufficient number of independent relations to determine the third-order elastic constants from wave velocities for an initially isotropic material. They used Murnaghan's form of the strain energy function, Eq. (3.26), and considered two types of stresses; hydrostatic pressure, P, and uniaxial compressive stress, T. The velocities were given by:

Hydrostatic pressure:

$$\rho_o V_L^2 = \lambda + 2\mu - \frac{P}{3K_o}[6\ell + 4m + 7\lambda + 10\mu]$$

$$\rho_o V_s^2 = \mu - \frac{P}{3K_o}[3m - \frac{n}{2} + 3\lambda + 6\mu] \qquad (3.14)$$

Uniaxial compressive stress:

$$\rho_o V_{Lzz}^2 = \lambda+2\mu - \frac{T}{3K_o}[2\ell+\lambda+ \frac{\lambda+\mu}{\mu}(4m+4\lambda+10\mu)]$$

$$\rho_o V_{Lyy}^2 = \lambda+2\mu - \frac{T}{3K_o}[2\ell- \frac{2\lambda}{\mu}(m+\lambda+2\mu)] \qquad (3.15)$$

$$\rho_o V_{sxz}^2 = \mu - \frac{T}{3K_o}[m + \frac{\lambda n}{4\mu} + 4\lambda + 4\mu]$$

$$\rho_o V_{syx}^2 = \mu - \frac{T}{3K_o}[m + \frac{\lambda n}{4\mu} + \lambda + 2\mu]$$

$$\rho_o V_{szx}^2 = \mu - \frac{T}{3K_o}[m - \frac{\lambda + 2\mu}{2\mu} n - 2\lambda]$$

where:

K_o = compressibility

ρ_o = density at zero stress

P = hydrostatic pressure

T = uniaxial compressive stress along z direction

ℓ,m,n = 3rd order elastic constants or Murnaghan constants.

Hughes and Kelly used ultrasonic pulse methods to measure the velocities of Eqs. (3.14) and (3.15). The values of ℓ,m and n were calculated from the known stresses. These values are presented in the table below. They are the only experimental values of ℓ,m and n that the present author found in the literature.

	Units 10^{11} dynes/cm^2				
Material	λ	μ	ℓ	m	n
Polystyrene	0.2889 ±0.001	0.1381 ±0.001	-1.89 ±0.32	-1.33 ±0.29	-1.00 ±0.14
Armco Iron	11.00 ±0.04	8.20 ±0.10	-34.8 ±6.5	-103.0 ±7.0	+110.0 ±110
Pyrex	1.353 ±0.003	2.75 ±0.03	1.4 ±4.0	+9.2 ±5	+42 ±35

3.2. Theoretical Derivation of Plane Wave Velocities in an Isotropic Material Subjected to Homogeneous Deformation

Expressions for wave velocities in an isotropic material subjected to hydrostatic compression or triaxial stress with uniaxial strain, will be developed by the present author in the following section. The equations derived will be used in Chapters IV and V to determine the third-order elastic constants of rock salt.

3.2.1. Strain

Consider an isotropic body which is initially unstressed and unstrained. In this initial state the body will be called in state A^o. When this body is subjected to known uniform stresses of the type $\sigma_{11}^o \neq \sigma_{22}^o \neq \sigma_{33}^o \neq 0$ with all shear stresses = 0 and with no rotation of the body as a whole it will be in state A'. Infinitesimal strains (due to plane waves) carry the body from state A' to the final state A.

Throughout the development a rectangular cartesian coordinate system will be used. The coordinates of a particle in each state are as follows:

State A^o : x_i^o $\quad (i = 1, 2, 3)$

State A' : x_i' $\quad (i = 1, 2, 3)$

State A : x_i $\quad (i = 1, 2, 3)$

x_i' and x_i can be expressed in terms of x_i^o as follows:

$$x_i' = x_i^o + U_1^o (x_i^o)$$

$$x_2' = x_2^o + U_2^o (x_2^o)$$

$$x_3' = x_3^o + U_3^o (x_3^o)$$

where:

U_i^o are the displacements due to the stresses

$$\sigma_{11}^o, \ \sigma_{22}^o, \ \sigma_{33}^o$$

The Jacobian matrix of the transformation $dx_i^o \rightarrow dx_i'$ is given by J_1

$$J_1 = \left[\frac{\partial x_i'}{\partial x_j^o}\right] = \begin{bmatrix} 1+B_{11} & 0 & 0 \\ 0 & 1+B_{22} & 0 \\ 0 & 0 & 1+B_{33} \end{bmatrix} \qquad (3.17)$$

where:

$$B_{11} = \frac{\partial U_i^o}{\partial x_i^o} \quad , \quad B_{22} = \frac{\partial U_2^o}{\partial x_2^o} \quad , \quad B_{33} = \frac{\partial U_3^o}{\partial x_3^o}$$

Thus:

$$dx' = J_1 \, dx^o \qquad (3.18)$$

Eq. (3.18) is a matrix equation between the differential elements dx_1^o and dx_i'. If the additional infinitesimal displacements are denoted by u_i, (i = 1,2,3), then the final coordinates of a particle that was originally at x_i^o are given by:

$$x_i = x_i' + u_i(x_j') \qquad 1,j = (1, 2, 3) \qquad (3.19)$$

Here u_i is a function of all three coordinates x_1', x_2' and x_3'. The Jacobian of the transformation $dx_i' \longrightarrow dx_i$ is given by J_2.

$$J_2 = \begin{bmatrix} 1+b_{11} & b_{12} & b_{13} \\ b_{21} & 1+b_{22} & b_{23} \\ b_{31} & b_{32} & 1+b_{33} \end{bmatrix} \qquad (3.20)$$

where:

$$b_{ij} = \frac{\partial u_i}{\partial x_j'} \qquad i,j = 1, 2, 3$$

J_2 can be written as the sum of a symmetric strain matrix and a skew symmetric rotation matrix as follows:

$$J_2 = E_3 + \left[\frac{\partial u_i}{\partial x'_j}\right]$$

$$= E_3 + \left[\frac{1}{2}\left(\frac{\partial u_i}{\partial x'_j} + \frac{\partial u_j}{\partial x'_i}\right)\right] + \left[\frac{1}{2}\left(\frac{\partial u_i}{\partial x'_j} - \frac{\partial u_j}{\partial x'_j}\right)\right]$$

$$J_2 = E_3 + \epsilon_{ij} + \bar{w}_{ij}$$

where:

$$\epsilon_{ij} = \frac{1}{2}\left(\frac{\partial u_i}{\partial x'_j} + \frac{\partial u_j}{\partial x'_i}\right) = \text{strain matrix}$$

$$\bar{w}_{ij} = \frac{1}{2}\left(\frac{\partial u_i}{\partial x'_j} - \frac{\partial u_j}{\partial x'_i}\right) = \text{rotation matrix}$$

E_3 = identity square matrix of dimension 3

The matrix equation for the transformation $dx' \longrightarrow dx$ can now be written as:

$$dx = J_2\, dx' \tag{3.21}$$

but $dx' = J_1\, dx^o$ (Eq. 3.18)

Therefore, $dx = J_2\, J_1\, dx^o$

or

$$dx = J\, dx^o \tag{3.22}$$

where:

$$J = J_2 J_1 = \begin{bmatrix} (1+b_{11})(1+B_{11}) & b_{12}(1+B_{22}) & b_{13}(1+B_{33}) \\ b_{21}(1+B_{11}) & (1+b_{22})(1+B_{22}) & b_{23}(1+B_{33}) \\ b_{31}(1+B_{11}) & b_{32}(1+B_{22}) & (1+b_{33})(1+B_{33}) \end{bmatrix} \tag{3.23}$$

The total strain from state A^o to state A will be designated by η. This strain is composed of two parts:

the large initial strain, which may be expressed in terms of B_{11}, B_{22} and B_{33}, and the additional infinitesimal strain ϵ_{ij}, which may be expressed in terms of b_{ij}. Throughout the development the initial strains will be treated as finite strains of order less than 0.1. The value of 0.1 represents 10% strain which is much higher than the maximum strain of 2.5% as measured in the tests during this investigation. To obtain a consistent order of accuracy the following rule of approximation will be adopted:

> In those terms which do not include b_{ij}, the first and 2nd powers of B_{11}, B_{22} and B_{33} will be retained. In coefficients of b_{ij} only the first powers of B_{11}, B_{22} and B_{33} will be retained. No terms involving b_{ij} to a higher power than the first will be retained.

The total strain η is given by:[47]

$$\eta = \frac{1}{2} [J^* J - E_3] \tag{3.24}$$

where:

J^* = transpose of J

The elements of this strain are developed in Appendix 1 using the approximation rule above. They are:

$$\eta_1 = b_{11} + B_{11} + 2b_{11}\, B_{11} + \frac{B_{11}^2}{2}$$

$$\eta_2 = b_{22} + B_{22} + 2b_{22}\, B_{22} + \frac{B_{22}^2}{2}$$

$$\eta_3 = b_{33} + B_{33} + 2b_{33}\, B_{33} + \frac{B_{33}^2}{2}$$

$$\eta_4 = \frac{b_{23} + b_{32}}{2} \quad (1 + B_{22} + B_{33}) \qquad (3.25)$$

$$\eta_5 = \frac{b_{13} + b_{31}}{2} \quad (1 + B_{11} + B_{33})$$

$$\eta_6 = \frac{b_{12} + b_{21}}{2} \quad (1 + B_{11} + B_{22})$$

where:

$$\eta_1 = \eta_{11} \;, \qquad \eta_2 = \eta_{22} \;, \qquad \eta_3 = \eta_{33}$$

$$\eta_4 = \eta_{23} = \eta_{32}$$

$$\eta_5 = \eta_{13} = \eta_{31}$$

$$\eta_6 = \eta_{12} = \eta_{21}$$

$$\text{or } [\eta] = \begin{bmatrix} \eta_1 & \eta_6 & \eta_5 \\ \eta_6 & \eta_2 & \eta_4 \\ \eta_5 & \eta_4 & \eta_3 \end{bmatrix}$$

3.2.2. The Strain Energy and the Relation Between Stress and Strain

Since the total strain η is considered to be finite, the strain energy can be represented by Eq. (3.10):

$$\Phi = \frac{1}{2} C_{ij}\, \eta_i\, \eta_j + C_{ijr}\, \eta_i\, \eta_j\, \eta_r + \text{higher order terms}$$

where:

Φ = strain energy per unit volume in A^{o} state.

All higher order terms in the expression of Φ will be omitted throughout the development. For an isotropic material, Φ can be expressed more conveniently as a function of the strain invariants as follows:[47]

$$\Phi = \frac{\lambda + 2\mu}{2} I_1^2 - 2\mu I_2 + \frac{\ell + 2m}{3} I_1^3 - 2m I_1 I_2 + n I_3 \tag{3.26}$$

where:

I_1, I_2, I_3 are first, second and third invarients of strain as given below

λ, μ = Lamé's constants

ℓ, m, n = Third-order elastic constants or Murnaghan constants.

$$I_1 = \eta_1 + \eta_2 + \eta_3 \tag{3.27}$$

$$I_2 = \det \begin{bmatrix} \eta_2 & \eta_4 \\ \eta_4 & \eta_3 \end{bmatrix} + \det \begin{bmatrix} \eta_3 & \eta_5 \\ \eta_5 & \eta_1 \end{bmatrix} + \det \begin{bmatrix} \eta_1 & \eta_5 \\ \eta_6 & \eta_2 \end{bmatrix}$$

$$= \eta_2 \eta_3 - \eta_4^2 + \eta_3 \eta_1 - \eta_5^2 + \eta_1 \eta_2 - \eta_6^2 \tag{3.28}$$

$$I_3 = \det \begin{bmatrix} \eta \end{bmatrix} \tag{3.29}$$

where:

det means determinant of the matrix.

The total stress σ in the A state is related to the total strain η by the formula:[47]

$$\sigma = \frac{\rho}{\rho_o} \; J \frac{\partial \phi}{\partial \eta} \; J^* \tag{3.30}$$

where:

ρ = density in A state

ρ_o = density in A^o state

$\frac{\rho}{\rho_o} \approx (1 - I_1)$

In this equation $\frac{\partial \phi}{\partial \eta}$ is a symmetric 3 x 3 matrix. The elements of this matrix can be developed using the following basic formulas from Murnaghan:[47]

$$\frac{\partial I_1}{\partial \eta} = E_3$$

$$\frac{\partial I_2}{\partial \eta} = I_1 \; E_3 - \eta \tag{3.31}$$

$$\frac{\partial I_3}{\partial \eta} = \text{cof } \eta$$

where:

cof η means cofactor of the matrix η.

Each of the $\frac{\partial I_1}{\partial \eta}$, $\frac{\partial I_2}{\partial \eta}$ and $\frac{\partial I_3}{\partial \eta}$ is a 3 x 3 symmetric matrix. Combining (3.31) and (3.26) leads to

$$\frac{\partial \phi}{\partial \eta} = \lambda \; I_1 \; E_3 + 2\mu \; \eta \; + (\ell I_1^{\,2} - 2mI_2) \; E_3 + 2mI_1 \; \eta + n \text{ cof } \eta \tag{3.32}$$

The elements of $\frac{\partial \phi}{\partial \eta}$ are developed in terms of λ, μ, ℓ, m, n, b_{ij} and B_{ij} in Appendix 2, Eqs. (A 19,20).

The stress matrix σ is then obtained from Eq. (3.30). The procedure for obtaining the stresses is outlined in Appendix 3. The results are:

$$\sigma_1 = \sigma_{11} \left[\lambda \left(B + \frac{3}{2} B_{11}^2 - \frac{B_{22}^2}{2} - \frac{B_{33}^2}{2} - 2B_{22} B_{33}\right)\right.$$

$$+ 2\mu \left(B_{11} + \frac{3}{2} B_{11}^2 - B_{11} B_{22} - B_{11} B_{33}\right)$$

$$\left. + \ell B^2 + 2m(B_{11}^2 - B_{22} B_{33}) + n(B_{22} B_{33})\right]$$

$$+ b_{11} \left[\lambda (1 + 4 B_{11}) + 2\mu (1+4 B_{11} - B_{22} - B_{33})\right.$$

$$\left. + 2\ell B + 4mB_{11}\right] \qquad (3.34)$$

$$+ b_{22} \left[\lambda(1-2 B_{33}) + 2\mu (-B_{11}) + 2\ell B + m(-2B_{33})\right.$$

$$\left. + nB_{33}\right]$$

$$+ b_{33} \left[\lambda(1-2 B_{22}) + 2\mu (-B_{11}) + 2\ell B + m (-2B_{22})\right.$$

$$\left. + nB_{22}\right]$$

where:

$$B = B_{11} + B_{22} + B_{33}$$

$\sigma_{22} = \sigma_2$ and $\sigma_{33} = \sigma_3$ are written from (3.34) by cyclic permulation of the numbers 1, 2 and 3.

$$\sigma_4 = \sigma_{23} = \sigma_{32} = \frac{b_{23} + b_{32}}{2} \left[2\mu (1+B_{22} + B_{33} - B_{11}) + (2m+2\lambda) B\right.$$

$$\left. - nB_{11}\right] + 2\mu (b_{32}B_{22}+b_{23}B_{33}) \qquad (3.35)$$

σ_4 and σ_5 are obtained from (3.35) by cyclic permutation of of the numbers 1, 2 and 3.

3.2.3. Hydrostatic Pressure

In this case $B_{11} = B_{22} = B_{33} = -\alpha$

$$\sigma_{11}^{o} = \sigma_{22}^{o} = \sigma_{33}^{o} = -P$$

The stresses of Eqs. (3.34) and (3.35) become:

$$\begin{aligned}
\sigma_1 &= [-\alpha\,(3\lambda + 2\mu) - \alpha^2\,(\tfrac{3}{2}\lambda + \mu - 9\ell - n)] \\
&\quad + b_{11}\,[\lambda + 2\mu - \alpha\,(4\lambda + 4\mu + 6\ell + 4m)] \\
&\quad + (b_{22} + b_{33})\,[\lambda + \alpha\,(2\lambda + 2\mu - 6\ell + 2m - n)] \\
\sigma_2 &= [-\alpha\,(3\lambda + 2\mu) - \alpha^2\,(\tfrac{3}{2}\lambda + \mu - 9\ell - n)] \\
&\quad + b_{22}\,[\lambda + 2\mu - \alpha\,(4\lambda + 4\mu + 6\ell + 4m)] \\
&\quad + (b_{33} + b_{11})\,[\lambda + \alpha\,(2\lambda + 2\mu - 6\ell + 2m - n)] \\
\sigma_3 &= [-\alpha\,(3\lambda + 2\mu) - \alpha^2\,(\tfrac{3}{2}\lambda + \mu - 9\ell - n)] \\
&\quad + b_{33}\,[\lambda + 2\mu - \alpha\,(4\lambda + 4\mu + 6\ell + 4m)] \qquad (3.36) \\
&\quad + (b_{11} + b_{22})\,[\lambda + \alpha\,(2\lambda + 2\mu - 6\ell + 2m - n)] \\
\sigma_4 &= \sigma_{23} = \sigma_{32} = \frac{b_{23} + b_{32}}{2}\,[2\mu - \alpha\,(6\lambda + 6\mu + 6m - n)] \\
\sigma_5 &= \sigma_{13} = \sigma_{31} = \frac{b_{13} + b_{31}}{2}\,[2\mu - \alpha\,(6\lambda + 6\mu + 6m - n)] \\
\sigma_6 &= \sigma_{12} = \sigma_{21} = \frac{b_{12} + b_{21}}{2}\,[2\mu - \alpha\,(6\lambda + 6\mu + 6m - n)]
\end{aligned}$$

or:

$$\begin{bmatrix}\sigma_1\\ \sigma_2\\ \sigma_3\\ \sigma_4\\ \sigma_5\\ \sigma_6\end{bmatrix} = \begin{bmatrix}-P\\ -P\\ -P\\ 0\\ 0\\ 0\end{bmatrix} + \begin{bmatrix}\lambda'+2\mu' & \lambda' & \lambda' & 0 & 0 & 0\\ \lambda' & \lambda'+2\mu' & \lambda' & 0 & 0 & 0\\ \lambda' & \lambda' & \lambda'+2\mu' & 0 & 0 & 0\\ 0 & 0 & 0 & \mu' & 0 & 0\\ 0 & 0 & 0 & 0 & \mu' & 0\\ 0 & 0 & 0 & 0 & 0 & \mu'\end{bmatrix}\begin{bmatrix}b_{11}\\ b_{22}\\ b_{33}\\ b_{23}+b_{32}\\ b_{13}+b_{31}\\ b_{12}+b_{21}\end{bmatrix} \qquad (3.37)$$

where:

$$-P = -\alpha(3\lambda+2\mu) - \alpha^2\left(\frac{3}{2}\lambda+\mu-9\ell-n\right)$$

$$\mu' = \mu - \alpha\left(3\lambda+3\mu+3m-\frac{n}{2}\right) \qquad (3.38)$$

$$\lambda' = \lambda+\alpha(2\lambda+2\mu-6\ell+2m-n)$$

$$\lambda'+2\mu' = \lambda+2\mu-\alpha(4\lambda+4\mu+6\ell+4m)$$

where:

λ' and μ' are the effective elastic constants for the state A'.

The stresses σ_1 to σ_6 are the stresses in the A state in the x, y, z directions; therefore they satisfy the equation of motion

$$\frac{\partial\sigma_{ij}}{x_j} + \rho X_i = \rho\frac{\partial^2 u_i}{\partial t^2} \qquad (3.39)$$

where:

σ_{ij} = total stress in A state

X_i = body force.

If the body forces X_i are neglected, the x component of the equation of motion becomes:

$$\frac{\partial \sigma_{xx}}{\partial x} + \frac{\partial \sigma_{xy}}{\partial y} + \frac{\partial \sigma_{xz}}{\partial z} = \rho \frac{\partial^2 u}{\partial t^2} \tag{3.40}$$

This equation can be transformed to the independent coordinates x_i' of the stressed state A' by the chain rule. For example, the first term $\frac{\partial \sigma_{xx}}{\partial x}$ becomes:

$$\frac{\partial \sigma_{xx}}{\partial x} = \frac{\partial \sigma_{xx}}{\partial x'} \frac{\partial x'}{\partial x} + \frac{\partial \sigma_{xx}}{\partial y'} \frac{\partial y'}{\partial x} + \frac{\partial \sigma_{xx}}{\partial z'} \frac{\partial z'}{\partial x} \tag{3.41}$$

The partial derivatives of x', y', z' with respect to x,y,z are given by the Jacobian transformations of the type:[49]

$$\frac{\partial x'}{\partial x_i} = \frac{\det \frac{\partial (f, g, h)}{\partial (x_i, y', z')}}{D}$$

where:

$$f = -x + x' + u$$

$$g = -y + y' + v$$

$$h = -z + z' + w$$

$$D = \det J_2$$

$$\frac{\partial x'}{\partial x} = -\frac{\det \frac{\partial (f, g, h)}{\partial (x, y', x')}}{D} = -\frac{\det \begin{bmatrix} -1 & \frac{\partial u}{\partial y'} & \frac{\partial u}{\partial z'} \\ 0 & 1 + \frac{\partial v}{\partial y'} & \frac{\partial v}{\partial z'} \\ 0 & \frac{\partial w}{\partial y'} & 1 + \frac{\partial w}{\partial z'} \end{bmatrix}}{D}$$

$$= \frac{1 + \frac{\partial v}{\partial y'} + \frac{\partial w}{\partial z'} + \frac{\partial v}{\partial y'} \frac{\partial w}{\partial z'} - \frac{\partial v}{\partial z'} \frac{\partial w}{\partial y'}}{D}$$

$$= \frac{1 + b_{22} + b_{33} + b_{22}\, b_{33} - b_{23}\, b_{32}}{D}$$

Neglecting products of the b_{ij} in the numerator yields:

$$\frac{\partial x'}{\partial x} = \frac{1 + b_{22} + b_{33}}{D}$$

Similarly,

$$\frac{\partial y'}{\partial x} = - \frac{\det \frac{\partial (f, g, h)}{\partial (x', x, z')}}{D} = - \frac{b_{21}}{D}$$

$$\frac{\partial z'}{\partial x} = - \frac{\det \frac{\partial (f, g, h)}{\partial (x', y', x)}}{D} = - \frac{b_{31}}{D}$$

Thus

$$\frac{\partial \sigma_{xx}}{\partial x} = \frac{\partial \sigma_{xx}}{\partial x'} \left(\frac{1+b_{22}+b_{33}}{D}\right) + \frac{\partial \sigma_{xx}}{\partial y'} \left(- \frac{b_{21}}{D}\right) + \frac{\partial \sigma_{xx}}{\partial z'} \left(- \frac{b_{31}}{D}\right)$$

$\frac{\partial \sigma_{xy}}{\partial y}$ and $\frac{\partial \sigma_{xz}}{\partial z}$ of Eq. (3.40) can be transformed by similar procedure. With the above transformations and the additional relation[47]

$$\rho = \frac{\rho'}{D}$$

Eq. (3.40) becomes:

$$\frac{\partial \sigma_{xx}}{\partial x'} \left(\frac{1+b_{22}+b_{33}}{D}\right) + \frac{\partial \sigma_{xx}}{\partial y'} \left(- \frac{b_{21}}{D}\right) + \frac{\partial \sigma_{xx}}{\partial z'} \left(- \frac{b_{31}}{D}\right)$$

$$+ \frac{\partial \sigma_{xy}}{\partial x'} \left(- \frac{b_{21}}{D}\right) + \frac{\partial \sigma_{xy}}{\partial y'} \left(\frac{1+b_{11}+b_{33}}{D}\right) + \frac{\partial \sigma_{xy}}{\partial z'} \left(- \frac{b_{32}}{D}\right)$$

$$+ \frac{\partial \sigma_{xz}}{\partial x'} \left(- \frac{b_{13}}{D}\right) + \frac{\partial \sigma_{xz}}{\partial y'} \left(- \frac{b_{23}}{D}\right) + \frac{\partial \sigma_{xz}}{\partial x'} \left(\frac{1+b_{11}+b_{22}}{D}\right)$$

$$= \frac{\rho'}{D} \frac{\partial^2 u}{\partial t^2} \qquad (3.42)$$

σ_{xx}, σ_{xy}, σ_{xz} are given by Eq. (3.37). They can be written as follows:

$$\sigma_{xx} = \sigma_{11} = -P + S_{xx}$$

$$\sigma_{xy} = \sigma_{6} = \sigma_{12} = \sigma_{21} = S_{xy} \tag{3.43}$$

$$\sigma_{xz} = \sigma_{5} = \sigma_{13} = \sigma_{31} = S_{xz}$$

where:

$-P$ = hydrostatic pressure = σ^{o}_{xx}

S_{ij} = additional stresses which are related to the infinitesimal strains ϵ_{ij} by the effective elastic constants λ', μ'.

With the above notation Eq. (3.42) becomes:

$$\frac{\partial S_{xx}}{\partial x'} + \frac{\partial S_{xy}}{\partial y'} + \frac{\partial S_{xz}}{\partial z'} = \rho' \frac{\partial^2 u}{\partial t^2} \tag{3.44}$$

Eq. (3.44) was derived using $\frac{\partial P}{\partial x'} = 0$, since P is homogeneous and neglecting the higher order terms $\frac{\partial S_{ij}}{\partial x'_i}$ (b_{ij}).

By similar procedure, the equations of motion for the y and z directions can be transferred to the x'_i coordinates, and Eq. (3.39) becomes:

$$\frac{\partial S_{ij}}{\partial x'_i} = \rho' \frac{\partial^2 u_i}{\partial t^2} \tag{3.45}$$

This equation is similar to the classical equation (2.12) from which the velocities V_L and V_s were derived. Thus, hydrostatic pressure does not produce any change

in the laws of propagation and the velocities are given by:

$$\text{Longitudinal velocity} = V_L = \sqrt{\frac{\lambda' + 2\mu'}{\rho'}}$$

$$\text{Shear velocity} = V_s = \sqrt{\frac{\mu'}{\rho'}}$$

Substituting for λ', μ' from Eq. (3.38) yields:

$$V_L = \sqrt{\frac{\lambda + 2\mu - \alpha\ (4\lambda + 4\mu + 6\ell + 4m)}{\rho'}} \tag{3.46}$$

$$V_s = \sqrt{\frac{\mu - \alpha\ (3\lambda + 3\mu + 3m - \frac{n}{2})}{\rho'}} \tag{3.47}$$

3.2.4. Uniform Triaxial Stress with Uniaxial Strain

In this case,

$$\begin{aligned} B_{11} &= B_{22} = 0 \\ B_{33} &= -e \\ \sigma^o_{33} &= -\sigma_z \\ \sigma^o_{11} &= \sigma^o_{22} = -\sigma_L \end{aligned} \tag{3.48}$$

The stresses of Eqs. (3.34) and (3.35) become:

$$\sigma_{11} = [-e\lambda - e^2 (\frac{\lambda}{2} - \ell)] + b_{11} [\lambda + 2\mu + 2\ell)]$$

$$+ b_{22} [\lambda + e (2\lambda - 2\ell + 2m - n)] + b_{33} [\lambda - 2\ell e]$$

$$\sigma_{22} = [-e\lambda - e^2 (\frac{\lambda}{2} - \ell)] + b_{22} [\lambda + 2\mu + e (2\mu - 2\ell)]$$

$$+ b_{11} [\lambda + e (2\lambda - 2\ell + 2m - n)] + b_{33} [\lambda - 2\ell e]$$

$$\sigma_{33} = [-e (\lambda + 2\mu) + e^2 (\frac{3}{2} \lambda + 3\mu + \ell + 2m)]$$

$$+ (b_{11} + b_{22}) [\lambda + e (2\mu - 2\ell)] \qquad (3.49)$$

$$+ b_{33} [\lambda + 2\mu - e (4\lambda + 8\mu + 2\ell + 4m)]$$

$$\sigma_4 = \frac{b_{23} + b_{32}}{2} [2\mu - e (2\lambda + 2\mu + 2m)] - 2 b_{23} \mu e$$

$$\sigma_5 = \frac{b_{13} + b_{31}}{2} [2\mu - e (2\lambda + 2\mu + 2m)] - 2 b_{13} \mu e$$

$$\sigma_6 = \frac{b_{12} + b_{21}}{2} [2\mu - e (2\lambda - 2\mu + 2m - n)]$$

or,

$$\sigma_1 = - \sigma_L + C'_{11} b_{11} + C'_{12} b_{22} + C'_{13} b_{33}$$

$$\sigma_2 = - \sigma_L + C'_{12} b_{11} + C'_{11} b_{22} + C'_{13} b_{33}$$

$$\sigma_3 = - \sigma_z + C'_{31} b_{11} + C'_{31} b_{22} + C'_{33} b_{33} \qquad (3.50)$$

$$\sigma_4 = C'_{44} b_{23} + C'_{55} b_{32}$$

$$\sigma_5 = C'_{44} b_{13} + C'_{55} b_{31}$$

$$\sigma_6 = \frac{1}{2} (C'_{11} - C'_{12}) (b_{12} + b_{21})$$

where the C'_{ij} are the effective elastic constants.

$$C'_{11} = \lambda + 2\mu + e\,(2\mu - 2\ell)$$

$$C'_{12} = \lambda + e\,(2\lambda - 2\ell + 2m-n)$$

$$C'_{13} = \lambda - 2\ell e$$

$$C'_{31} = \lambda + e\,(2\mu - 2\ell)$$

$$C'_{33} = \lambda + 2\mu - e\,(4\lambda + 8\mu + 2\ell + 4m) \qquad (3.51)$$

$$C'_{44} = \mu - e\,(\lambda + 3\mu + m)$$

$$C'_{55} = \mu - e\,(\lambda + \mu + m)$$

$$\frac{1}{2}\,(C'_{11}-C'_{12}) = \mu - e\,(\lambda - \mu + m-\frac{n}{2})$$

The initial stresses σ_L and σ_z are given by

$$-\sigma_L = -e\lambda - e^2\,(\frac{\lambda}{2} - \ell)$$

$$(3.52)$$

$$-\sigma_z = -e(\lambda + 2\mu) + e^2\,(\frac{3}{2}\,\lambda + 3\mu + \ell + 2m)$$

Thus the stresses S_{ij} are related to the infinitesimal strains b_{ij} by:

$$S_1 = S_{xx} = C'_{11}\,b_{11} + C'_{12}\,b_{22} + C'_{13}\,b_{33}$$

$$S_2 = S_{yy} = C'_{12}\,b_{11} + C'_{11}\,b_{22} + C'_{13}\,b_{33}$$

$$S_3 = S_{zz} = C'_{31}\,(b_{11} + b_{22}) + C'_{33}\,b_{33} \qquad (3.53)$$

$$S_4 = S_{yz} = S_{zy} = C'_{44}\,b_{23} + C'_{55}\,b_{32}$$

$$S_5 = S_{xz} = S_{zx} = C'_{44}\,b_{13} + C'_{55}\,b_{31}$$

$$S_6 = S_{xy} = S_{yx} = \frac{1}{2}\,(C'_{11} - C'_{12})(b_{12} + b_{21})$$

These are the stress-strain relationships for the material in the A' state. It is interesting to note the differences between these equations and the equations which are derived from the classical theory for an unstressed body which has the same symmetry as A'.

In the classical theory, an unstressed body which has the same symmetry as A', i.e., symmetric about the z axis, would have only five independent elastic constants.[40] The stress-strain relationships are given by:

$$\begin{bmatrix} S_1 \\ S_2 \\ S_3 \\ S_4 \\ S_5 \\ S_6 \end{bmatrix} = \begin{bmatrix} d_{11} & d_{12} & d_{13} & 0 & 0 & 0 \\ d_{12} & d_{11} & d_{13} & 0 & 0 & 0 \\ d_{13} & d_{13} & d_{33} & 0 & 0 & 0 \\ 0 & 0 & 0 & d_{44} & 0 & 0 \\ 0 & 0 & 0 & 0 & d_{44} & 0 \\ 0 & 0 & 0 & 0 & 0 & \frac{1}{2}(d_{11} - d_{12}) \end{bmatrix} \begin{bmatrix} b_{11} \\ b_{22} \\ b_{33} \\ b_{23}+b_{32} \\ b_{13}+b_{31} \\ b_{12}+b_{21} \end{bmatrix} \tag{3.54}$$

Thus, in the classical theory the elastic constant matrix is symmetric while in (3.53) $C'_{13} \neq C'_{31}$. Furthermore, in the classical theory $d_{44} = d_{55}$ and the shear stresses S_4 and S_5 are related to twice the strains $(b_{23}+b_{32})$ and $(b_{13}+b_{31})$ by d_{44}; whereas in (3.53) $C'_{44} \neq C'_{55}$ and the shear stresses S_4 and S_5 are related to the deformation gradients b_{23}, b_{32}, b_{13} and b_{31} by C'_{44} and C'_{55}.

These differences are due to the presence of initial stresses in A'. Similar relations to Eq. (3.53)

were obtained by Green[24] and Biot.[9] Both of them also obtained the following relations between the effective elastic constants:

$$C'_{31} - C'_{13} = C'_{55} - C'_{44} = \sigma_z - \sigma_L \tag{3.54}$$

These relations can be obtained from Eqs. (3.51) and (3.52) by approximating σ_z and σ_L to the first powers of e.

The equations of motion for the state A are:

$$\frac{\partial \sigma_{ij}}{\partial x_j} + \rho X_i = \rho \frac{\partial^2 u_i}{\partial t^2}$$

This is the same as Eq. (3.39) and it can be transformed to the independent coordinate of body A' by the same procedure leading to Eq. (3.45). When the body forces are neglected the equations of motion become:

$$\frac{\partial S_{xx}}{\partial x'} + \frac{\partial S_{xy}}{\partial y'} + \frac{\partial S_{xz}}{\partial z'} = \rho' \frac{\partial^2 u}{\partial t^2} \tag{3.55a}$$

$$\frac{\partial S_{yx}}{\partial x'} = \frac{\partial S_{yy}}{\partial y'} + \frac{\partial S_{yz}}{\partial z'} = \rho' \frac{\partial^2 v}{\partial t^2} \tag{3.55b}$$

$$\frac{\partial S_{zx}}{\partial x'} = \frac{\partial S_{zy}}{\partial y'} + \frac{\partial S_{zz}}{\partial z'} = \rho' \frac{\partial^2 w}{\partial t^2} \tag{3.55c}$$

where:

S_{ij} are the stresses given in Eq. (3.53)

u, v, w are particle displacements

For a plane longitudinal wave propagating in the z direction, the particle motion can be described as:

$$w = f\,(V_{Lzz}\cdot t - z')$$

$$u = v = 0$$

The velocity V_{Lzz} can be found from Eq. (3.55c)

$$\frac{\partial S_{zx}}{\partial x'} + \frac{\partial S_{zy}}{\partial y'} + \frac{\partial S_{zz}}{\partial z'} = \rho' \frac{\partial^2 w}{\partial t^2} \tag{3.66}$$

Substituting for the stresses from (3.53) and noting that $b_{ij} = \frac{\partial u_i}{\partial x'_j}$ yields:

$$S_{zx} = C'_{44} b_{13} + C'_{55} b_{31}$$

$$= C'_{44} \frac{\partial u}{\partial z'} + C'_{55} \frac{\partial w}{\partial x'}$$

$$S_{zy} = C'_{44} \frac{\partial v}{\partial x'} + C'_{55} \frac{\partial w}{\partial y'}$$

$$S_{zz} = C'_{31} \left(\frac{\partial u}{\partial x'} + \frac{\partial v}{\partial y'}\right) + C'_{33} \frac{\partial w}{\partial z'}$$

and

$$\frac{\partial S_{zx}}{\partial x'} = 0 \qquad \frac{\partial S_{zy}}{\partial y'} = 0 \qquad \frac{\partial S_{zz}}{\partial z'} = C_{33} \frac{\partial^2 w}{\partial z'^2}$$

Thus, (3.66) reduces to

$$C'_{33} \frac{\partial^2 w}{\partial z'^2} = \rho' \frac{\partial^2 w}{\partial t^2} \tag{3.67}$$

This is a wave equation and the velocity is given by

$$V_{Lzz} = \sqrt{\frac{C'_{33}}{\rho'}} = \sqrt{\frac{\lambda + 2\mu - e\,(4\lambda + 8\mu + 2\ell + 4m)}{\rho'}} \tag{3.68}$$

By similar procedure the velocities of plane longitudinal waves in the x and y directions are:

$$V_{Lxx} = V_{Lyy} = \sqrt{\frac{C'_{11}}{\rho'}} = \sqrt{\frac{\lambda + 2\mu + e\,(2\mu - 2\ell)}{\rho'}} \tag{3.69}$$

For a plane shear wave propagating in the z direction with a particle motion (u) in the x direction, the particle motion can be described as:

$$u = f\ (V_{sxz}\ t - z)$$
$$v = w = 0 \tag{3.70}$$

The wave velocity V_{sxz} can be obtained from (3.55a).

$$\frac{\partial S_{xx}}{\partial x'} + \frac{\partial S_{xy}}{\partial y'} + \frac{\partial S_{xz}}{\partial z'} = \rho' \frac{\partial^2 u}{\partial t^2} \tag{3.71}$$

$$S_{xx} = C'_{11} \frac{\partial u}{\partial x} + C'_{12} \frac{\partial v}{\partial y} + C'_{13} \frac{\partial w}{\partial x'}$$

$$\frac{\partial S_{xx}}{\partial x'} = 0$$

$$S_{xy} = \frac{1}{2} (C'_{11} - C'_{12}) \left(\frac{\partial u}{\partial y'} + \frac{\partial v}{\partial x'}\right)$$

$$\frac{\partial S_{xy}}{\partial y'} = 0$$

$$S_{xz} = C'_{44} \frac{\partial u}{\partial z'} + C'_{55} \frac{\partial w}{\partial x'}$$

$$\frac{\partial S_{xz}}{\partial z'} = C'_{44} \frac{\partial^2 u}{\partial z'^2}$$

Thus, (3.71) reduces to the wave equation:

$$C'_{44} \frac{\partial^2 u}{\partial z'^2} = \rho' \frac{\partial^2 u}{\partial t^2}$$

and

$$V_{sxz} = \sqrt{\frac{C_{44}}{\rho'}} = \sqrt{\frac{\mu - e\ (\lambda + 3\mu + m)}{\rho'}} \tag{3.72}$$

By similar procedure, the wave velocity of a plane wave propagating in z direction with a single particle motion (v) in y direction is given by V_{syz}.

$$V_{syz} = V_{sxz} \tag{3.73}$$

Similarly,

$$V_{sxy} = V_{syx} = \sqrt{\frac{\frac{1}{2}(C'_{11} - C'_{12})}{\rho'}} = \sqrt{\frac{\mu - e(\lambda - \mu + m - \frac{n}{2})}{\rho'}} \tag{3.74}$$

$$V_{szx} = V_{szy} = \sqrt{\frac{C'_{55}}{\rho'}} = \sqrt{\frac{\mu - e(\lambda + \mu + m)}{\rho'}} \tag{3.75}$$

IV. EXPERIMENTAL INVESTIGATION

The experimental investigation may be divided into two major parts; preliminary and major investigations.

In the preliminary investigation, the changes in ultrasonic attenuation and velocity of longitudinal waves were measured in steel and rock salt specimens subjected to uniaxial compressive stress. Measurements made in a direction parallel to the applied load will be designated as "axial" measurements. Measurements made in a direction perpendicular to the applied load will be called "lateral" measurements.

In the major investigation the following four velocities were measured:

$$V_{Lh} = \sqrt{\frac{\lambda' + 2\mu'}{\rho_h}} = \sqrt{\frac{\lambda + 2\mu - \alpha(4\lambda + 4\mu + 6\ell + 4m}{\rho_h}} \tag{4.1}$$

$$V_{sh} = \sqrt{\frac{\mu'}{\rho_h}} = \sqrt{\frac{\mu - \alpha\ (3\lambda + 3\mu + 3m - \frac{n}{2})}{\rho_h}} \tag{4.2}$$

$$V_{Lt} = \sqrt{\frac{\lambda + 2\mu - e\ (4\lambda + 8\mu + 2\ell + 4m)}{\rho_t}} \tag{4.3}$$

$$V_{st} = \sqrt{\frac{\mu - e\ (\lambda + 3\mu + m)}{\rho_t}} \tag{4.4}$$

where:

The first subscript of V indicates type of wave; L for longitudinal and s for shear, and the 2nd subscript of V indicates stress condition; h for hydrostatic pressure, t for triaxial stress with uniaxial strain in z direction.

$V_{Lt} = V_{Lzz}$ of Eq. (3.68), i.e., longitudinal velocity in z direction.

$V_{st} = V_{sxz} = V_{syz}$ of Eqs. (3.72) and (3.73), i.e., shear wave velocities in z direction.

λ, μ = Lamé's constants for unstressed rock salt.

ρ_t, ρ_h = density at a certain stress level.

α = measured linear hydrostatic strain.

e = measured strain in the triaxial test.

4.1. Objectives

The main objective of the tests on steel was to gain experience in ultrasonic systems. The main objective of the preliminary investigation of rock salt was to determine if changes in wave velocity and attenuation could be used to detect anisotropy due to compression or predict yield before it occurs. The main objectives of the major investigations were:

1. To determine the third-order elastic constants, ℓ, m and n of rock salt.

2. To investigate the feasibility of using ultrasonic pulse methods to determine the initial stresses (hydrostatic pressure or triaxial stress with uniaxial strain cases only) from wave velocities as predicted by the equations above.
3. To determine if the velocity measurements would detect the transition from elastic to plastic states of stress in the triaxial test.

4.2. Apparatus

The principal components of the apparatus may be divided into six major groups; specimens, loading systems, strain equipment, electronic equipment, transducers and optical equipment.

Specimens

Rock salt: The rock salt used in all the tests was mined from the International Salt Company mine in Avery Island, Louisiana. Large specimens, about one foot cubes or larger, were cut from the mine floor without the use of explosives. These specimens were cut in the laboratory to the desired dimensions for each test. The rock salt was compact, white in color and 99.9% pure NaCl. The macroscopic grain size of the crystals ranged from 0.4 to 1.2 cm.

Steel: Hot rolled, mild steel "C1018" columns. The ends and two sides were polished to final dimensions of 1.97 x 1.98 x 6 inches.

Loading Systems

Loading machines: An Olson loading machine, with a loading capacity of 300,000 lbs was used in the uniaxial stress tests (Fig. 4.6). A Forney, Jobsite Press tester model FT-20, was used in the triaxial tests. This tester is designed for testing specimens in compression. It has a manually operated pump and an accuracy of 500 lbs (Fig. 4.23).

Thick walled steel cylinder: A thick-walled stainless steel cylinder, 3.25 inches long with inside and outside diameters of 3.25 and 4 inches, was used in the triaxial tests (Fig. 4.19). This cylinder provided the lateral stresses by restricting the lateral expansion of the salt.

High-pressure vessel: The pressure vessel used in the hydrostatic test had a capacity of over 10,000 psi. It consisted of an 11 inch long steel cylinder with a 5 inch inside diameter and 7 inch outside diameter, circular end plates and high strength bolts to fasten the plates. Sealing was accomplished by teflon and oil rings placed between the cylinder and the end plates. Insulated wires were threaded through bolts in the top plate to provide electrical connection through the vessel (Fig. 4.13). Leakage was prevented by using Hyso cement to fill the holes in the bolts.

Pressure pump: A Blackhawk model P-85 hand pump was used to develop the oil pressure in the vessel.

Strain Equipment

SR-4 strain gages: Post-yield strain gages, type PA-3, were used in the uniaxial stress tests. Two-element rosette gages, type FABX-50-12, were used on the outer surface of the thick walled cylinder in the triaxial test. Type A-1 gages were used to measure linear strain in salt in the hydrostatic test.

Dial gages: Half-inch displacement Ames dial gages, with an accuracy of 0.0001 inch, were used to measure the strain in the salt.

Strain indicators: A Sanborn Strain Recorder (Fig. 4.6) and Baldwin Strain Indicator (Fig. 4.23) were used in the uniaxial and triaxial compression tests respectively.

Electronic Equipment

Oscilloscopes: Tektronic types 541 and 551 with type D or CA plug-in units.

Pulsers: A Hewlett-Packard type 212A and a Rutherford pulse generator type B7 were used. These pulsers give rectangular 70 volt pulses. The pulse repetition rate and width are adjustable in both pulsers. Both pulsers are equipped with an adjustable delay time between the trigger-in or trigger-out and the main output pulse.

Transducers

One inch diameter barium titanate disks vibrating in thickness mode were used to produce and detect longitudinal waves. The disks used for the uniaxial stress tests were 0.5 inch thick with a fundamental frequency of 180 kcs. The disks used for the triaxial and hydrostatic tests were 0.2 inch thick with a fundamental frequency of 500 kcs.

Barium titanate shear plates were used for shear velocity measurements. The plates were 0.8 x 0.8 x 0.13 inches and had a fundamental frequency of 350 kcs.

The two opposite faces of each transducer were coated with a layer of conductive silver paint or silver epoxy cement. The paint on the face to be attached to the specimen was extended to the edge of the back face. The silver epoxy cement was used to attach thin phonographic wire leads to the transducers.

Optical Equipment

A Dumont Oscillograph Record Camera, type 321A, was used in the uniaxial stress tests (Fig. 4.6). This camera accommodates a 50 foot roll of 35 mm film. The film could be driven at different speeds. A projector equipped with a mirror that reflects the image to a gridded paper was used to analyze the film. Different enlargements were obtained by changing the distance between the mirror and the paper.

A Polaroid Oscillograph Camera was used in the hydrostatic and triaxial tests. The films were analyzed using a two-dimensional measuring microscope which is manufactured by PYE Company of England. This device has an accuracy of $\pm$ 0.01 mm per 20 cm and a magnification of 5 and 25.

4.3. Uniaxial Compressive Stress

Changes of attenuation and velocity of longitudinal waves were measured in two directions; parallel to the applied load (axial tests) and perpendicular to the applied load (lateral tests). The same experimental procedure was used for the rock salt and steel tests. Specimen dimensions and transducers were as follows:

Steel:	1.97 x 1.96 x 6 inch steel columns
Salt:	2.5 and 3.5 inch cubic specimens
Transducers:	180 kcs barium titanate disks placed in a holder.

Experimental Setup

A schematic diagram of the transducer attachment in the axial and lateral tests is shown in Figure 4.1.

In the lateral tests two identical transducers were placed on opposite sides of the specimen and held tightly by rubber bands. High-vacuum Dow-Corning grease was used as a couplant. Figures 4.2 and 4.3 show the transducer attachment for steel and rock salt specimens.

In the axial tests the transducers were cemented, using plybond rubber cement, to one-inch steel disks placed on both ends of the specimen. Hollow thick-walled steel cylinders were placed around the transducers in order to transmit the load without compressing the transducer (Fig. 4.4). The steel disks provided uniform stress distribution in the sample. The interfaces between the steel disks and the specimen were coated with vacuum grease. Figure 4.5 shows the specimen assembly. Figure 4.6 shows the various test components.

A schematic diagram of the electrical circuit is shown in Figure 4.7. The basic principles of this circuit are the same as those of the through transmission test discussed in Section 2.3.2.

Figure 4.8 shows a schematic diagram of two successive pulses as they appear on the scope screen when a low sweep rate is used. The pulse is applied to the transmitting transducer at point A, which is the point at which the sweep starts. Point B represents the instant when the wave reaches the receiving transducer. The output of the receiving transducer, after point B, shows a complicated damped oscillatory motion, D, which disappears before point A' (the instant when the second pulse from the pulser is applied to the transmitter).

The received signal D consists of many wave components that travel with different velocities in addition to waves that are reflected from the sides of the sample.

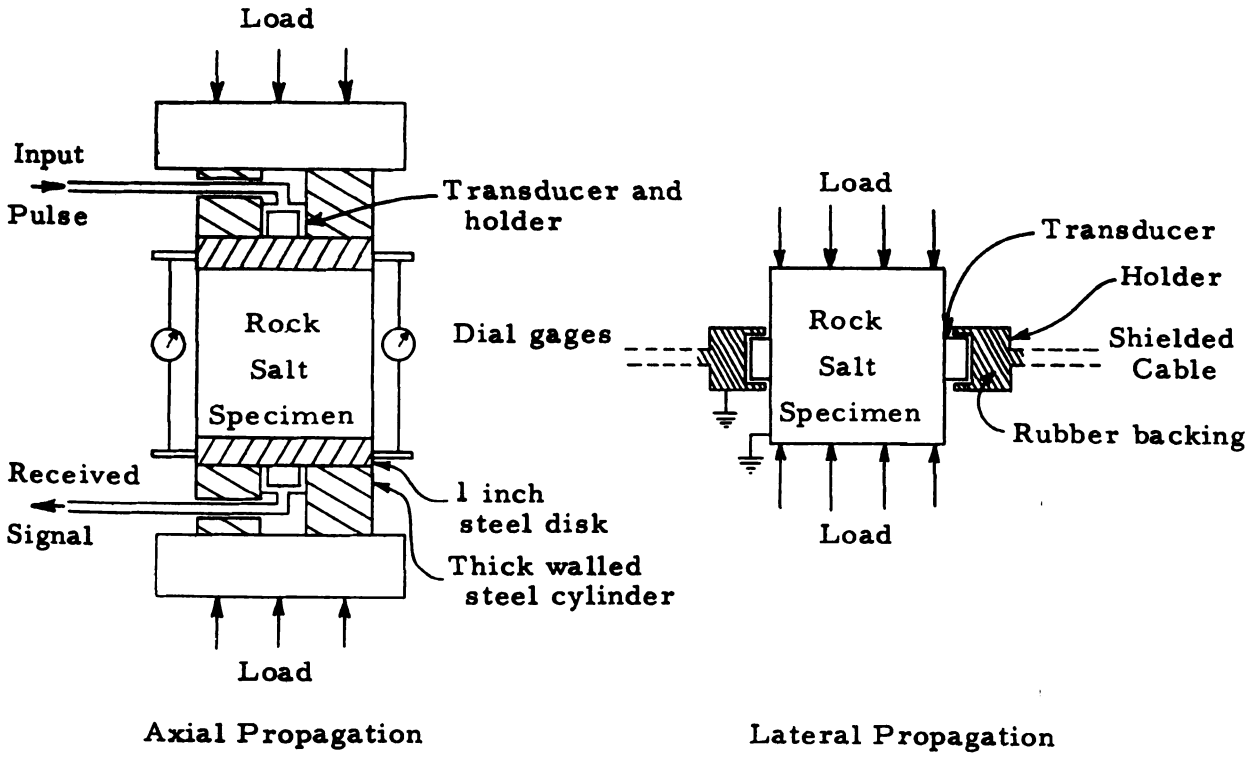

Fig. 4.1 Arrangement of specimen and transducers for the axial and lateral tests.

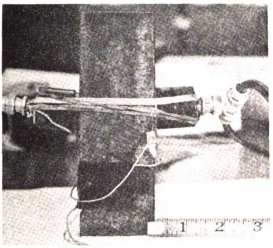

Figure 4. 2. Transducer attachment for lateral propagation in steel.

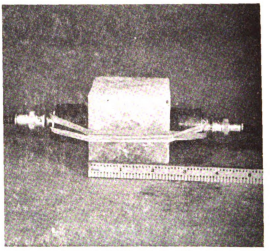

Figure 4. 3. Transducer attachment for lateral propagation in rock salt.

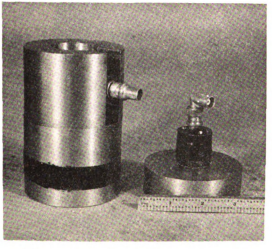

Figure 4. 4. Steel disks and transducers for axial propagation.

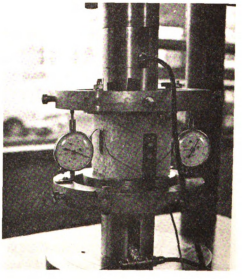

Figure 4. 5. Axial test on rock salt.

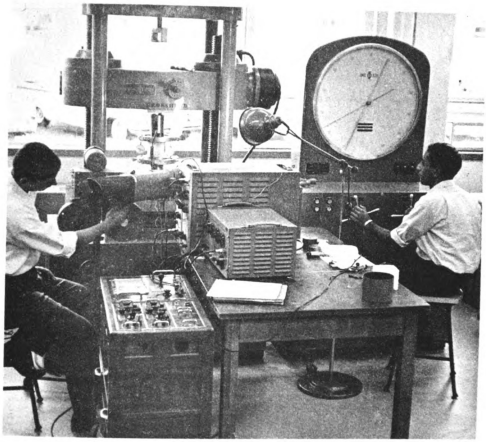

Figure 4.6. Testing machine, oscilloscope, camera, pulser and strain recorder used in uniaxial compression tests.

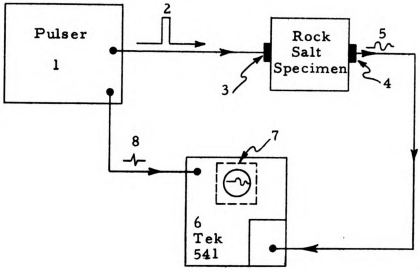

1. Pulse Generator
2. Output pulse: Amplitude 70 volts
3. Driving Barium Titanate transducer: 1 inch dia., $\frac{1}{2}$ inch thick, 180 kc frequency, silver plated on both faces.
4. Receiving transducer; same as the driving transducer
5. Received signal
6. Tektronix type 541 oscilloscope
7. Dumont oscillograph record camera
8. Sweep trigger signal

Fig. 4.7 Block diagram of ultrasonic wave apparatus

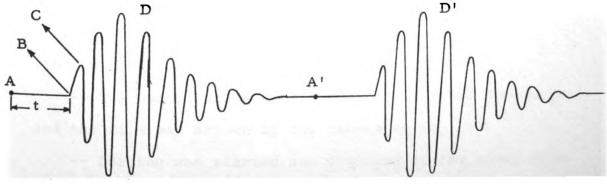

Fig. 4.8 Schematic diagram of two successive pulses as they appear on the oscilloscope screen.

An analysis of the complicated pattern D is quite difficult and for all practical purpcses all measurements of this kind are confined to the measurement of the time, t, which will be the propagation time of the fastest wave between the two transducers. Relative attenuation was determined from the changes in amplitude of the first received signal (C in Figure 4.8).

Procedure

-- Sweep speed and amplifier gain were adjusted to give a trace similar to that of Figure 4.8.

-- Load was raised slowly to 500 lbs.

-- Pictures of the trace were taken with a Polaroid camera to determine the best screen adjustments (illumination, focus, astigmatism and intensity).

-- The Dumont camera was attached to the oscilloscope.

-- The oscilloscope screen scale was illuminated and pictures of the grid were taken.

-- Scale illumination was turned off.

-- The scope intensity was adjusted so that the point of zero time (sweep start) would show as a continuous line on the film (Fig. 4.9).

-- The oscilloscope single sweep switch was turned on and the film was driven by the camera motor.

-- Loading was started and pictures of the trace were taken at different loads by pressing the single sweep buttom of the oscilloscope.

-- The camera timing light served as a record to determine the load at which a picture was taken. When this light is on, it leaves a trace on the left side of the film (Fig. 4.9).

-- Strain and dial gage readings were recorded.

-- Steel was loaded up to 45,000 psi. Yield occurred at about 30,000 psi.

-- Salt was loaded to 4,000 psi which is about 80% of the crushing strength.

Data Reduction

As mentioned in the apparatus, the film was analyzed by projecting the trace on a gridded paper. The grids on this paper were drawn by projecting a picture of the oscilloscope grid.

In the axial test, the wave propagates through the steel disks and the salt. Therefore, it was necessary to measure the changes in propagation time and amplitude of the first arrival in the steel disks alone. The results of this test were combined with the results of the axial test (steel disks and salt) in order to determine the propagation time and amplitude of the first arrival for the salt alone.

Table 4.1 shows typical reduced data for the axial test on steel specimens. Velocity is obtained by dividing the path length by the propagation time. The propagation time was measured from the straight line portion (Fig. 4.9)

Table 4.1. Reduced data for axial measurements in steel specimens.

Axial Stress 1000 PSI	Axial Strain 1000 μ in/in	Axial Dimension L inches	Propagation Time t μ-sec.	Velocity V m/sec	Percent Change in Velocity $\frac{V-V_o}{V_o} = \frac{\Delta V}{V_o}$ %	Amplitude A milivolts	Percent Change in Amplitude $\frac{A-A_o}{A_o} = \frac{\Delta A}{A_o}$ %
0	0	6.0000	25.11	6126	0	27.2	0
5	0.17	5.9989	24.87	6126	0	51.8	94.4
10	0.35	5.9979	24.87	6125	0.02	123.3	355.3
15	0.52	5.9969	24.69	6169	0.69	130.5	380.1
20	0.70	5.9958	24.69	6168	0.68	132.2	386.0
25	0.87	5.9958	24.60	6189	1.03	134.3	393.7
30	1.00	5.9940	24.50	6214	1.46	139.2	411.7
32	---	----	24.42	--	--	138.9	---
35	11.00	5.9341	24.13	6246	1.95	139.6	413.2
37	15.00	5.9103	23.95	6268	2.31	139.1	411.7
40	19.00	5.886	23.72	6303	2.87	139.4	411.7
42	24.00	5.8572	23.58	6309	2.98	139.4	412.4
43	26.00	5.8455	23.58	6296	2.77	139.4	412.0
45	27.50	5.8368	---	--	--	---	---
unload							
37	27.20	5.8385	23.53	6302	2.87	135.9	399.6
31	27.00	5.8397	23.72	6253	2.06	135.4	397.7
25	26.80	5.8408	23.76	6244	1.91	134.6	395.0
20	26.60	5.8420	23.76	6245	1.93	130.2	378.6
12	26.30	5.8438	23.82	6342	1.71	122.7	351.4
6	26.10	5.8449	23.82	6232	1.73	30.2	110.3
0	25.80	5.8467	23.82	6234	1.76	---	---

with an accuracy of 1%. Percent change in velocity was calculated as:

$$\frac{\Delta V}{V}\ \% = \frac{V - V_o}{V_o} \times 100$$

where:

V = velocity at a certain stress

V_o = velocity at zero stress

Relative attenuation was calculated from the changes in the amplitude of the first received signal. For steel specimens, percent change in amplitude was calculated as:

$$\frac{\Delta A}{A_o}\ \% = \frac{A - A_o}{A} \times 100$$

where:

A_o = amplitude in mv at zero load

A = amplitude at any load

For rock salt, relative attenuation was calculated in decibels as follows:

$$db = 20 \log_{10} \frac{A}{A_o}$$

The results are presented in Chapter V.

4.4. Velocities in Unstressed Specimens

The circuit shown in Fig. 4.7 was used to measure the longitudinal and shear wave velocities of different size specimens. Longitudinal and shear wave velocities were measured using different size specimens. The transducers were attached to the specimens by Phenyl Salicylate. This compound was heated to its melting point (40^{o}C) and a few

drops were applied between the transducers and the salt. The bond obtained after cooling was found to be satisfactory for both longitudinal and shear waves.

Care was taken to have the two opposite faces of the specimens parallel to each other and to align the shear transducers so that their particle motions (directions of polarization) were in the same direction.

Figure 4.10 shows typical signals from the longitudinal transducers. The straight line portions of the trace indicate the propagation time in the specimens. Figure 4.11 shows typical signals from the shear transducers. The first small signals on the straight line portion of the trace are early arrivals of some longitudinal components. The arrival of the shear wave is indicated by the first large signal.

Figure 5.4 indicates the propagation time in different length specimens. The longitudinal and shear wave velocities are the slopes of the lines in the figure.

Lamé's constants were calculated as follows:

$$\mu = \rho V_s^2$$

$$\lambda = \rho V_L^2 - 2\mu$$

where:

ρ = average density

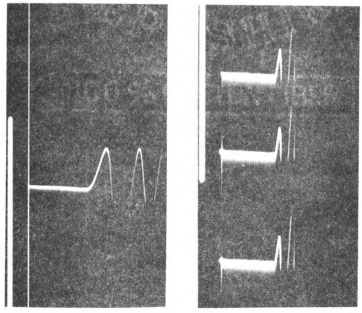

Figure 4.9. Typical traces from the uniaxial compression tests showing the camera timing lights, zero time and signals.

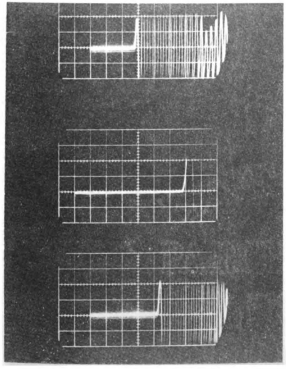

Figure 4.10. Typical longitudinal waves.

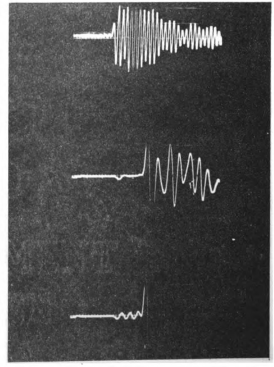

Figure 4.11. Typical shear waves.

4.5. The Effect of Hydrostatic Pressure On Velocity

The purpose of this test was to measure the longitudinal and shear wave velocities given by Eqs. (4.1) and (4.2).

$$V_{Lh} = \sqrt{\frac{\lambda + 2\mu - \alpha\,(4\lambda + 4\mu + 6\ell + 4m)}{\rho_h}}$$

$$V_{sh} = \sqrt{\frac{\mu - \alpha\,(3\lambda + 3\mu + 3m - \frac{n}{2})}{\rho_h}}$$

In the above equation, the hydrostatic linear strain (α) and the density ρ_h depend on the hydrostatic pressure. Thus, it was necessary to determine α. Then:

$$\rho_h = \rho_o\,(1 + 3\alpha)$$

where:

ρ_o = density at zero pressure

α = linear hydrostatic strain

Strain Measurement

The following procedure was used to determine the strain α.

-- A thin coat of SR-4 strain gage cement was applied to specimens and allowed to dry. This coat served the purpose of filling any holes or cracks on the surface of the specimen.

-- The coat was polished with sand paper and SR-4 gages of type A-1 were attached.

-- The strain gages and salt specimens were coated with a Dow-Corning silicone rubber caulk (commercially known as Dow-Corning Bathtub Caulk) to prevent oil leakage to the strain gages or the specimen.

-- After drying, the whole assembly was coated with approximately a 1/4 inch layer of Gulf Microwax 75. Coating was accomplished by dipping the specimen in the melted wax. Figure 4.12 shows the layers of silicone, rubber and wax.

-- A similar procedure was followed for coating and attaching a similar strain gage to a steel specimen. This gage was used as a compensating gage.

-- The steel and rock salt specimens were placed in the high-pressure vessel. The electrical connections to the strain gages were the same as discussed in the apparatus.

-- The gages from the steel and salt were connected to form adjacent arms of a wheatstone bridge. This arrangement provided for temperature and pressure compensation. The strain output was the difference between the strain in salt and steel.

-- α was calculated by adding recorded strain to the strain in steel which was calculated from the known compressibility of steel.

-- The results indicated a linear relation between pressure and strain (α). The curve was very close to the theoretical value of α:

$$\alpha = \frac{P}{3\lambda + 2\mu}$$

where:

P = pressure

λ, μ = Lamé's constants calculated from Section 4.4.

Experimental Setup for Velocity Measurements

Longitudinal transducers were attached to the specimens with a thin coat of high vacuum grease. The transducers and the salt were then covered with coats of Dow-Corning silicone rubber and Gulf Microwax 75 (Fig. 4.12). The electrical leads from the transducers were soldered to the electrical wires on the end plate of the vessel (Fig. 4.13).

Shear transducers were cemented to the specimens with regular office sealing wax. This was accomplished by warming the surfaces of the transducers and the salt and applying a thin coat of the melted wax (melting point 120°C) to the two surfaces. The transducers were then clamped to the salt and allowed to cool slowly.

It was mentioned in Section 4.3 that the accuracy obtained by using the circuit of Fig. 4.7 to measure the delay time in the specimen was of the order of $\pm$ 1%. Better accuracy was needed in the hydrostatic and triaxial compression tests. This was obtained by using a modified comparison method to measure the changes in the delay time due to stress, rather than the absolute time at each stress level. A block diagram of this method is

shown in Fig. 4.15. A description of this method as developed by the present author, is included in the following procedure.

Procedure

-- The 1-inch steel disks with the transducers attached (Fig. 4.4) were used to represent the unstressed specimen in the circuit of Fig. 4.15. The delay time in the steel disks was about 9 μ sec.

-- The test specimens were placed in the pressure vessel and the circuit was connected as shown in Fig. 4.15. Figure 4.14, shows the various components used in the test. The unstressed specimen assembly is shown to the right of the pressure gage.

-- The straight line portions of the two signals were superimposed to appear as a single straight line.

-- The oscilloscope sweep speed was increased to 1 or $\frac{2}{5}$ μ sec/cm scope division. At these speeds, only a small portion of the straight line appeared.

-- The amplitude of the signal from the test specimen was adjusted to coincide with the top horizontal grid line of the oscilloscope screen. This adjustment was accomplished by using the oscilloscope gain.

-- Loading was started. At each load level the amplitude of the signal from the stressed specimen was adjusted back to its original level. Figure 4.17 shows three pictures from a longitudinal test. Each picture was taken at several

load levels. For example, the top picture was taken at 5 load levels. The traces of the received signal from the test specimen are the thin approximately parallel traces. The thick slanting trace represents the signals from the unstressed specimen at different load levels. A single curved trace from the unstressed specimen indicates that the zero time (scope trigger), which is not shown in the picture, did not change. Thus, the horizontal distance between any two signals represents a true change in propagation time.

-- Measurements were taken for two cycles of loading and unloading. Maximum pressure was 9,000 psi. In the unloading of the first cycle and during the second cycle, the changes in propagation time were small as shown in the bottom picture of Fig. 4.17. Thus, measurements were taken at larger load intervals.

-- Four specimens were used; two for longitudinal tests and two for shear tests.

-- The same procedure was used for the shear and longitudinal measurements. Typical traces from a shear test are shown in Fig. 4.18. This figure shows the early arrival of the longitudinal components.

Data Reduction

The polaroid pictures were analyzed using a two dimensional traveling microscope. The change in propagation time between any two pressure levels was calculated from

the horizontal distance between the two traces. This distance was measured along the center of the scope grid. The accuracy of the time measurements was of the order of $\pm$ 0.005 μ sec.

Table 4.2 shows typical data for a hydrostatic test. The quantities were calculated as follows:

-- Hydrostatic strain α was determined from the results described in the hydrostatic strain measurements:

$$\alpha = \frac{P}{3\lambda + 2\mu}$$

where:

P = pressure in psi

$3\lambda+2\mu = 9.238 \times 10^6$ psi; determined from measurement of V_L and V_s at zero pressure.

-- The path length at any pressure is given by $L_o + \Delta L$ where:

L_o = path length at zero pressure

$\Delta L = - \alpha L_o$

-- Δt step: represents the change in propagation time between two consecutive loads.

-- $t_o + \Sigma \Delta t$: represents the propagation time at any pressure.

-- $\Sigma \Delta t$ = total change in propagation time.

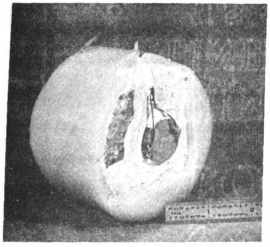

Figure 4.12. Transducer and specimen coating in the hydrostatic test.

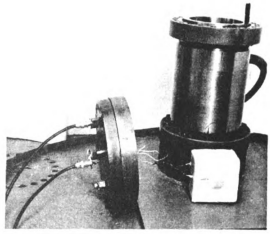

Figure 4.13. High pressure vessel and electrical connections.

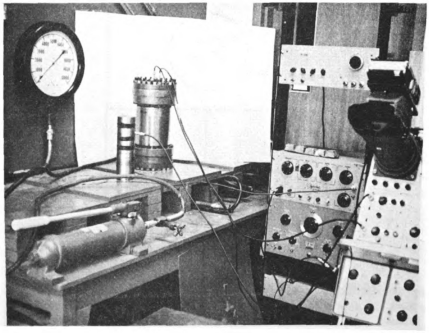

Figure 4.14. Various components of the hydrostatic test.

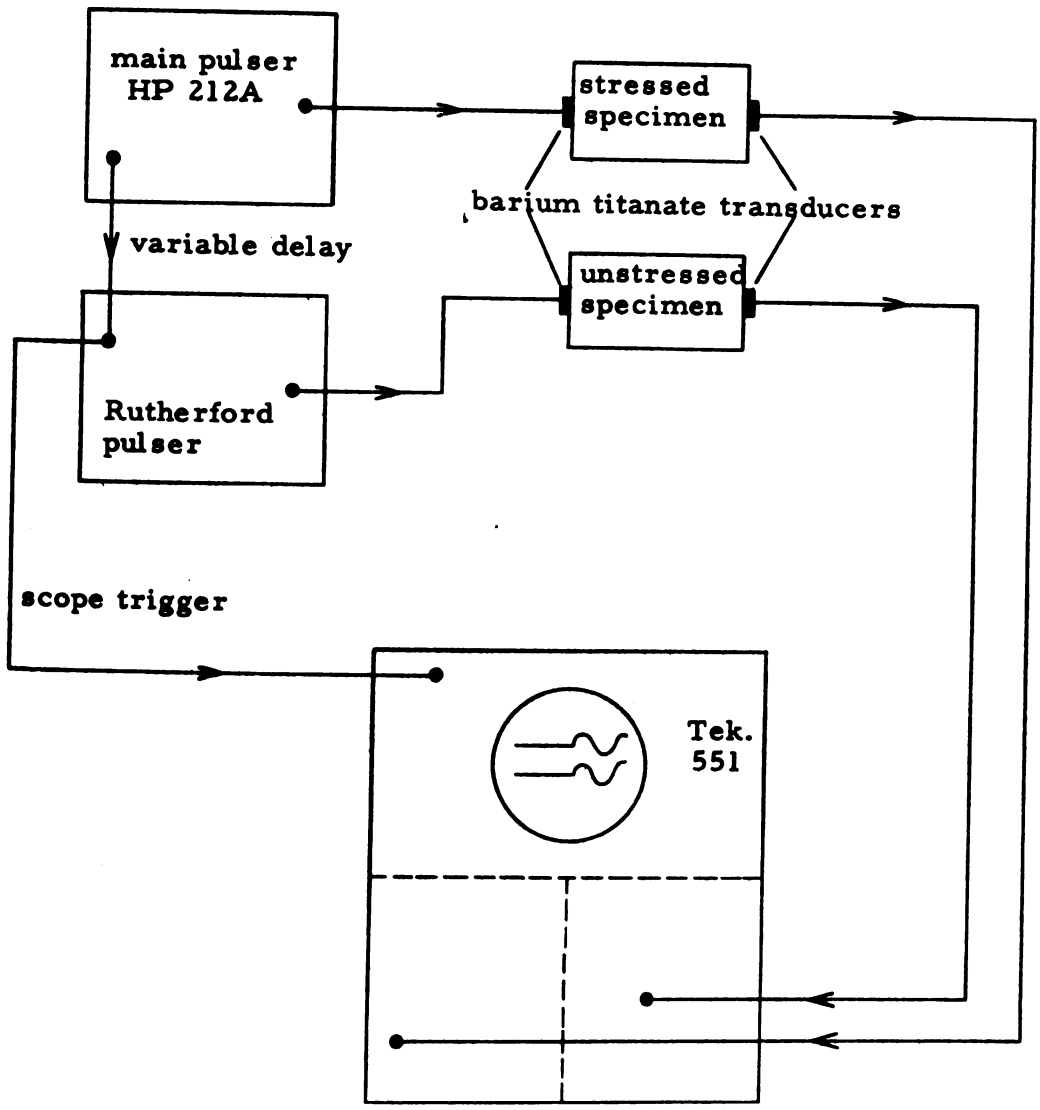

Fig. 4.15. A block diagram of the comparison method for measuring small changes in velocity in the hydrostatic and triaxial compression tests.

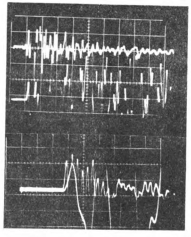

4.16. Delay time adjustment in comparison method.

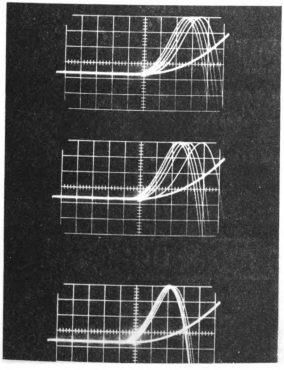

4.17. Typical traces from a longitudinal test at 2/5 μ sec/scope div.

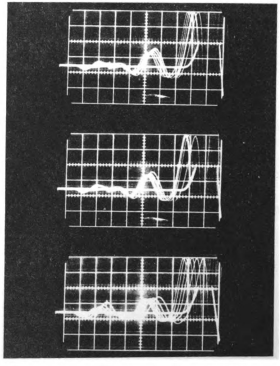

4.18. Typical traces from a shear test at 2 μ sec/ scope div.

Table 4.2. Reduced data for the longitudinal wave velocity in the hydrostatic test.

			Specimen HL3					
			first cycle			second cycle		
P Pressure psi	α Strain μ in/in	$L_o + \Delta L$ inch	Δt Step μ sec.	$t_o + \Sigma \Delta t$ μ sec.	Velocity m/sec	Δt Step μ sec.	$t_o + \Sigma \Delta t$ μ sec.	Velocity m/sec.
0	0	2.4800	0	14.909	4225	--	--	--
500	55	2.4799	-0.55	14.359	4387	--	13.990	4502
1000	108	2.4797	-0.21	14.149	4451	-0.225	13.765	4576
2000	216	2.4795	-0.31	13.839	4551	-0.110	13.655	4612
3000	324	2.4792	-0.138	13.701	4596	-0.050	13.605	4628
4000	432	2.4789	-0.086	13.615	4624	--	--	--
5000	540	2.4786	-0.056	13.559	4643	-0.054	13.551	4646
6000	648	2.4784	--	--	--	--	--	--
7000	756	2.4781	-0.078	13.481	4669	-0.040	13.511	4659
8000	864	2.4779	--	--	--	--	--	--
9000	972	2.4776	-0.057	13.424	4688	-0.034	13.477	4669
unload								
8000	864	--	--	--	--	--	--	--
7000	756	2.4781	+0.037	13.461	4676	+0.046	13.523	4655
6000	648	--	--	--	--	--	--	--
5000	540	2.4786	+0.042	13.501	4662	+0.024	13.547	4647
4000	432	2.4789	+0.02	13.523	4656	--	--	--
3000	324	2.4792	+0.025	13.548	4648	+0.050	13.597	4631
2000	216	2.4795	+0.041	13.589	4635	+0.038	13.635	4619
1000	108	2.4797	+0.113	13.702	4597	+0.112	13.747	4582
500	55	2.4799	+0.288	13.990	4502	+0.285	14.032	4489

t_o = propagation time at zero pressure. This was calculated from the average velocities in unstressed specimens. The actual calculation is given in Section 5.4.

V_L = 4225 meters/sec.

V_s = 2450 meters/sec.

$$t_o = \frac{L_o}{V_{average}}$$

-- The velocity at any pressure is given by V:

$$V\left(\frac{meter}{sec}\right) = \frac{L_o + \Delta L}{t_o + \Delta t} \left(\frac{inch}{\mu\ sec}\right) 10^6 \left(\frac{\mu\ sec}{sec}\right)(0.0254)\left(\frac{meter}{sec}\right)$$

The results are presented in Chapter V.

4.6. Triaxial Compressive Stress With Uniaxial Strains

The purpose of this test was to measure the longitudinal and shear wave velocities of Eqs. 4.3 and 4.4,

$$V_{Lt} = \sqrt{\frac{\lambda + 2\mu - e\ (4\lambda + 8\mu + 2\ell + 4m)}{\rho_t}}$$

$$V_{st} = \sqrt{\frac{\mu - e\ (\lambda + 3\mu + m)}{\rho_t}}$$

where:

V_{Lt} and V_{st} are the longitudinal and shear wave velocities in the direction of uniaxial strain e.

Experimental Setup

A plastic sheet was coated on both sides with a grease-graphite mixture. The sheet was wrapped around the solid cylindrical salt specimens. The diameter of the specimen was 3.24 inches and the height was about 3.15 inches. The specimen was then tightly fitted into the thick-walled steel cylinder described in Section 4.2. Figure 4.19 shows the thick-walled steel cylinder and the salt specimen.

The assembly for the longitudinal wave measurements was the same as for the axial test of Fig. 4.1. Figure 4.20 shows the transducer attached to the one-inch steel disk, the dial gages used to measure the strain in the salt, and the thick-walled cylinder.

Shear transducers were embedded in Armstrong adhesive cement, type C-4, which filled the center of $\frac{1}{2}$ inch thick steel rings (Fig. 4.21). Electrical wires from the transducers were embedded in two thin grooves in the back of the rings (left ring of Fig. 4.21). The front faces of the rings were placed in direct contact with the salt. Loading was applied to the back faces of the rings. This arrangement provided uniform stress on the salt and at the same time direct contact between the transducers and the specimens. Figure 4.22 shows the assembly for a shear test.

Procedure

Figure 4.23 shows the experimental setup. Load was applied to the specimens by the hand pump of the press tester. The electrical circuit was the same as the circuit used for the hydrostatic tests (Fig. 4.15). The same procedure was used for measuring the change in propagation time.

At each load the following readings were taken: (1) picture of trace, (2) dial gage reading, and (3) tangential strain from SR-4 gages attached on the thick-walled cylinder. Measurements were taken for two cycles of loading and unloading. Maximum axial stress was 13,800 psi. Four specimens were used; two for longitudinal waves and two for shear waves.

Data Reduction

The films were analyzed by the same procedure described in the hydrostatic test. Uniaxial strain e was calculated from the average reading, ΔL, of the two dial gages:

$$e = \frac{\Delta L}{L_o}$$

where:

ΔL = average change in path length

L_o = path length at zero stress.

Velocity was calculated by the same procedure as used in the hydrostatic test:

$$V = \frac{L_o + \Delta L}{t_o + \Delta t}$$

Lateral stress on the salt was calculated from the tangential strain (ϵ_{t_s}) on the outer surface of the thick-walled steel cylinder as follows.[45]

$$\sigma_L = - \frac{b^2 - a^2}{2a^2} \sigma_{t_s}$$

where:

σ_L = lateral stress in the salt.

σ_{t_s} = tangential stress on the surface of the thick-walled cylinder.

b = 2 inches, outside radius of steel cylinder.

a = 1.625 inches, inside radius of steel cylinder.

$$\sigma_{t_s} = E \epsilon_{t_s} + \nu (\sigma_{r_s} + \sigma_{z_s})$$

where:

ν = Poisson's ratio of steel.

σ_{z_s}, σ_{r_s} = axial and radial stress on the outer surface of the steel.

$\sigma_{r_s} = \sigma_{z_s} = 0$ on the outer surface

$E = 30 \times 10^6$ psi.

Substituting for a, b and σ_{t_s} yields:

$$\sigma_L = - \frac{b^2 - a^2}{2a^2} E \epsilon_{t_s} = -7.72 \epsilon_{t_s}$$

where:

ϵ_{t_s} = measured tesile strain in μ in/in

σ_L = compressive lateral stress on rock salt, psi.

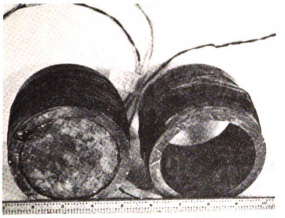

Figure 4.19. Thick walled steel cylinder.

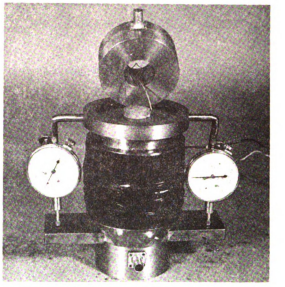

Figure 4.20. Longitudinal transducer and specimen assembly in triaxial test.

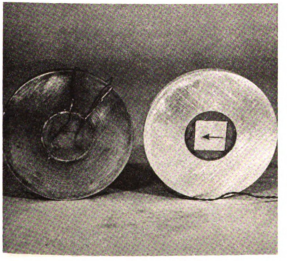

Figure 4.21. Shear transducers.

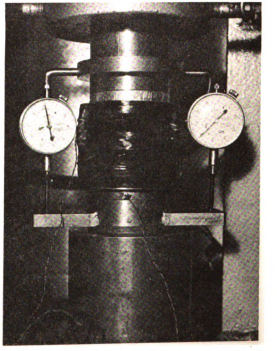

Figure 4.22. Assembly for shear wave measurements.

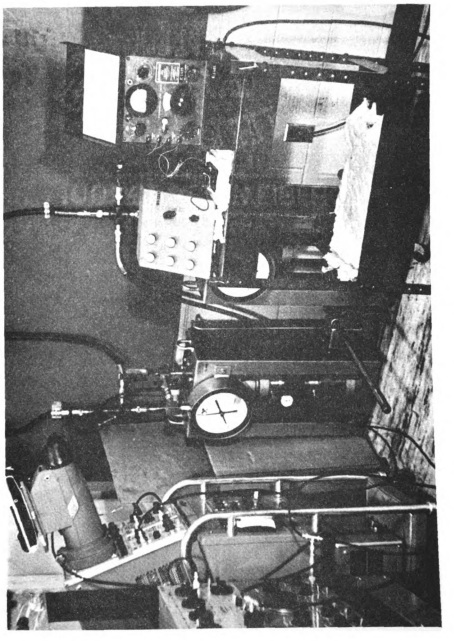

Figure 4. 23. Various components of triaxial compression test.

V. RESULTS AND DISCUSSION

5.1. General Remarks

Before discussing the results, it might be desirable to state that the velocities measured in this investigation are assumed to be equal to the wave velocities in an infinite medium. Furthermore, it was assumed that the waves in the hydrostatic and triaxial tests are plane.

The assumption that the velocities measured are equal to the velocities in an infinite medium can be verified from the experimental results of Sileava (Fig. 2.6) as follows:

The lowest frequency used was 180 kcs.

The longitudinal wave velocity in rock salt was about 4225 meters/second.

Thus, the maximum wave length was:

$$L = \frac{422,500 \text{ cm/sec}}{180,000 \text{ cycle/sec}} = 2.35 \text{ cm}$$

The minimum value of the ratio $\frac{a}{L}$, where

a = minimum radius of specimen, was

$$\frac{3.2 \text{ cm}}{2.35 \text{ cm}} = 1.36.$$

The maximum length of the specimens, x, was 3.5 inches = 8.9 cm. Therefore, the maximum ratio $\frac{x}{L}$ was:

$$\frac{8.9}{2.35} = 3.8$$

From Figure 2.6 it can be seen that the velocities measured for these extreme values of $\frac{a}{L}$ and $\frac{x}{L}$ are the wave velocities in infinite media.

The plane wave region (sketch, Sect. 2.4.4) in the hydrostatic and triaxial tests extended to 2.3 cm, while specimen length ranged from 2 to 3.1 inches. It was pointed out that this would cause large errors in absolute attenuation measurements. However, attenuation was not measured in these tests. The assumption of plane waves was justified by the sharp rise time in the received signals and by the fact that velocity was measured along the main beam.

5.2. Uniaxial Compressive Stress Tests on Steel

The results obtained from these tests are presented in Fig. 5.1. Fig. 5.1a shows the stress-strain relationship for the steel used. Fig. 5.1b shows the results of the axial and lateral measurements.

For the axial test, attenuation is most probably due to improvement of the coupling between the transducers, end blocks, and the specimen interfaces. For the lateral test, no improvement of coupling is expected since the holders are fixed in position by rubber bands across them and the change in the lateral dimension is too small to affect the force with which the rubber bands are stretched.

In both the axial and the lateral test, the velocity was found to increase with increasing stress with a steeper slop near the yield region. The maximum velocity is reached at the maximum load. The maximum velocities are 1.4% and 2.8% higher than the zero stress velocity for the lateral and axial tests respectively. This is higher than the resolution of the method; therefore, the change is assumed to be the true behavior of steel. During unloading, the velocity and attenuation showed a small change in both tests.

5.3. Uniaxial Compressive Stress Tests on Rock Salt

Figures 5.2 and 5.3 show the results obtained from uniaxial compressive stress tests of six identical 3.5 inch cubic rock salt specimens. Similar results were obtained for six identical 2.5 inch cubic specimens. Relative attenuation is calculated in decibels as discussed in Section 4.3. Negative values indicate an increase in attenuation and vice versa.

The behavior indicated by the results may be explained by Serata's[60] observations on the development of fracture or cracks at the lateral surfaces and the development of a triaxially stressed zone at the loading surfaces of the specimen. A schematic diagram of these two zones is presented below.

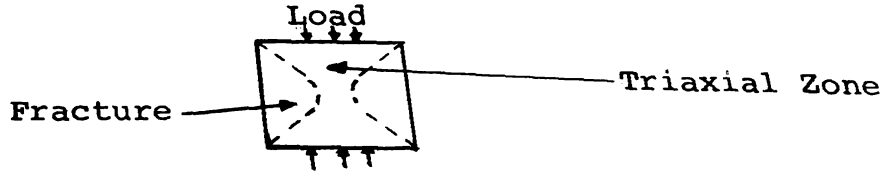

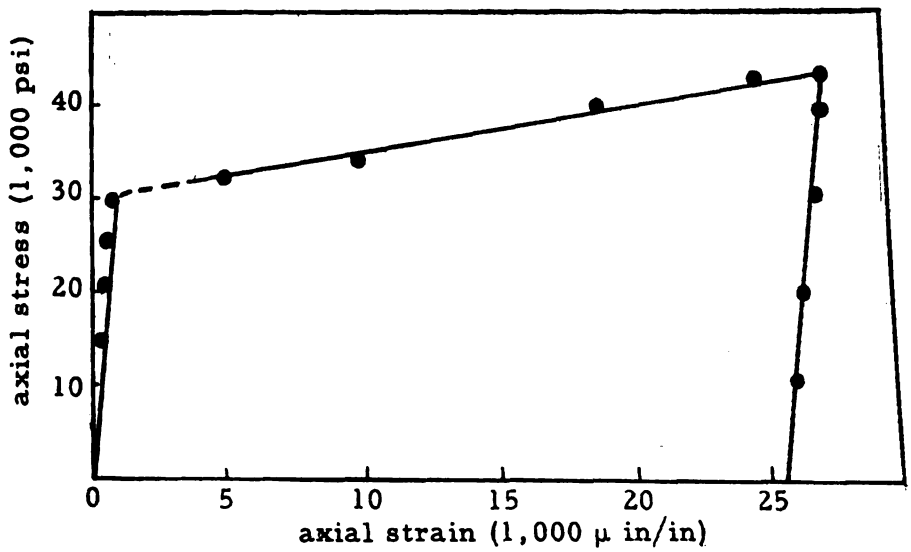

Fig. 5.1a Stress-strain relationship.

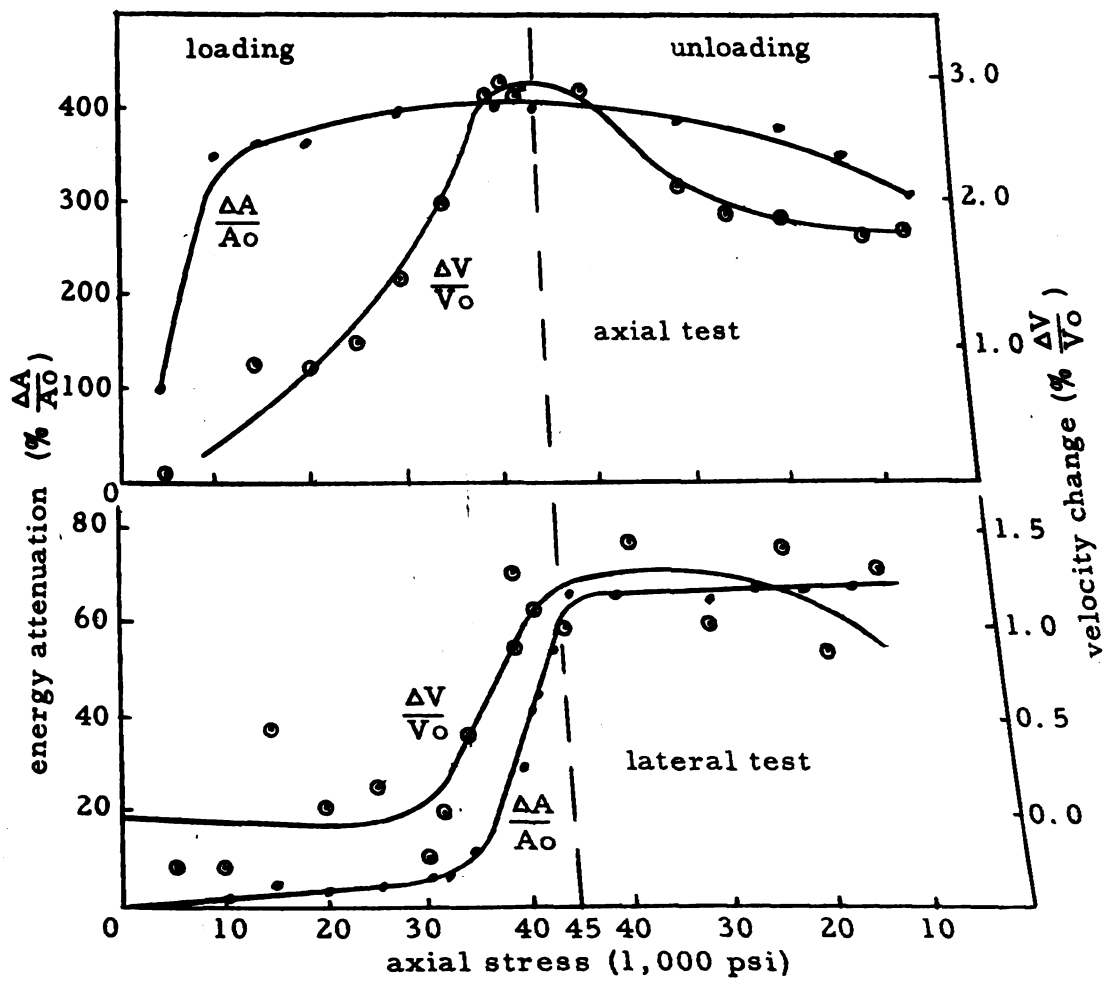

Fig. 5.1b Energy attenuation and velocity changes versus axial stress in steel.

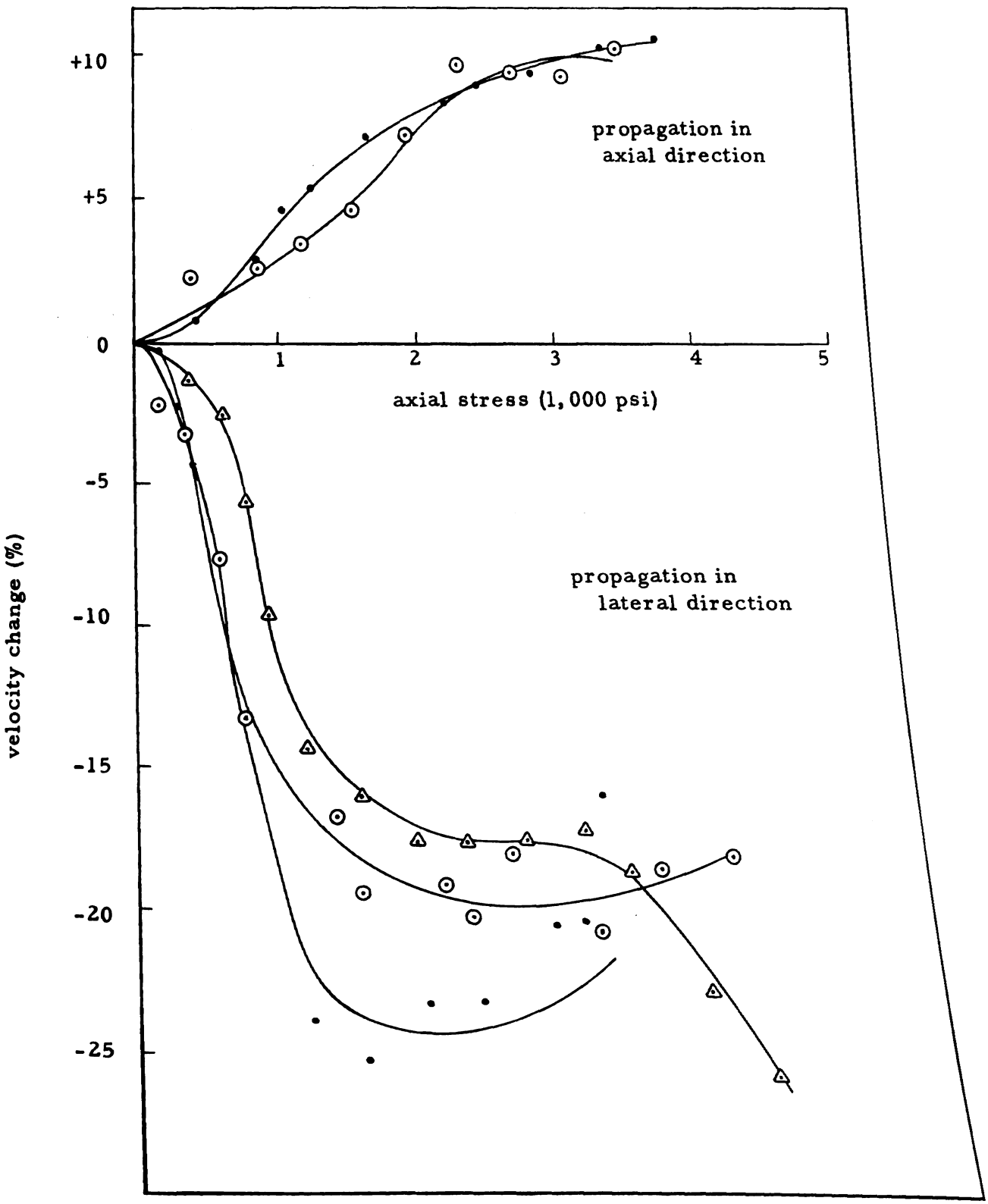

Fig. 5.2 Velocity change of ultrasonic longitidunal waves propagating through five identical 3.5-inch cubic specimens with increase of uniaxial compression

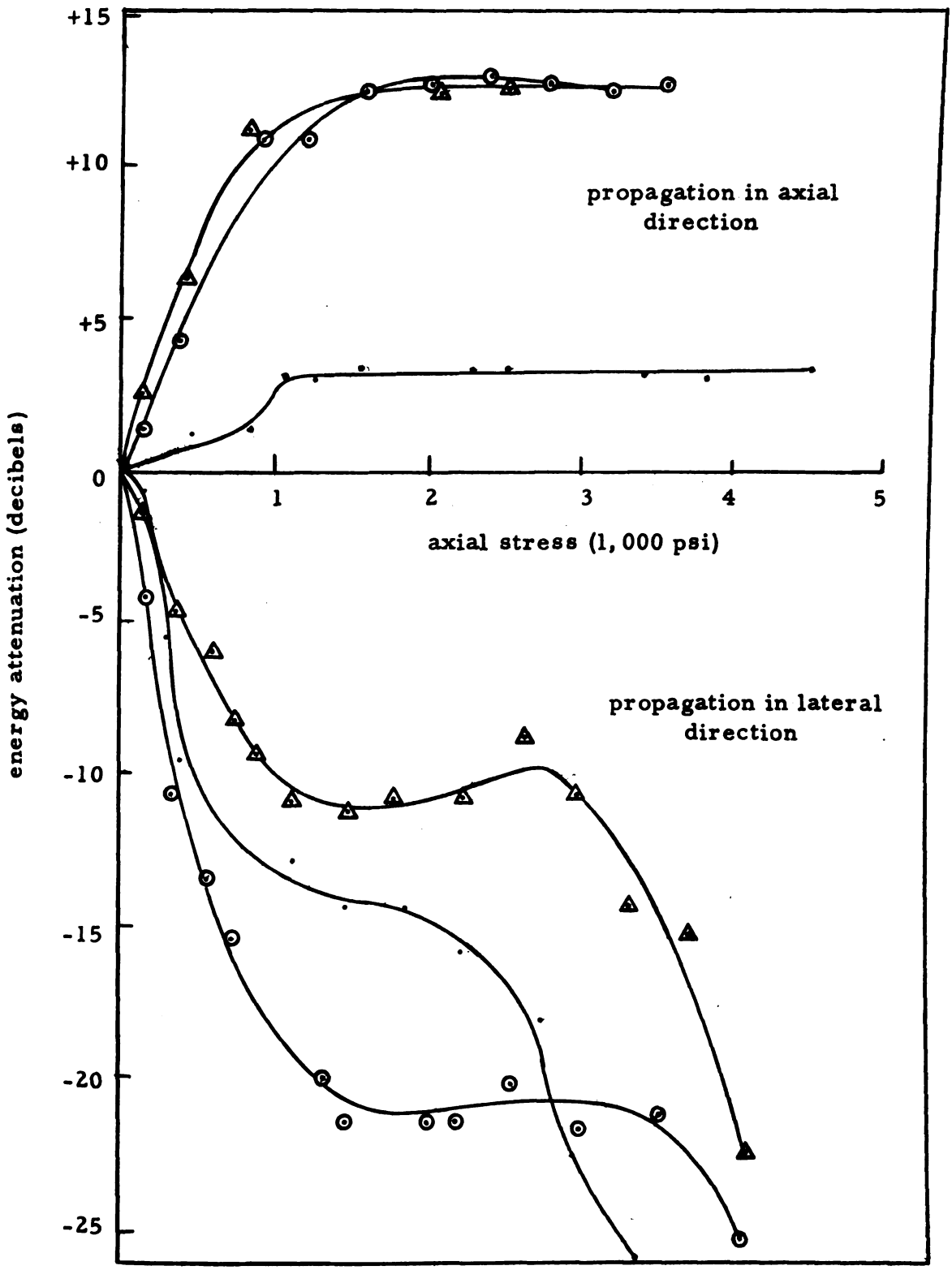

Fig. 5.3 Energy attenuation of Ultrasonic wave propagating through six identical 3.5-inch cubic specimens with increase of uniaxial compression.

In the triaxially stressed zone, the salt becomes more compact and better transmission is expected as indicated by the increase in velocity and decrease in attenuation in the axial measurements. Opposite behavior is observed in the lateral direction due to propagation in a fractured zone.

As the load increases, the triaxial zone extends to the center of the specimen. From 1,000 to $\approx$ 3,000 psi, lateral waves are partially propagating in the triaxial zone; this explains the relatively constant values of attenuation and velocity in this stress range. At higher loads, the specimen starts to fracture and attenuation in the lateral direction increases very fast.

Attenuation measurements are further complicated by changes in coupling between the transducers and specimens. The effect of this coupling cannot be separated from the true changes in attenuation in the salt.

The difference between the velocities measured in the axial and lateral directions increases with increasing axial stress. The velocity difference reaches 25% at 3,000 psi (about 75% of the crushing strength).

5.4. Lamé's Constants

Velocities were measured in different-length specimens and in three mutually perpendicular directions in cubic specimens. The purpose of using different-length specimens was to determine the effect of the couplant on

the propagation time. The purpose of the measurements made in three directions was to determine if the assumption of isotropy is valid for rock salt in its unstressed state.

Figure 5.4 shows the propagation time for longitudinal and shear waves versus specimen length. The straight lines connecting the points pass through the origin indicating that the couplant effect is negligible.

Velocities were calculated from the slopes of the straight lines.

longitudinal velocity = 4255 meters/sec $\pm$ 1%

shear velocity = 2450 meters/sec $\pm$ 2%

The accuracies indicated are determined from the accuracy with which the propagation time (straight line portions, Figs. 4.10, 4.11) was measured.

The cluster of six points at the end of the longitudinal line (Fig. 5.4) was determined from measurements in 3 perpendicular directions in two approximately 5-inch cubic specimens. They indicate that the velocity is the same in all directions and thus the assumption of isotropy is valid.

Lamé's constants were calculated as follows:

$$\mu = \rho V_s^2 \qquad (5.1)$$

where:

ρ = average density of all samples = 2.157 gm/cm^3

$\mu = (2.157 \text{ gm/cm}^3) \times (245{,}000 \text{ cm/sec})^2$

$\mu = 1.2947 \times 10^{11}$ dynes/cm^2

$$\lambda = \rho V_L^2 - 2\mu$$

$$\lambda = 1.261 \times 10^{11} \text{ dynes/cm}^2 \qquad (5.2)$$

$$\lambda + 2\mu = 3.85 \times 10^{11} \text{ dynes/cm}^2$$

$$1 \text{ dyne/cm}^2 = 1.45 \times 10^{-5} \text{ psi}$$

Thus,

$$\mu = 1.877 \times 10^6 \text{ psi}$$

$$\lambda = 1.828 \times 10^6 \text{ psi}$$

$$\lambda + 2\mu = 5.58 \times 10^6 \text{ spi}$$

Poisson's ratio, ν, was calculated as:

$$\nu = \frac{1 - 2(\frac{V_s}{V_L})^2}{2 - 2(\frac{V_s}{V_L})^2} = 0.247$$

The dynamic value of Young's modulus was calculated as:

$$E = 2\mu (1 + \nu) = \frac{\mu (3\lambda + 2\mu)}{\lambda + \mu}$$

$$= 4.68 \times 10^6 \text{ psi}$$

The bulk modulus, $K = \frac{1}{3}(3\lambda + 2\mu) = 3.08 \times 10^6$ psi.

The values of V_L, V_s, λ, μ obtained from velocity measurements in situ (Section 2.4) are slightly higher than the values obtained by the present author. The value of ν compares very closely (Table 5.1). The differences are due to the fact that rock salt in situ is in a triaxially compressed state while the specimens used by the author are in an unstressed state. Compression causes an increase in V_L, V_s, λ and μ as will be discussed in the following sections.

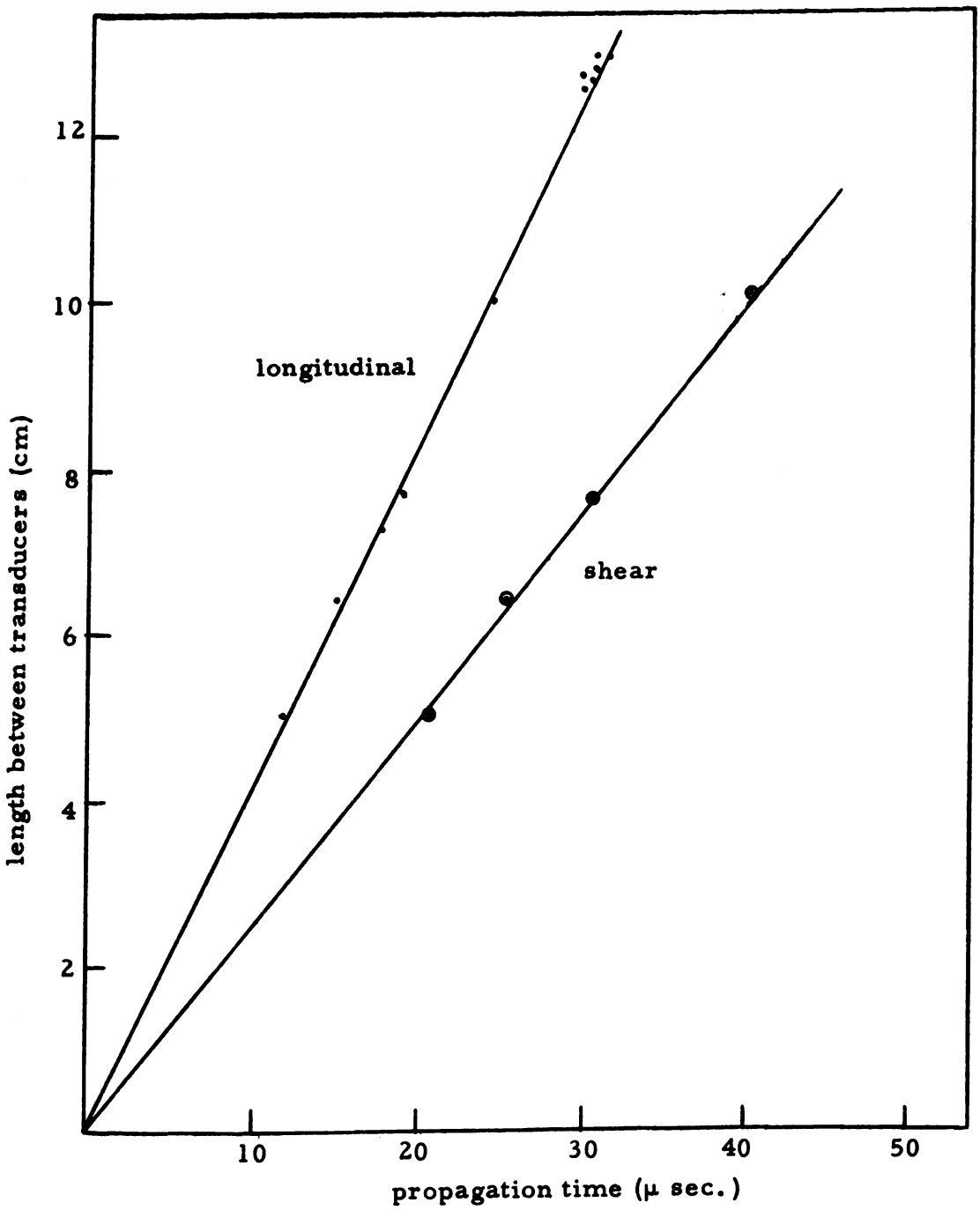

Fig. 5.4 Propagation time of longitudinal and shear waves in rock salt specimens of various lengths

Table 5.1. Dynamic elastic moduli of rock salt.

	Present author	In situ[48]
V_L (meter/sec)	4225	4370
V_s (meter/sec)	2450	2550
ν = Poisson's ratio	0.247	0.241
μ = G (10^6 psi)	1.877	2.05
λ (10^6 psi)	1.828	1.91
E (10^6 psi)	4.68	5.09
K (10^6 psi)	3.08	3.28

It is also interesting to note that the values of λ and μ are very close to each other. This is in line with the quantum mechanical assumption regarding the existence of central forces between the particles of single crystals of NaCl.[68a] This assumption leads to the conclusions that $C_{44} = C_{12}$ in single crystals of NaCl and $\lambda = \mu$ in isotropic bodies.[68a] For NaCl:[68a]

$$C_{12} = 1.25 \times 10^{11} \text{ dynes/cm}^2$$

$$C_{44} = 1.26 \times 10^{11} \text{ dynes/cm}^2$$

and $C_{12} \approx C_{44}$

For the rock salt tested:

$$\lambda = 1.261 \times 10^{11} \text{ dynes/cm}^2 \approx C_{12} \text{ of NaCl}$$

$$\mu = 1.295 \times 10^{11} \text{ dynes/cm}^2 \approx C_{44} \text{ of NaCl}$$

and $\lambda \approx \mu$.

5.5. Hydrostatic Compression

Figure 5.5 shows the variation of longitudinal velocity due to hydrostatic pressure in two specimens. Figure 5.6 shows the variation of shear wave velocities.

In both figures, velocity increases very fast with an increase of hydrostatic pressure from zero to about 1,000 psi. Velocity increases at a progressively slower rate with an increase of hydrostatic pressure from 1,000 to 4,000 psi. Velocity shows a slow but steady increase with increasing hydrostatic pressure from 4,000 to 9,000 psi. Velocities measured during unloading of the first cycle are slightly higher than the corresponding velocities measured during loading. Velocities measured during the second loading and unloading cycles are very close to the velocities measured during unloading of the first cycle.

Similar results for different types of rocks were obtained by many investigators and reported in Section 2.4. The characteristic shape of velocity versus pressure curves was interpreted by the hypothesis of pore closure. Birch[14] explained this hypothesis as follows: "Pressure affects the elastic constants of rocks first by reducing porosity and eventually, as pressure is increased, by an

intrinsic effect upon the crystalline components." For example, "in igneous rocks, porosity is of the order of one tenth of one percent and under pressure of order of one kilobar solid contact is restored and above this point the pressure effect is close to the intrinsic one."

The higher velocities obtained during unloading are interpreted as due to the fact that some pores remain closed while unloading.

The present author agrees with the above descriptive hypothesis. The fast increase of velocity at low pressures is not reproducible and is most probably due to difference in porosity between the specimens. However, the "intrinsic" increase of velocity at higher pressures is reproducible. Rinehart[53] has stated that no satisfactory mathematical explanation has been given for this intrinsic change in rocks. The present author will give a mathematical explanation for this effect in the following sections based on the equations derived in Chapter III.

5.6. Triaxial Stress with Uniaxial Strain

Figures 5.7 and 5.8 show the variation of longitudinal and shear wave velocities, measured in the direction of uniaxial strain, as a function of the axial stress. The shape of these curves is similar to the one obtained in the hydrostatic tests and the same discussion applies here.

One of the objectives of this test was to determine if ultrasonic methods would detect transition from elastic

to plastic states of stress as discussed in Serata's transition theory (Fig. 2.4, Section 2.1). Figure 5.9 shows a typical experimental plot of lateral stress σ_L versus axial stress σ_z. This figure shows a close agreement with Serata's transition theory. However, no correlation is observed between the transition points of this figure and the velocity curves of Figs. 5.7 and 5.8. The absence of correlation may possibly be explained by Sternglass and Stuart's[65] experimental results which indicated that the wave front of longitudinal waves propagating in metal bars, which are prestressed to the plastic region, travels with the elastic wave velocity.

5.7 Determination of the Third-Order Elastic Constants of Rock Salt

The following theoretical equations, for the measured longitudinal and shear wave velocities during the first loading cycle in the hydrostatic and triaxial compression tests, were derived in Chapter III and redefined in Chapter IV.

Hydrostatic Compression :

$$V_{Lh} = \sqrt{\frac{\lambda + 2\mu - \alpha\,(4\lambda + 4\mu + 6\ell + 4m)}{\rho_h}} \tag{5.3}$$

$$V_{sh} = \sqrt{\frac{\mu - \alpha\,(3\lambda + 3\mu + 3m - \frac{n}{2})}{\rho_h}} \tag{5.4}$$

Triaxial Stress:

$$V_{Lt} = \sqrt{\frac{\lambda + 2\mu - e\,(4\lambda + 8\mu + 2\ell + 4m)}{\rho_t}} \tag{5.5}$$

$$V_{st} = \sqrt{\frac{\mu - e\,(\lambda + 3\mu + m)}{\rho_t}} \tag{5.6}$$

where:

$\lambda = 1.261 \times 10^{11}$ dynes/cm^2

$\mu = 1.295 \times 10^{11}$ dynes/cm^2

$-\alpha$ = hydrostatic linear strain

$-e$ = uniaxial strain in triaxial tests

ρ_h = density at a given strain α

ρ_t = density at a given strain e

$\rho_h \approx \rho_o\,(1 + 3\alpha)$

$\rho_t \approx \rho_o\,(1 + e)$

$\rho_o = 2.157$ gm/cm^3

ℓ, m, n = unknown third-order elastic constants

V_{Lh}, V_{sh}, V_{Lt} and V_{st} are the measured velocities in the first loading cycle of Figures 5.5 through 5.8 respectively.

The unknown third-order elastic constants can be calculated from the above equations. For example, the constant function $(6\ell + 4m)$ can be calculated from Eq. 5.3.

$$V_{Lh}^2\,\rho_h = \lambda + 2\mu - \alpha\,(4\lambda + 4\mu + 6\ell + 4m)$$

$$6\ell + 4m = \frac{\lambda + 2\mu - V_{Lh}^2\,\rho_h}{\alpha} - (4\lambda + 4\mu) \tag{5.7}$$

Similar procedures can be used to calculate the remaining functions $(3m - \frac{n}{2})$, $(2\ell + 4m)$ and (m). These four functions of ℓ, m, and n should be constant for any strain α or e and the corresponding velocity. However, due to pore closure effects and non-reproducibility of velocities at low pressures, the four functions of ℓ, m, and n were calculated by a differential approach. Table 5.2 shows a typical calculation for the constant function $(2\ell + 4m)$ by the following procedure:

$$V_{Lt_1}^2 \rho_{t_1} = \lambda + 2\mu - e_1 (4\lambda + 8\mu + 2\ell + 4m)$$

$$V_{Lt_2}^2 \rho_{t_2} = \lambda + 2\mu - e_2 (4\lambda + 8\mu + 2\ell + 4m)$$

Thus:

$$2\ell + 4m = \frac{V_{Lt_1}^2 \rho_{t_1} - V_{Lt_2}^2 \rho_{t_2}}{e_2 - e_1} - (4\lambda + 8\mu) \qquad (5.8)$$

where:

e_1 = strain at a stress σ_1

e_2 = strain at a stress $\sigma_2 > \sigma_1$

$e_2 > e_1$, e is positive

$V_{Lt_2} > V_{Lt_1}$

$e_2 - e_1 = \Delta e$

A similar procedure was used to calculate the other functions $(6\ell + 4m)$, $(3m - \frac{n}{2})$ and (m). The results are tabulated in Tables 5.3 and 5.4.

Since rock salt remains isotropic in the hydrostatic test, the same procedure was used to calculate $(6\ell + 4m)$ and $(3m - \frac{n}{2})$ for the second loading cycle. The only change in the seconc cycle is that λ and μ are different from their values in the first loading cycle. The new values of λ and μ were calculated from the average longitudinal and shear wave velocities at the beginning of the second loading cycle.

V_{Lh} = 4450 meters/sec.

V_{sh} = 2640 meters/sec.

ρ = 2.157 gm/cm^3

Using Eqs. 5.1 and 5.2 yields:

$\mu = 1.51 \times 10^{11}$ dynes/cm^2

$\lambda = 1.24 \times 10^{11}$ dynes/cm^2

These values were substituted in the velocity equations. The results are included in Table 5.3. A similar procedure for the second loading cycle in the triaxial tests would not be valid because of the induced anisotropy.

Table 5.2. Calculation of $(2\ell + 4m)$ for specimen TL2 from 1st cycle of loading.

Table 5.2. Calculation of $(2\ell + 4m)$ for specimen TL2 from 1st cycle of loading.

Axial stress σ_z 100 psi	Strain e in/in	Δe $e_2 - e_1$	Velocity V_{Lt} 100 cm/sec	Density ρ_t gm/cm^3	$V^2\rho$	$V_1^2\rho_1 - V_2^2\rho_2$	$\frac{V_1^2\rho_1 - V_2^2\rho_2}{\Delta e}$	$2\ell + 4m$
					dynes/cm^2			
					10^{10} +	10^{10} -	10^{11} -	10^{11} -
0	0	0	4225	2.157	38.504	---	---	---
6	.0006	.0006	4290	2.158	39.716	1.212	202.0	217
12	.0022	.0016	4353	2.162	40.967	1.251	78.2	94
18	.0047	.0025	4407	2.167	42.087	1.120	44.8	60
30	.0089	.0042	4493	2.176	43.927	1.840	43.8	59
42	.0117	.0028	4564	2.182	45.451	1.524	54.4	70
54	.0145	.0028	4630	2.188	46.904	1.453	51.9	67
66	.0162	.0017	4653	2.192	47.458	0.554	32.6	48
78	.0177	.0015	4672	2.195	47.911	0.453	30.2	46
90	.0192	.0015	4690	2.198	48.347	0.436	29.1	44
102	.0205	.0013	4699	2.201	48.599	0.252	19.3	35
114	.0216	.0011	4707	2.203	48.809	0.210	19.1	35
126	.0229	.0013	4717	2.206	49.084	0.275	21.1	36
138	.0240	.0011	4724	2.209	49.296	0.212	19.3	35

Table 5.3. Calculated values of $(6\ell + 4m)$ and $(3m - \frac{n}{2})$ from hydrostatic tests.

Pressure 100 psi	$-(6\ell + 4m)$ 10^{11} dynes/cm^2				$-(3m - \frac{n}{2})$ 10^{11} dynes/cm^2			
	First Cycle		Second Cycle		First Cycle		Second Cycle	
	HL2	HL3	HL2	HL3	HS1	HS2	HS1	HS2
0	--	--	--	--	--	--	--	--
5	6330	5555	--	--	2762	3442	--	--
10	1524	1107	842	2798	1580	1982	799	615
20	--	1811	227	677	303	568	245	--
30	261	836	194	274	210	292	91	161
40	--	530	--	--	117	120	--	--
50	--	366	140	146	63	76	45	77
60	127	--	--	--	--	--	--	--
70	--	256	130	127	31	32	34	27
80	--	--	--	--	--	--	--	--
90	121	192	105	109	20	21	23	21
Selected values:			107 $\pm$ 16				22 $\pm$ 5	

Table 5.4. Calculated values of $(2\ell + 4m)$ and (m) from the first cycle of triaxial tests.

Axial Stress 100 psi	$-(2\ell + 4m)$ 10^{11} dynes/cm^2		$-m$ 10^{11} dynes/cm^2	
	TL1	TL2	TS1	TS2
0	---	---	---	---
6	218	217	---	---
12	85	94	17	20
18	72	60	54	57
30	59	59	63	---
42	63	70	75	47
54	53	67	63	---
66	60	48	52	41
78	55	46	51	---
90	46	44	---	30
102	40	35	34	---
114	43	35	---	17
126	35	36	---	---
138	19	35	16	9
Selected Values:		35		< 9

Figures 5.10-5.12 show a plot of the four functions of ℓ, m, and n, tabulated in Tables 5.2 and 5.3, with respect to the stress. The horizontal straight line segments indicate the stress ranges for which the functions were calculated by the procedure illustrated in Eq. (5.8).

The results indicate the following:

-- The four functions of ℓ, m and n increase with an increase in stress. This increase is attributed to porosity effects. At high stresses, porosity effects become less and the four functions of ℓ, m and n approach constant values.

-- Differences between two replications are also due to differences in initial porosity. Lower values of any of the functions were obtained from specimens that showed higher changes in velocity (Figs. 5.5-5.8). Thus, it is reasonable to reject low values of the functions obtained from specimens which showed large changes in velocity. For example, in the first cycle of the hydrostatic longitudinal test, the results of specimen HL3 are rejected and the results of specimen HL2 and accepted.

-- Figure 5.10 shows that the difference between the two specimens HL2 and HL3 becomes small during the second cycle. Furthermore, the function $(6\ell + 4m)$ seems to converge faster at higher loads. Therefore, the value of $(6\ell + 4m)$ is taken as:

$$-(6\ell + 4m) = (107 \pm 16) \times 10^{11} \text{ dynes/cm}^2 \qquad (5.9)$$

where:

107×10^{11} is the average value from 7,000 to 9,000 psi.

$\pm 16 \times 10^{11}$ represents 67% of the difference between 107×10^{11} and the average value in the load range of 5,000 - 7,000 psi.

-- By similar argument, the average value of $(3m - \frac{n}{2})$ is taken as:

$$- (3m - \tfrac{n}{2}) = (22 \pm 5)\ 10^{11}\ \text{dynes/cm}^2 \qquad (5.10)$$

-- The results of specimen TL2 (Fig. 5.12) incidated that $(2\ell + 4m)$ converged to a constant value of -35×10^{11} dynes/cm^2 over a wide pressure range (9,000 - 13,800 psi axial stress). The average value of $(2\ell + 4m)$ from specimen TL1, over the same stress range, is also -35×10^{11} dynes/cm^2. Therefore;

$$(2\ell + 4m) = - 35 \times 10^{11}\ \text{dynes/cm}^2 \qquad (5.11)$$

-- The value of (m) as determined from the triaxial shear test (Fig. 5.12) did not indicate good convergence. The results of specimen TS2 indicate that (m) can be assumed as:

$$- (m) < 9 \qquad (5.12)$$

-- The four equations above do not yield a unique solution for ℓ, m and n. This behavior can be explained as due to differences in testing procedures; the functions $(6\ell + 4m)$

and $(3m - \frac{n}{2})$ were determined from a hydrostatic test while the functions $(2\ell + 4m)$ and (m) were determined from triaxial tests.

-- Large errors can be expected in the measurement of uniaxial strain, in the triaxial test, due to creep and plastic behavior of the salt. In fact, the strain e at each stress level was measured after a waiting period of 3 minutes during which some creep did occur. Thus, it is reasonable to assume that the true values of Δe are less than the values used in the calculation of the functions $(2\ell + 4m)$ and (m). Careful examination of Eq. (5.8) would indicate that the true values of $-(2\ell + 4m)$ and $(-m)$ must then be higher than those of Table 5.4.

-- It can be assumed that the unknown creep effects are the same in the longitudinal and shear velocity measurements of the triaxial test. Therefore, the results of the test can be represented by the following single formula:

$$\frac{N(2\ell + 4m)}{N(m)} = \text{constant} \qquad (5.13)$$

N = unknown factor

$-N(2\ell + 4m) = 35$

$-N(m) < 9$

-- The third order elastic constants can be calculated from Eqs. (5.9, 5.10 and 5.13) by assuming different $\frac{(2\ell + 4m)(N)}{m(N)}$ ratios.

Table 5.5. Third-order elastic constants of rock salt.

$\frac{N(2\ell + 4m)}{Nm}$	10^{11} dynes/cm^2			
	+ Nm	m	ℓ	n
------	------	------	------	------
4.38	-8	-20.5 ± 3	-39 ± 0.5	-79 ± 21
5	-7	-15.3 ± 2.3	-7.6 ± 1.1	-48 ± 17
5.84	-6	-10.0 ± 1.6	-9.4 ± 1.5	-12 ± 14

A sample calculation is given below:

Assume $-(N)m = 7 \times 10^{11}$

then,

$$\frac{N(2\ell + 4m)}{N(m)} = \frac{35}{7} = 5$$

Therefore,

$$2\ell = m$$

From Eq. (5.9):

$$6\ell + 4m = (-107 \pm 16) \times 10^{11}$$

$$7m = (-107 \pm 16) \times 10^{11}$$

Therefore:

$$m = (-15.3 \pm 2.3) \times 10^{11} \text{ dynes/cm}^2$$

$$\ell = (-7.6 \pm 1.1) \times 10^{11} \text{ dynes/cm}^2$$

From Eq. (5.12):

$$3m - \frac{n}{2} = (-22 \pm 5) \times 10^{11}$$

$$n = 6m + (44 \pm 10) \times 10^{11}$$

$$n = [(-92 \pm 13.7) + (44 \pm 10)]10^{11}$$

$$n = (-48 \pm 17)\ 10^{11} \text{ dynes/cm}^2$$

where:

$$\pm 17 = \sqrt{(10)^2 + (13.7)^2}$$

-- Figure 5.13 shows the average values of $(2\ell + 4m)$ and (m) for the second loading cycle in the triaxial tests. The salt was assumed to be isotropic at the beginning of the second loading cycle, and the functions $(2\ell + 4m)$ and (m) were calculated by the same procedure used to calculate $(6\ell + 4m)$ and $(3m - \frac{n}{2})$ in the second loading cycle of the hydrostatic test. It was pointed out that the assumption of isotropy is not valid in the triaxial test. However, it is assumed that the errors introduced in this assumption are less than the advantages obtained in the calculation of $(2\ell + 4m)$ and (m), due to less creep effect in the second loading cycle. Figure 5.14 shows the strain behavior for two typical specimens. The strain in the second loading cycle shows a linear behavior up to about 12,000 psi. Very little creep was observed in this range. After 12,000 psi the strain increments become large and start to show creep similar to that observed in the first loading cycle. This behavior justifies the elimination of the values of $(2\ell + 4m)$ and (m) in Figure 5.13, at loads higher than 12,000 psi.

-- It can be concluded that the average values of $(2\ell + 4m)$ and (m) for the second cycle of the triaxial test (Fig. 5.13) are:

$$2\ell + 4m = (-55 \pm 3) \times 10^{11} \text{ dynes/cm}^2$$

$$m = (-12 \pm 1) \times 10^{11} \text{ dynes/cm}^2$$

-- These values suggest the following choice of ℓ, m and n from Table 5.4:

$$m = (-12 \pm 1)\ 10^{11} \text{ dynes/cm}^2$$

$$\ell = (-9 \pm 1)\ 10^{11} \text{ dynes/cm}^2$$

$$n = (-26 \pm 6)\ 10^{11} \text{ dynes/cm}^2$$

-- This choice was made by plotting the values of ℓ, m and n from Table 5.4 as shown in Fig. 5.15. The value of (m) was chosen as $(-12 \pm 1)\ 10^{11}$. Three horizontal lines were drawn to intersect the (m) curve at the selected values of $(-11, -12, -13) \times 10^{11}$ dynes/cm^2. Three vertical lines were then drawn from these points. The values of ℓ and n were obtained from the points at which the three vertical lines intersected the ℓ and n curves.

-- The measured values of $(6\ell + 4m)$ and $(3m - \frac{n}{2})$ in the first and second cycles of the hydrostatic test (Figs. 5.10, 5.11) and the average values of $(2\ell + 4m)$ and (m) in the second cycle of the triaxial test, are all in close agreement with the final selected values of ℓ, m and n. Similarly, the measured value of (m) in the first cycle of the triaxial test was -9×10^{11} for specimen TS2 and -17×10^{11} for specimen TS1. The average of these two values is also in close agreement with the final choice of m.

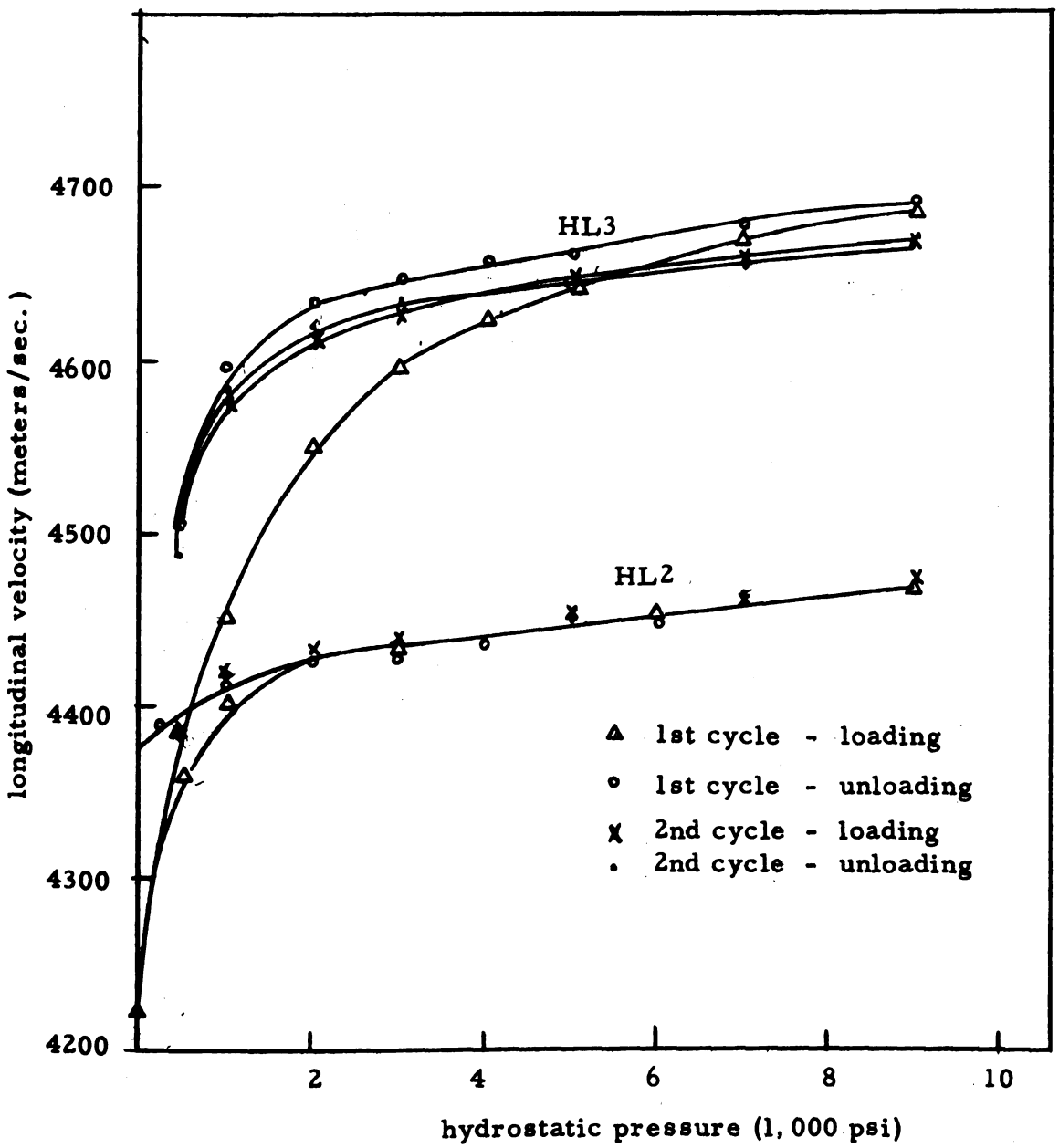

Fig. 5.5 Change of longitudinal velocity with hydrostatic pressure

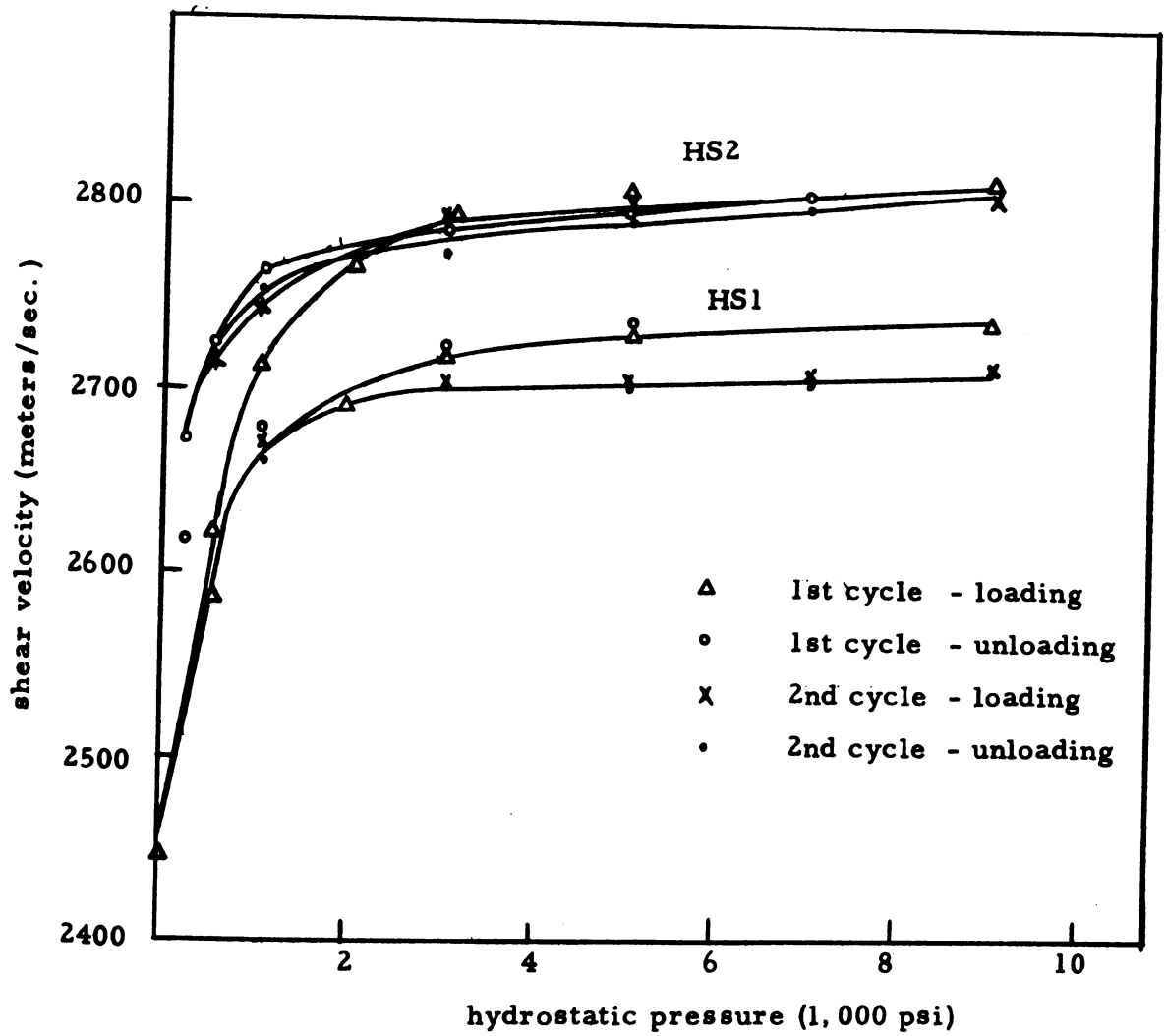

Fig. 5.6 Change of shear velocity with hydrostatic pressure

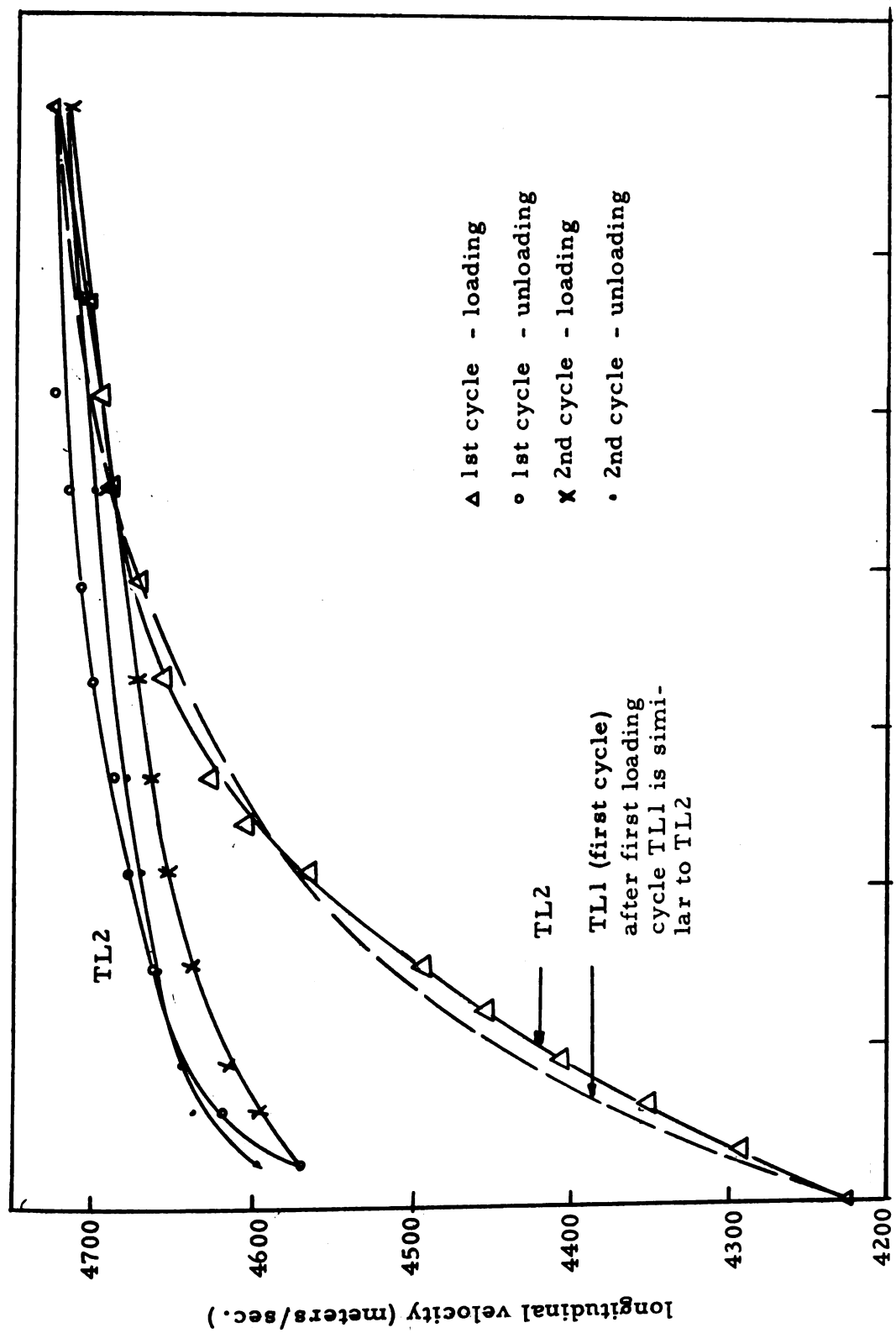

Fig. 5.7 Longitudinal velocity versus axial stress in triaxial tests

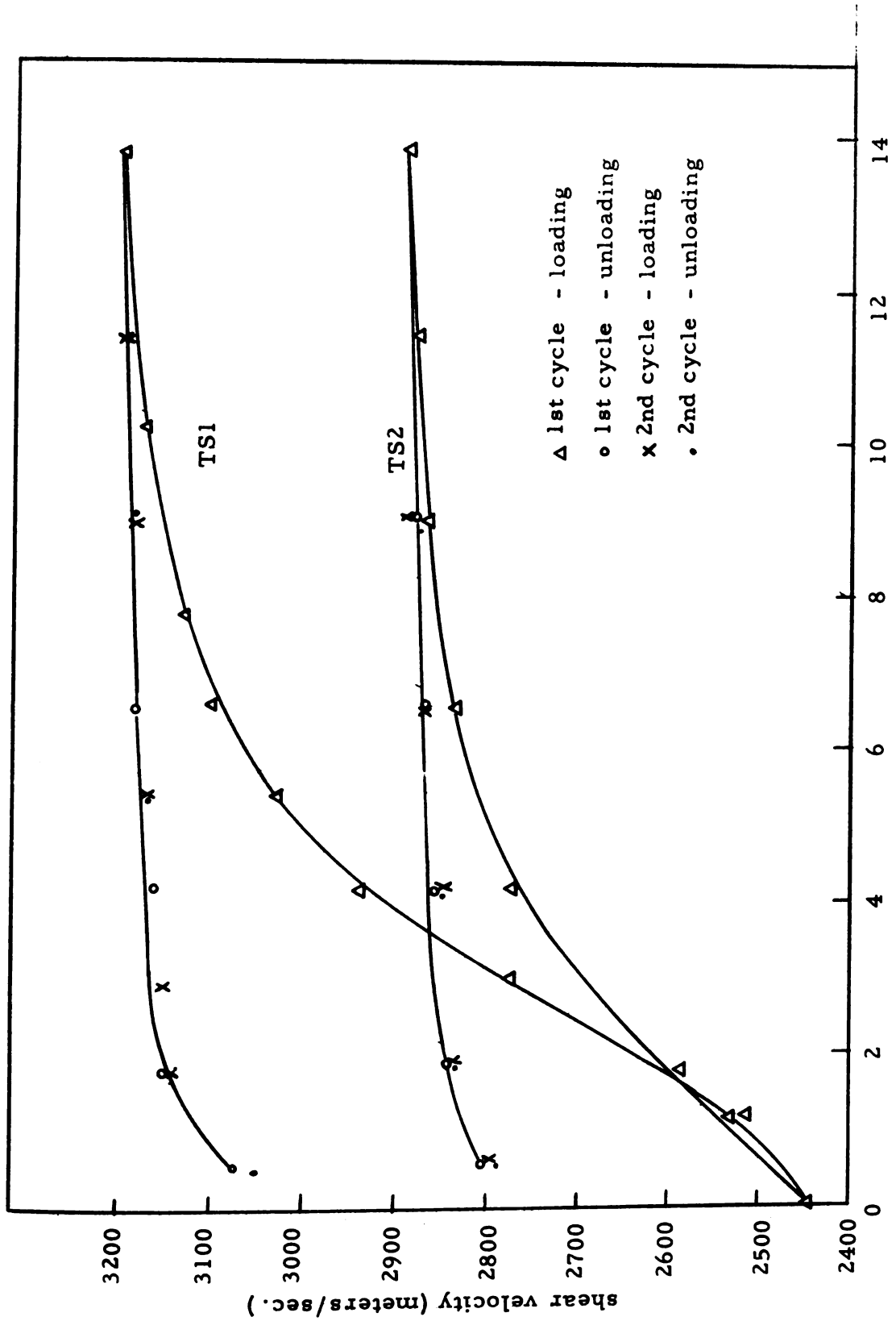

Fig. 5.8 Shear velocity versus axial stress in triaxial tests

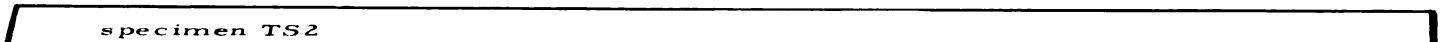
specimen TS2

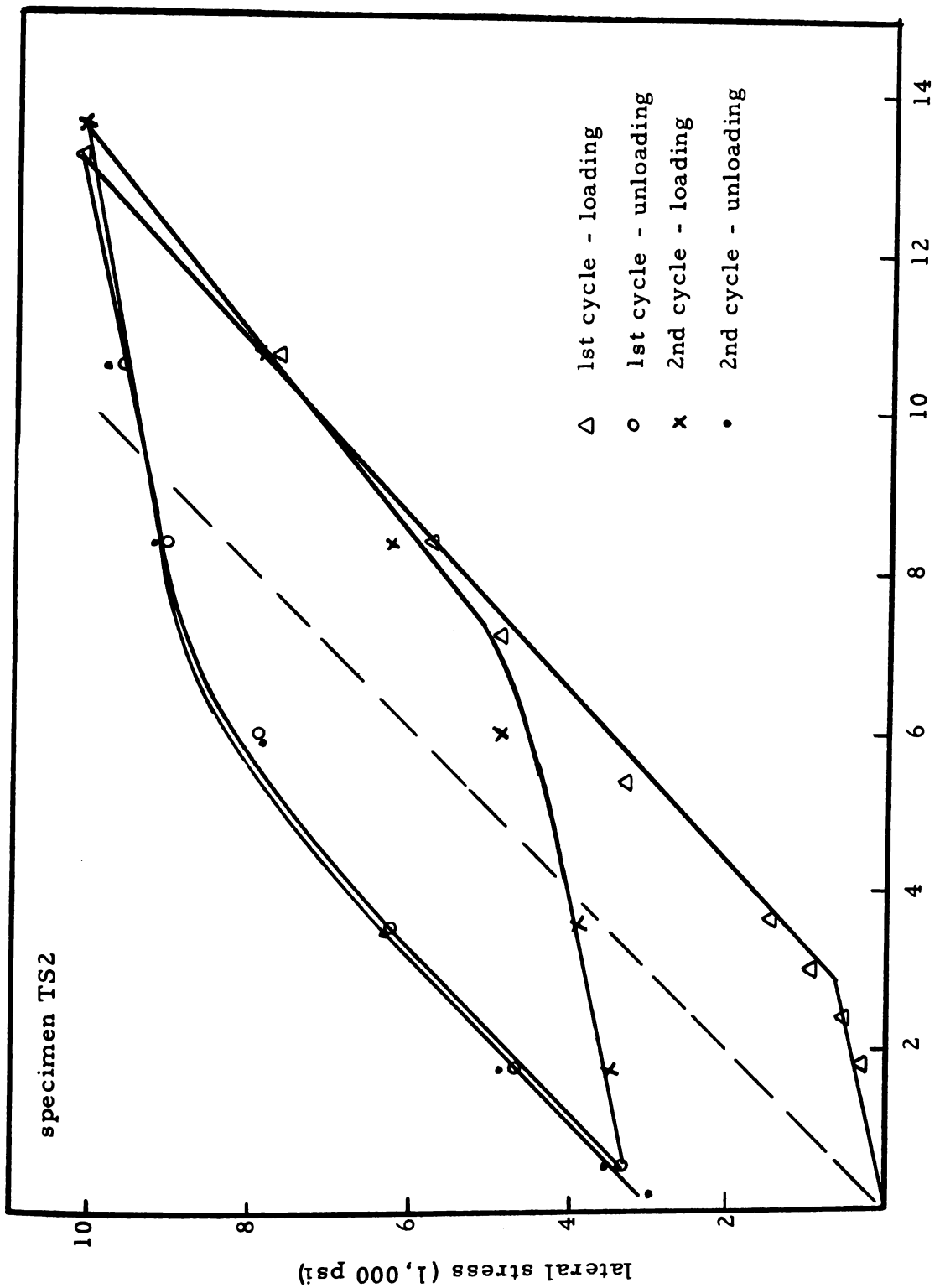

Fig. 5.9 Lateral stress versus axial stress in triaxial tests

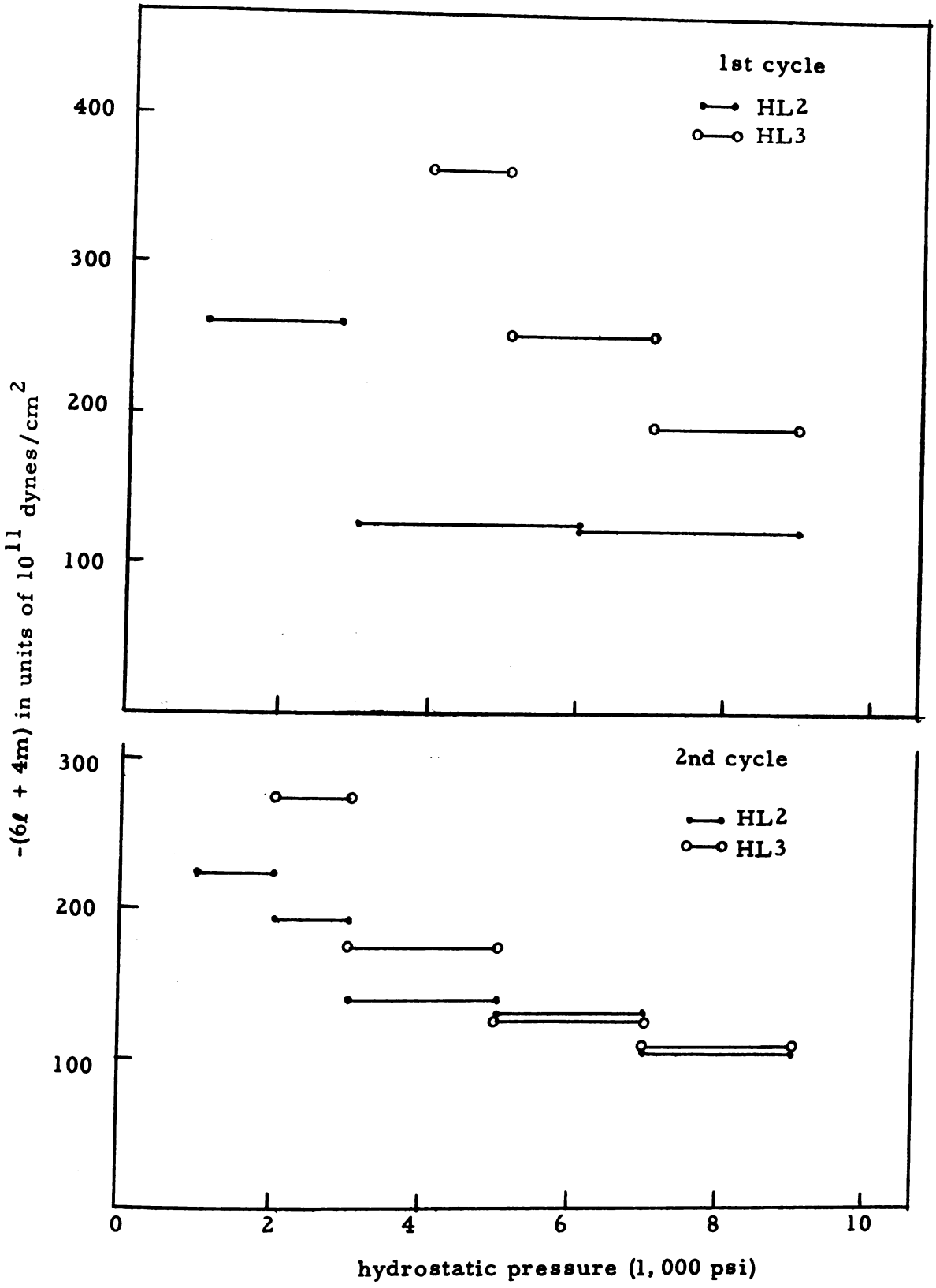

Fig. 5.10 Change of (6ℓ + 4m) with hydrostatic pressure

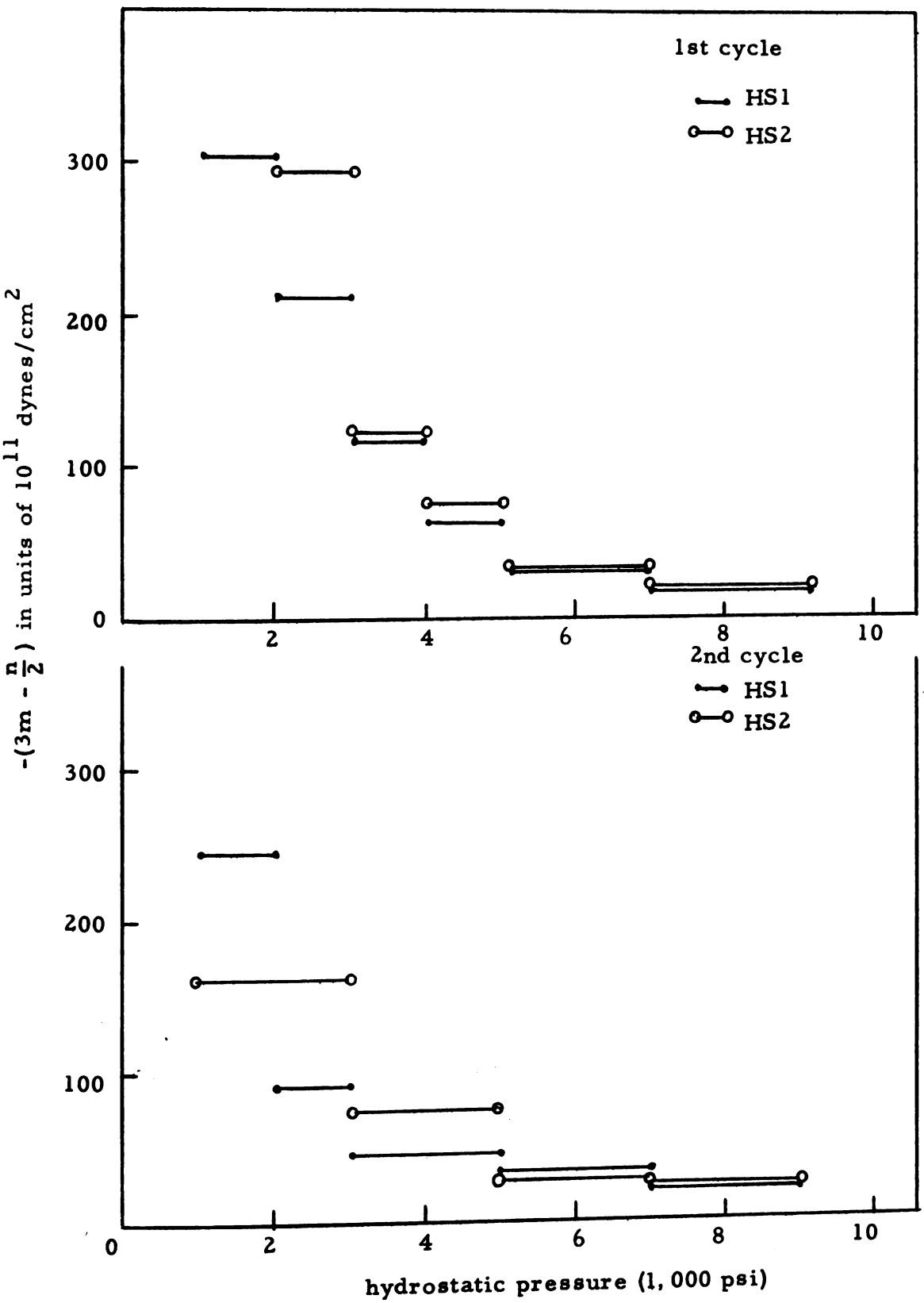

Fig. 5.11 Change of (3m - n/2) with hydrostatic pressure

$-(2\ell + 4m)$ in units of 10^{11} dynes/cm^2

$-(m)$ in units of 10^{11} dynes/cm^2

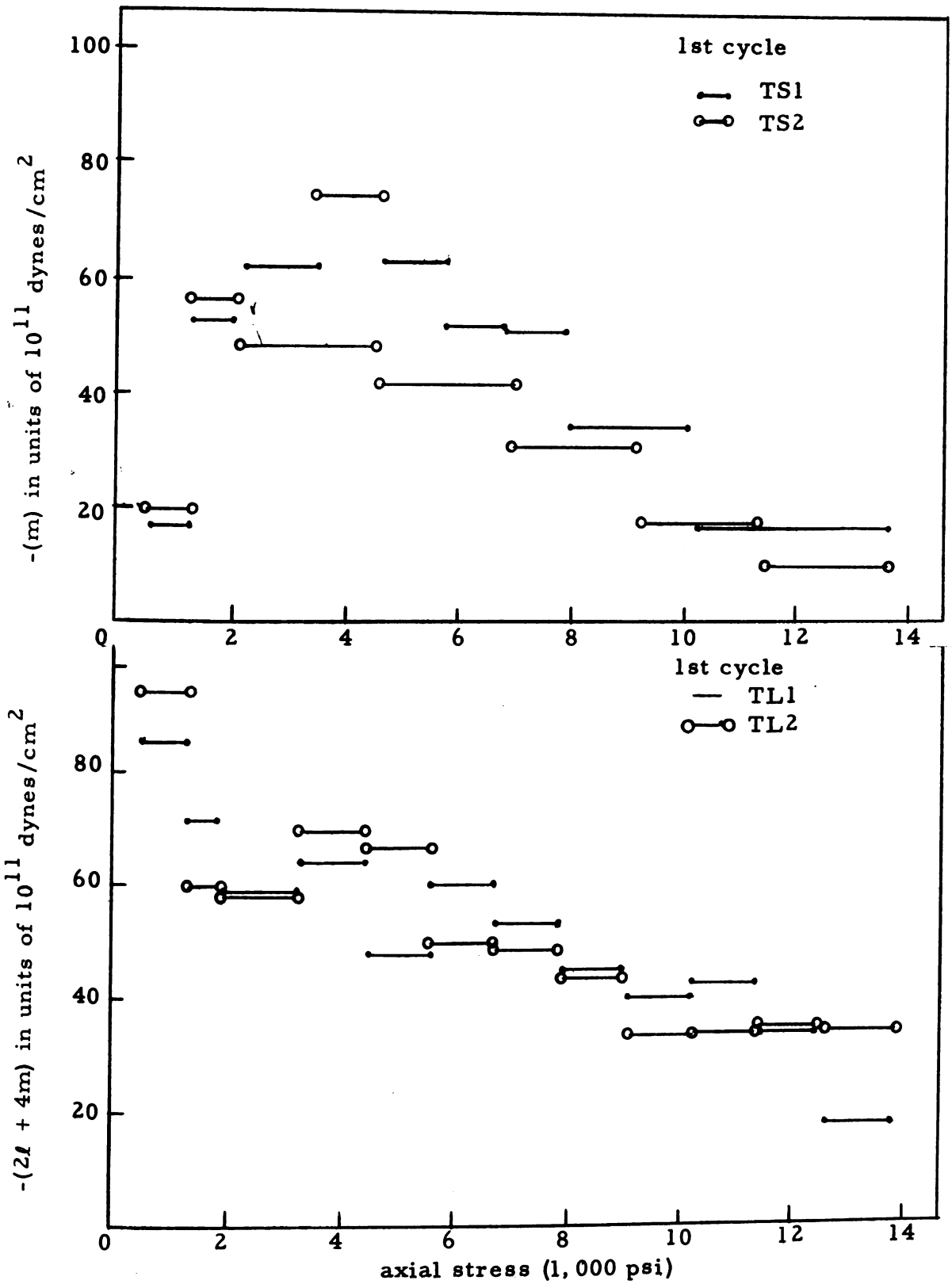

Fig. 5.12 Change of (2ℓ + 4m) and (m) in the triaxial test-first cycle

-(2ℓ + 4m) in unit of 10^{11} dynes/cm^2
80
60
40
20
(-m) in units of 10^{1} dynes/cm^2
60
40
20

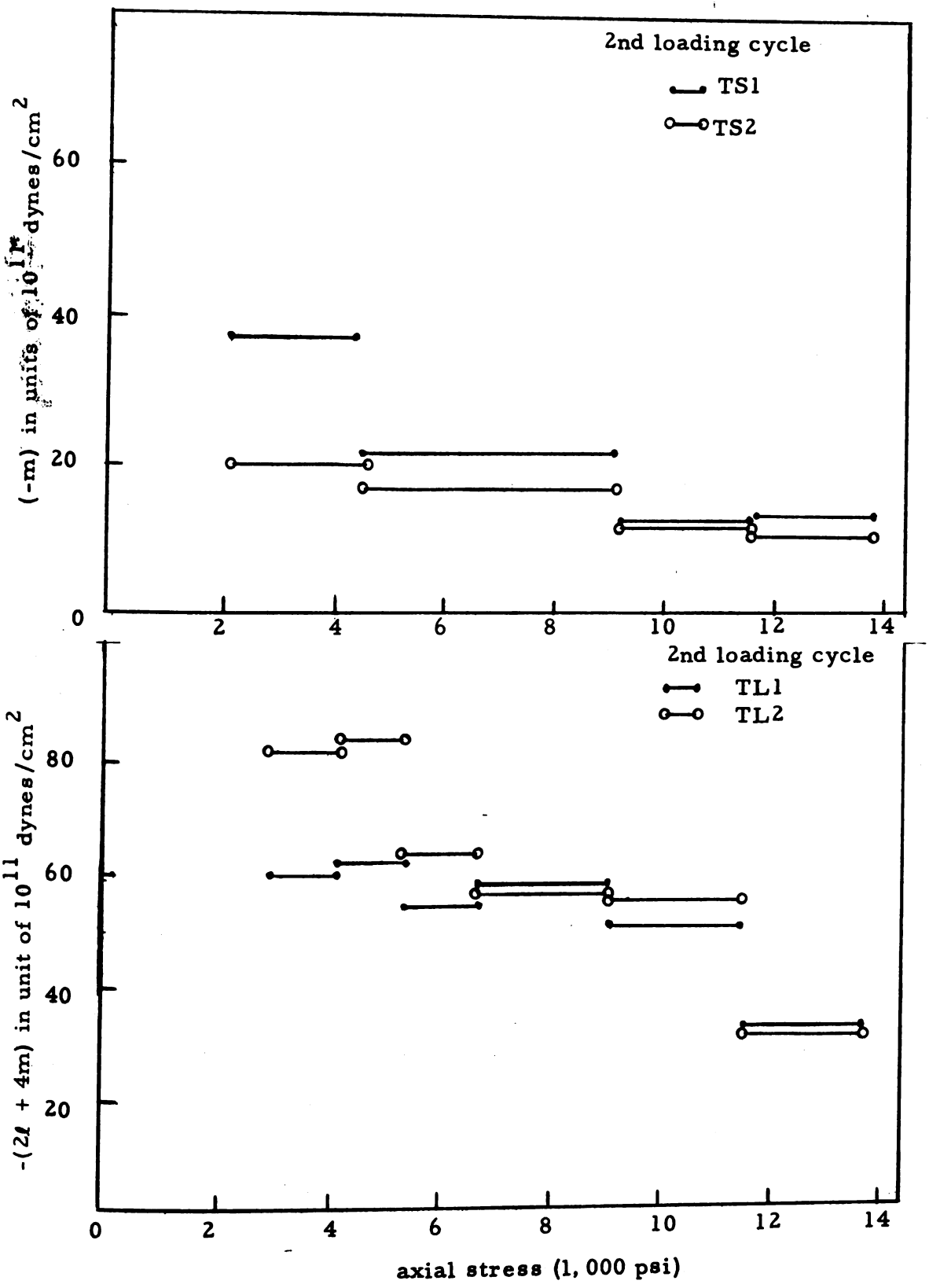

Fig. 5.13 Change of (2ℓ + 4m) and (m) in the triaxial test-second cycle

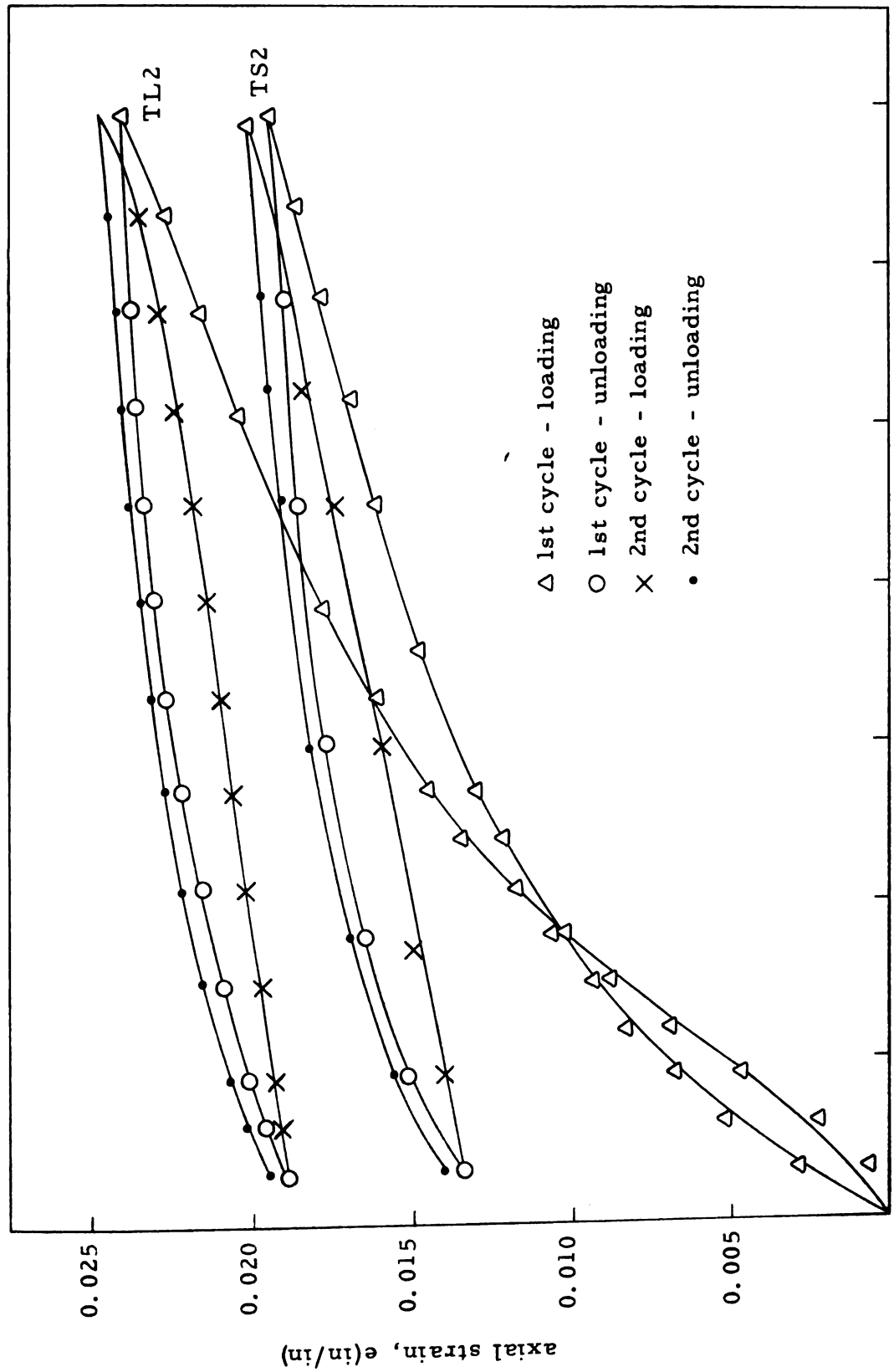

Fig. 5.14 Typical axial strain versus axial stress in triaxial tests

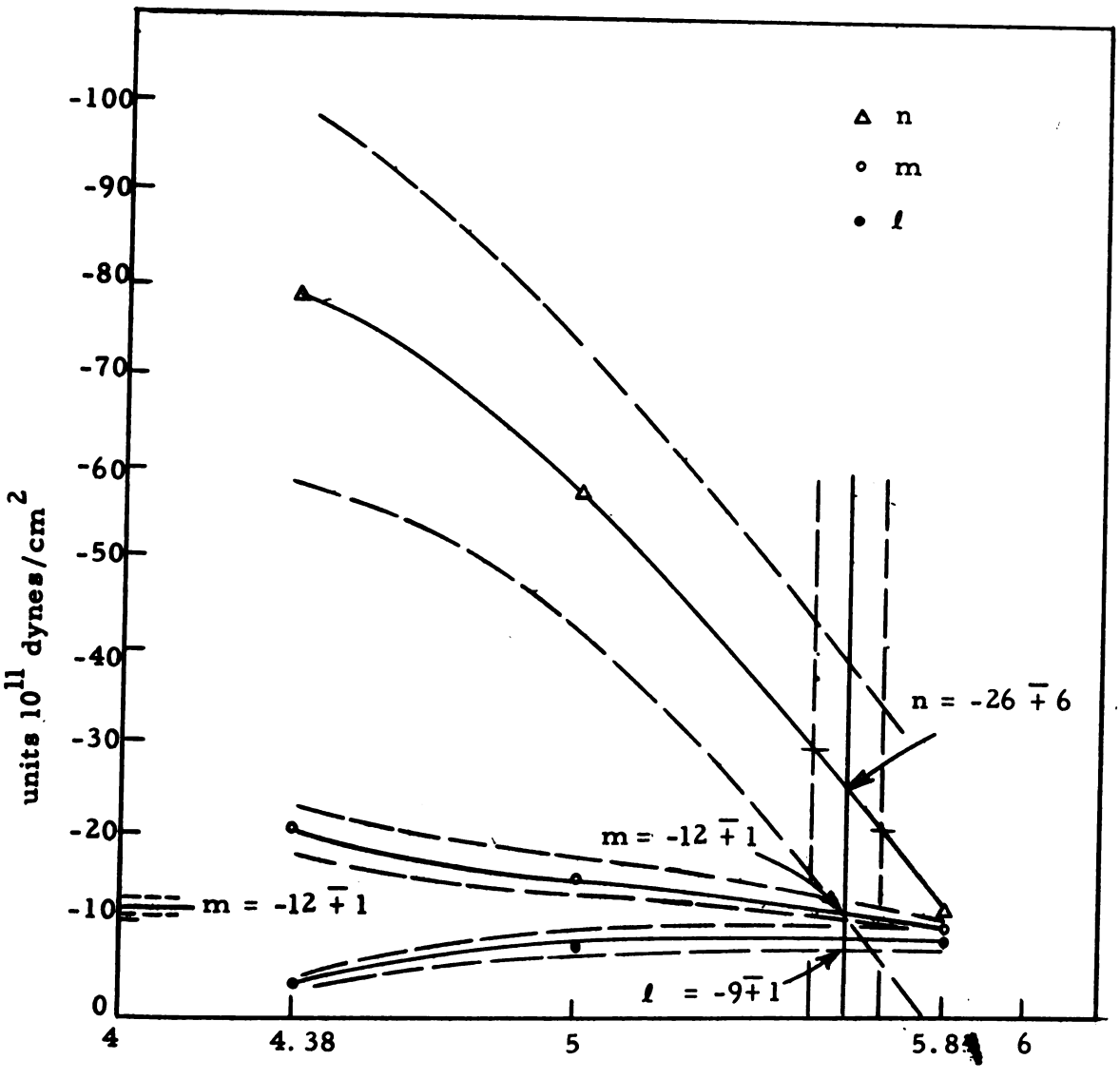

Fig. 5.15 Determination of the third order elastic constants of rock salt

Therefore, the final choice of ℓ, m and n is in close agreement with the measured values in seven tests but disagrees with $(2\ell + 4m)$ in the first loading cycle of the triaxial test. Therefore, the probability of the final choice of the values of ℓ, m and n is $\frac{7}{8}$.

5.8 Evaluation

The literature review did not reveal any work on the third-order elastic constants of rocks. However, the experimental values of ℓ, m and n obtained in this investigation are in agreement with Brillouin's predictions and Hughes'[30] experimental results which indicated that the third-order elastic constants are negative and larger than the second-order elastic constants λ and μ.

Bergman and Shahbender[5] measured the changes in longitudinal and shear wave velocities propagating in a direction perpendicular to the applied uniaxial stress in aluminum columns. They concluded that changes in shear wave velocities could be explained by changes in density and shear modulus while changes in longitudinal velocities could be explained by changes in density alone. However, the theoretical development of Hughes,[30] Rivlin,[56] Biot,[10] Bhagvantum,[6] and the present author indicate that changes in both longitudinal and shear waves are due to changes in both density and effective elastic moduli. Furthermore, the experimental results of Hughes and the present author

were in close agreement with the theory. Therefore, the present author cannot find any theoretical justification for Bergman and Shahbender's assumption that changes in longitudinal velocity are due to changes in density alone.

Hughes' experimental results provided the third-order elastic constants of Polystyrene, Armco iron and Pyrex. In the present investigation, the third-order elastic constants of rock salt were calculated from the changes in velocities at high stresses where the porosity effect is small. This suggests the possibility of measuring the third-order elastic constants of other solids. Consequently, it is reasonable to assume that for compact isotropic materials the changes in wave velocities due to known applied stresses can be predicted from theoretical considerations provided that ρ_o, λ, μ, ℓ, m and n are known.

The question arises whether a reverse procedure is possible, i.e., given ρ_o, λ, μ, ℓ, m and n for a compact material which is under the influence of unknown forces, is it possible to calculate the stresses from absolute velocity measurements in the material? This question is difficult to answer because of the limited available data on this subject. Furthermore, the theoretical development is restricted to the special cases of uniaxial stress (Hughes), hydrostatic compression (Hughes and present author), and homogeneous triaxial stress (Rivlin and present author). Essenaitlly, there are two things that must be considered.

First an assumption must be made regarding the stress distribution in the material to be tested, and second the stress-strain relationship and the history of the deformation must be known. The stress-strain relationship and history of the deformation are needed because the velocity equations include some functions of the strains and not stresses. Therefore, the answer to the question may be affirmative if the stresses can be uniquely determined from the strains and if an intelligent assumption can be made regarding the stress distribution, provided that all necessary velocities can be measured.

VI. GEOPHYSICAL APPLICATIONS

The theoretical and experimental investigations in this study may be extended to certain geophysical applications. Ultrasonic transducers might be placed at the ends of drill holes, which are filled with liquid pressure, for detection and transmission of waves.

The data obtained in the uniaxial compressive stress tests suggest that measurement of longitudinal velocities in the vertical and horizontal directions of mine pillars may indicate structural stability of the pillars.

Currently there are two theories regarding the nature of the underground stress field; the common hydrostatic theory and Serata's[61] triaxial theory which was reviewed in Section 2. Measurement of velocity in three mutually perpendicular directions could provide an experimental verification of either theory. Equal velocities indicate that the rock is still isotropic and thus the underground stress field is hydrostatic. If two velocities in the horizontal direction are equal but different from the velocity in the vertical direction, then the underground stress field is triaxial.

The data obtained in this investigation revealed that the changes in velocity at high pressure are reproducible.

The third-order elastic constants of rock salt were calculated from the intrinsic change in velocity. This suggests the possibility of extending the experimental data to determine the changes in overburden pressure with increasing depth by measuring the velocity of longitudinal or shear waves.

Wave velocity logging around underground cavities might indicate some correlation with the stress and strain distribution.

VII. CONCLUSIONS

1. Unstressed rock salt is nearly isotropic. The velocities measured in three mutually perpendicular directions in five-inch cubic specimens were relatively consistent with a maximum variation of less than 3%.
2. The average longitudinal velocity in rock salt is 4225 $\pm$ 1% meters/sec. The average shear wave velocity is 2450 $\pm$ 2% meters/sec.
3. The dynamic elastic moduli of rock salt are:

$$\text{Lamé's constants} \begin{cases} \lambda = (1.83 \pm 0.05) \times 10^6 \text{ psi} \\ \quad = (1.26 \pm 0.05) \times 10^{11} \text{ dynes/cm}^2 \\ \mu = (1.88 \pm 0.05) \times 10^6 \text{ psi} \\ \quad = (1.29 \pm 0.05) \times 10^{11} \text{ dynes/cm}^2 \end{cases}$$

Poisson's ratio, $\nu = (0.247 \pm 0.01)$

Young's modulus, $E = (4.68 \pm 0.10) \times 10^6$ psi

Bulk modulus, $K = (3.08 \pm 0.07) \times 10^6$ psi

4. The dynamic elastic moduli of rock salt are much higher than the corresponding static moduli. The dynamic value of the bulk modulus is in close agreement with the static bulk modulus as measured from a hydrostatic test.

5. Uniaxial compressive stress in rock salt produces an increase in velocity of longitudinal waves propagating along the axis of compression and a decrease in the velocity of longitudinal waves propagating in the lateral direction. The difference between the two velocities reaches 25% at 3,000 psi (about 75% of the salt crushing strength).
6. Longitudinal and shear wave velocities increase with an increase in hydrostatic pressure or triaxial stress with uniaxial strain. The rate of velocity increase is very fast at early stages of loading and approaches a steady slow rate at high loads. The initial rapid increase in velocity is not reproducible and can be explained as due to porosity effects. The small but steady increase in velocity at higher loads is reproducible and can be explained as due to intrinsic changes in the effective elastic moduli of rock salt.
7. The third-order elastic constants of rock salt were determined from the changes in velocity at high loads assuming that the porosity effects are negligible at the highest loads used. The calculated values are:

$$\ell = (-13.0 \pm 1.4) \times 10^{6} \text{ psi}$$
$$= (-9 \pm 1) \times 10^{11} \text{ dynes/cm}^2$$

$$m = (-17.4 \pm 1.4) \times 10^6 \text{ psi}$$
$$= (-12 \pm 1) \times 10^{11} \text{ dynes/cm}^2$$
$$n = (37.7 \pm 8.7) \times 10^6 \text{ psi}$$
$$= (-26 \pm 6) \times 10^{11} \text{ dynes/cm}^2$$

8. The experimental results did not show any correlation between the measured absolute velocities and magnitude of stress. Furthermore, there was no correlation with the transition from elastic to plastic states of stress.
9. Velocity changes at high stress levels were reproducible and indicated a correlation with the change in stress. This behavior might possibly be used to determine changes in overburden pressure with increasing depth in salt formations.
10. The data obtained from the uniaxial compressive stress tests suggest that measurement of longitudinal velocities in the vertical and horizontal directions of mine pillars may provide information about the development of fracture zones in the pillar.
11. Since ultrasonic waves are sensitive for the detection of the degree of anisotropy in a stressed medium, ultrasonic wave methods might be used to determine if the underground stress field is hydrostatic.

VIII. RECOMMENDATIONS FOR FUTURE STUDY

The following aspects of the effect of stress on wave propagation in solids are recommended for future study:

1. The literature review revealed a lack of experimental data on the third-order elastic constants of solids. A study of these constants is essential for any investigation of material behavior under high static stresses.

2. A general theoretical development to determine the necessary and sufficient velocities to be measured in order to determine unknown stresses.

3. A theoretical and experimental investigation to correlate the third-order elastic constants of single crystals with the non-linearity of intermolecular interactions as predicted by quantum mechanical analysis such as Born-Mayer theory of ionic crystals.

4. Determine the best experimental procedure to measure attenuation in stressed solids.

5. An experimental investigation, using wave reflection and refraction techniques, to detect the development of a plastic region in stressed solids.

6. Certain difficulties were encountered during the course of this study. Based on these difficulties, the following laboratory investigations on rock salt or other rocks are recommended:

   a. Repeat the same experiments with higher hydrostatic and triaxial compressions.
   b. Measure the longitudinal and shear wave velocities in the lateral direction in the triaxial test.
   c. Measure the changes of longitudinal and shear waves in the same specimen.
   d. Measure the wave velocities in biaxially compressed salt blocks.
   e. Measure the wave velocity in triaxially or biaxially stressed hollow salt blocks.
   f. During the course of this investigation the phenomenon of acoustic emission was observed. A laboratory investigation of this phenomenon in rocks might be helpful in studying slip between the grain boundaries of rocks.

BIBLIOGRAPHY

BIBLIOGRAPHY

1. Auberger, M. and J. S. Rinehart. "A new method for measurement of attenuation of ultrasonic longitudinal waves in plastics and rocks," Colorado School of Mines Bulletin, July, 1960.

2. Balakrishna, S. "Isotropic behavior of rocks," Current Science, Vol. 24, No. 4 (April, 1955), 117-118.

3. Benson, R. W. "Ultrasonic stress analysis," Ultrasonic News, Spring, 1962.

4. _____., and V. J. Realson. "Acoustoelasticity," Product Engineering, July 20, 1959, 56-59.

5. Bergman, R. H. and R. A. Shahbender. "Effect of statically applied stresses on velocity of propagation of ultrasonic waves," J. Appl. Phys., Vol. 29 (December, 1958), 1736-1738.

6. Bhagavantam, S. "Third order elasticity," Proc. of the Third Congress on Theoretical and Applied Mech., Bangalore, India, December, 1957.

7. _____., and T. R. Seshagiri. "Elastic properties of polycrystalline agregates," Proc. Indian Acad. of Sciences, Vol. 35A, No. 3 (1952), 129-135.

8. _____., and E. V. Chelam. "Elastic behavior of matter under very high pressure. Uniform compression," Proc. Indian Acad. of Sci., Vol. 52A, No. 1 (1960), 1-19.

9. Biot, M. A. "Non-linear theory of elasticity and the linearized case for a body under initial stress," Phil. Mag. 7th Series, Vol. 27 (1939), 468-487.

10. _____. "The influence of initial stress on elastic waves," J. of Appl. Phys., Vol. 11 (1940), 522-530.

11. Birch, F. "Finite elastic strains of cubic crystals," Physical Review, Vol. 71, No. 11 (June, 1947), 809-824.

12. _____. "The effect of pressure upon the elastic parameters of isotropic solids according to Murnaghan's theory of finite strains," J. of Appl. Phys., Vol. 9 (April, 1958), 279-288.

13. _____. "The velocity of compressional waves in rocks to 10 kilobars. Part I," J. Geophys. Research, Vol. 65, No. 4 (April, 1960), 1083-1102.

14. _____. "The velocity of compressional waves in rocks to 10 kilobars. Part 2," J. Geophys. Research, Vol. 66, No. 7 (July, 1961), 2199-2224.

15. Breck, H. R., S. W. Schoellhorns and R. B. Baum. "Velocity logging and its geological and geophysical applications," Bull. Am. Assoc. Petrol. Geologists., Vol. 41, No. 8 (1957).

16. Brillouin, L. Les Tenseurs. New York: Dover Publications, 1946.

17. Cady, W. G. Piezoelectricity. New York: McGraw-Hill Book Co., Inc., 1946.

18. Carlin, B. Ultrasonics. 2nd Edition. New York: McGraw-Hill Book Co., Inc., 1960.

19. Cook, R. K. "Variation of elastic constants and static strains with hydrostatic pressure: A method of calculation from ultrasonic measurements," J. Acoust. Soc. Am., Vol. 29 (1957), 445-449.

20. Chowdiah, A. M. "Stress and strain distribution around openings in underground salt formations," Ph.D. Thesis, Michigan State University, East Lansing, 1963.

21. Daniels, W. B. and C. S. Smith. "Pressure derivatives of the elastic constants of Copper, Silver and Gold to 10,000 bars," Physical Review, Vol. 111 (1958), 713-721.

22. Davids, N., editor. International Symposium on Stress Wave Propagation in Materials. New York: Interscience Publishers, Inc., 1960.

23. Eringen, A. C. Nonlinear Theory of Continuous Media. New York: McGraw-Hill Book Co., Inc., 1962.

24. Green, A. E., R. S. Rivlin, and R. T. Shield. "General theory of small elastic deformations superposed on finite elastic deformations," Proc. Roy. Soc. of London, Series A, Vol. 211 (February, 1952), 128-154.

25. Green, A. W. and W. Zerna. Theoretical Elasticity. New York: Oxford University Press, 1954.

26. Handin, J. W. and R. V. Hager, Jr. "Experimental deformation of sedimentary rocks under confining pressure: Tests at room temperature on dry samples," Am. Assoc. Pet. Geol., Bulletin 41, 1957, 1-50.

27. Hikata, A., R. Truell, A. Granato, B. Chick, and K. Lucke. "Sensitivity of ultrasonic attenuation and velocity changes to plastic deformation and recovery in Aluminum," J. Appl. Phys., Vol. 27 (1956), 396-404.

28. Holyman, H. W. "Seismograph evidence on the depth of salt columns, Moss Bluff Dome, Texas," Geophysics, 11, No. 2 (1946), 128-134.

29. Hughes, D. S. and J. H. Cross. "Elastic wave velocities in rocks at high pressures and temperatures," Geophysics, Vol. 16, No. 4 (October, 1951), 577-593.

30. _____., and J. L. Kelly. "Second-order elastic deformation of solids," Physical Review, Vol. 92, No. 5 (December, 1953), 1145-1149.

31. _____., and H. J. Jones. "Elastic wave velocities of sedimentary rocks," Am. Geophys. Union. Trans., Vol. 32, No. 2 (April, 1951), 173-178.

32. _____., and C. Maurette. "Variation of elastic wave velocities in basic igneous rocks with pressure and temperature," Geophysics, Vol. 22, No. 1 (January, 1957), 23-31.

33. _____., _____. "Variation of elastic wave velocities in granites with pressure and temperature," Geophysics, Vol. 21, No. 2 (April, 1956), 277-284.

34. Karus, E. V. and V. B. Zuckernik. "An ultrasonic apparatus for studying the physical and mechanical properties of rocks intersected by a drill-hole," Bull. Acad. Sci. USSR, Geophys. Ser., No. 4 (1958), 755-761.

35. Kittel, C. Introduction to Solid State Physics. 2nd Edition. New York: John Wiley and Sons, 1961.

36. Kolsky, H. Stress Waves in Solids. Oxford at the Clarendon Press, 1953.

37. Krishnamurthi, M. and S. Bulakrishna. "Measurement of ultrasonic velocity in some Indian rocks," Proc. Indian, Acad. Sciences, Vol. 38A (1953), 495-501.

38. _____., _____. "Attenuation of sound in rocks," Geophysics, Vol. 22, No. 2 (April, 1957), 268-274.

39. Lazarus, D. "The variation of adiabatic elastic constants of KCl, NaCl, CuZn, Cu and Al with pressure to 10,000 bars," Physical Review, Vol. 76 (1949), 545-553.

40. Love, A. E. H. A Treatise on the Mathematical Theory of Elasticity. 4th edition. New York: Dover Publications, 1926.

41. Mason, W. P. Physical Accoustics and Properties of Solids. Bell Laboratory series. Princeton: D. Van Nostrand Co., 1958.

42. _____. Piezoelectric Cyrstals and Their Application to Ultrasonics. Princeton: D. Van Nostrand Co., Inc., 1950.

43. McMaster, R. C., editor. Nondestructive Testing Handbook, Vol. II. New York: The Ronald Press Company, 1959.

44. McSkimin, H. J. "Notes and references for the measurement of elastic moduli by means of ultrasonic waves," J. Acoust. Soc. Am., Vol. 33, No. 5 (May, 1961), 606-615.

45. Morrison, D. M. "The transition test as a method for determining the triaxial properties of rocks in the condition of underground formations," M.S. Thesis, Michigan State University, E. Lansing, 1962.

46. Murnaghan, F. D. "Finite deformation of an elastic solid," Am. J. Math., Vol. 59 (1937), 235-260.

47. _____. Finite Deformation of an Elastic Solid. New York: John Wiley and Sons, Inc., 1951.

48. Nicholls, H. R., V. Hooker, and W. I, Duvall. "Dynamic rock mechanics investigations," Project Cowboy, U.S. Bureau of Mines, Applied Physics Research Laboratory, College Park, Maryland, September, 1960.

49. Olmsted, J. M. H. Advanced Calculus. New York: Appleton-Century-Crofts, Inc., 1961.

50. Pochhammer, L. "Ueber die Fortpflanzungeschwindigkeit Kliener Schwingungen in einem unbegrenzten isotropen Kreiscylinder," J. reine u. angew. Math, 81, 324, 1876.

51. Raman, A. B. "Elastic plastic transition tests," M.S. Thesis, Michigan State University, E. Lansing, 1962.

52. Rayleigh, L. Theory of Sound, Vol. 1. New York: Dover Publications, 1945.

53. Rinehart, J S., J. P. Fortin, and L. Burgin. "Propagation velocity of longitudinal waves in rocks. Effect of state of stress, stress level of the wave, water content, porosity, temperature, stratification and texture," Proceedings of the Fourth Symposium on Rock Mechanics, The Pennsylvania State University, University Park, Pennsylvania, March, 1961.

54. Rivlin, R. S. "Large elastic deformations of isotropic materials. I. Fundamental concepts," Phil. Trans. Roy. Soc. London, Vol. 240A (1948), 459-490.

55. _____. "Large elastic deformation of isotropic materials. IV. Further developments of the general theory," Phil. Trans. Roy. Soc. London. Vol. 241A (1948), 379-397.

56. _____., and M. Hayes. "Propagation of a plane wave in an isotropic elastic material subjected to pure homogeneous deformation," Arch. Rational Mech. and Analysis, Vol. 8 (1961), 15-22.

57. Riznichenko, Y. V. "The development of ultrasonic methods in seismology," Bull. Acad. Sci. USSR, Geophys. Ser., No. 11 (1957), 31-37.

58. Rollins, F. R. "Study of methods for nondestructive measurement of residual stress," WADC Tech. Report 59-561, Midwest Research Institute, December, 1959.

59. Seitz, F. The Modern Theory of Solids. New York: McGraw-Hill Book Co., 1940.

60. Serata, S. "Development of design principle for disposal of reactor fuel waste into underground salt cavities," Ph.D. Thesis, University of Texas, 1959.

61. _____. "Transition from Elastic to plastic states of rocks under triaxial compression." Proceedings of the 4th Symposium of Rock Mechanics held at Pennsylvania State University, University Park, Pennsylvania, April, 1961.

62. _____., and E. F. Gloyna. "Principles of structural stability of underground salt cavities," Journal of Geophysical Research, Vol. 65, No. 9 (September, 1960).

63. Silaeva, O. I. "Methods for the study of Elastic properties of rock samples under pressure," Bull. Acad. Sci. USSR Geophys. Series, 145-149, 1959.

64. _____., and O. G. Shamina. "The distribution of elastic pulses in cylindrical specimens," Bull. Acad. Sci. USSR, Geophys. Series (1958), 17-24.

65. Sternglass, E. J. and D. A. Stuart. "An experimental study of the propagation of transient longitudinal deformations in elastoplastic media," J. Appl. Mech., Vol. 20, No. 3 (September, 1953), 427-434.

66. The Committee on Waste Disposal of the Division of Earth Sciences, National Research Council, "The disposal of Radioactive waste on land," National Acad. of Science, April, 1957.

67. Tocher, D. "Anisotropy in Rocks under simple compression," Am. Geophys. Union. Trans., Vol. 38, No. 1 (Feburary, 1957), 89-94.

68. Toupin, R. A. and B. Bernstein. "Sound waves in deformed perfectly elastic materials. Acoustoelastic effect," J. Acoust. Soc. Am., Vol. 33, No. 2 (February, 1961), 216-225.

68a. Triffet, T. "Introduction to the mechanics of discontinua," Unpublished class notes. Applied Mechanics Department, Michigan State University, E. Lansing, Michigan, 1962.

69. Truesdell, C. "General and exact theory of waves in finite elastic strain," Arch. for Rational Mech. and Analysis, Vol. 8 (1961), 263-297.

70. Tu, L. Y., J. N. Brennan and J. A. Sauer. "Dispersion of ultrasonic pulse velocity in cylindrical rods," J. Acoust. Soc. Am., Vol. 27, No. 3 (May, 1955), 550-555.

71. Turnbull, H. W. The Theory of Determinants, Matrices, and Invariants. New York: Dover Publications, Inc., 1960.

72. Volarovich, M. P., D. B. Bulashov. "Study on the velocities of elastic waves in rock specimens at pressures up to 5,000 kg/cm^2," Bull. Acad. Sci. USSR, Geophys. Ser., No. 3 (1957), 319-324.

73. Wyllie, M. R. J., A. R. Gregory and G. H. F. Gardner. "An experimental investigation of factor affecting elastic wave velocities in porous media," Geophysics, Vol. 23, No. 3 (July, 1958), 459-493.

74. _____., _____., and L. W. Gardner. "Elastic wave velocities in heterogeneous and porous media," Geophysics, Vol. 21, No. 1 (January, 1956), 41-70.

75. Zener, C. Elasticity and Anelasticity of Metals. Chicago: The University of Chicago Press, 1960.

APPENDICES

APPENDIX I

$$\eta = \frac{1}{2}\,[J^{*}J - E_3]$$

$$J^{*} = [J^{*}_{ij}] = \begin{bmatrix} (1+b_{11})(1+B_{11}) & b_{21}(1+B_{11}) & b_{31}(1+B_{11}) \\ b_{12}(1+B_{22}) & (1+b_{22})(1+B_{22}) & b_{32}(1+B_{22}) \\ b_{13}(1+B_{33}) & b_{23}(1+B_{33}) & (1+b_{33})(1+B_{33}) \end{bmatrix} \quad \text{(A-1)}$$

$$J = [J_{ij}] = \begin{bmatrix} (1+b_{11})(1+B_{11}) & b_{12}(1+B_{22}) & b_{13}(1+B_{33}) \\ b_{21}(1+B_{11}) & (1+b_{22})(1+B_{22}) & b_{23}(1+B_{33}) \\ b_{31}(1+B_{11}) & b_{32}(1+B_{22}) & (1+b_{33})(1+B_{33}) \end{bmatrix} \quad \text{(A-2)}$$

$$E_3 = \begin{bmatrix} 1 & 0 & 0 \\ 0 & 1 & 0 \\ 0 & 0 & 1 \end{bmatrix}$$

where:

i indicates row and j column. For example $(J_{32}) = b_{23}(1+B_{33})$.

By regular matrix multiplication, $J^{*}J$ is a square matrix of dimension 3 whose elements are:[71]

$$(J^{*}J)_{ik} = \sum_{j=1}^{3} J^{*}_{ij}\, J_{jk}$$

$$(J^{*}J)_{11} = \sum_{j=1}^{3} J^{*}_{1j}\, J_{j1}$$

$$= J^{*}_{11}\, J_{11} + J^{*}_{12}\, J_{21} + J^{*}_{13}\, J_{31}$$

$$= (1+b_{11})^2(1+B_{11})^2 + b_{21}^2\,(1+B_{11})^2 + b_{31}^2\,(1+B_{11})^2$$

$$= 1 + 2B_{11} + B_{11}^2 + 2b_{11} + 4b_{11}B_{11} + \text{higher order terms.}$$

Thus:

$$\eta_1 = \eta_{11} = \frac{1}{2}[(J^*J)_{11} - 1]$$

$$= b_{11} + B_{11} + 2b_{11}\,B_{11} + \frac{B_{11}^2}{2} \qquad \text{(A-3)}$$

By similar procedure,

$$\eta_2 = \eta_{22} = b_{22} + B_{22} + 2b_{22}\,B_{22} + \frac{B_{22}^2}{2}$$

$$\eta_3 = \eta_{33} = b_{33} + B_{33} + 2b_{33}\,B_{33} + \frac{B_{33}^2}{2}$$

$$(J^*J)_{12} = \sum_{j=1}^{3} J_{1j}^*\,J_{j2} = J_{11}^*\,J_{12} + J_{12}^*\,J_{22} + J_{13}^*\,J_{32}$$

$$= (1+b_{11})(1+B_{11})\,b_{12}(1+B_{22}) + b_{21}(1+B_{11})(1+b_{22})(1+B_{22})$$

$$+ b_{31}(1+B_{11})\,b_{32}(1+B_{22})$$

$$= (b_{12} + b_{21})(1+B_{11} + B_{22}) + \text{higher order terms.}$$

Similarly $(J^*J)_{21} = (J^*J)_{12}$

Therefore,

$$\eta_6 = \eta_{12} = \eta_{21} = \frac{1}{2}\,[(J^*J)_{12} - 0]$$

$$= \frac{b_{12} + b_{21}}{2}\,(1+B_{11} + B_{22})$$

By similar procedure,

$$\eta_5 = \eta_{13} = \eta_{31} = \frac{b_{13} + b_{31}}{2}\,(1+B_{11} + B_{33})$$

$$\eta_4 = \eta_{23} = \eta_{32} = \frac{b_{23} + b_{32}}{2}\,(1+B_{22} + B_{33})$$

APPENDIX II

$$\phi = \left(\frac{\lambda + 2\mu}{2}\right) I_1^2 - 2\mu I_2 + \left(\frac{\ell+2m}{3}\right) I_1^3 - 2mI_1I_2 + nI_3 \quad \text{(A-5)}$$

I_1, I_2 and I_3 are functions of the symmetric matrix η.

Therefore,

$$\frac{\partial\phi}{\partial\eta} = (\lambda+2\mu)\, I_1\left(\frac{\partial I_1}{\partial\eta}\right) - 2\mu\left(\frac{\partial I_2}{\partial\eta}\right) + (\ell+2m) I_1^2 \left(\frac{\partial I_1}{\partial\eta}\right)$$

$$-2mI_1 \left(\frac{\partial I_2}{\partial\eta}\right) - 2mI_2\left(\frac{\partial I_1}{\partial\eta}\right) + n\left(\frac{\partial I_3}{\partial\eta}\right) \quad \text{(A-6)}$$

$\frac{\partial\phi}{\partial\eta}$ is a symmetric matrix according to the following theorem from Murnaghan.[47]

> "If f(A) is a function, written symmetrically, of the symmetric matrix A, then $\frac{\partial f}{\partial A}$ is, like A, a symmetric matrix."

By the same theorem, the gradients of I_1, I_2 and I_3 with respect to η, are symmetric, given by:[47]

$$\frac{\partial I_1}{\partial\eta} = E_3$$

$$\frac{\partial I_2}{\partial\eta} = I_1\, E_3 - \eta \quad \text{(A-7)}$$

$$\frac{\partial I_3}{\partial\eta} = \text{cof}\ \eta$$

where:

cof η means cofactor* of η

$$\text{cof } \eta = \begin{bmatrix} \begin{vmatrix} \eta_2 & \eta_4 \\ \eta_4 & \eta_3 \end{vmatrix} & - \begin{vmatrix} \eta_6 & \eta_4 \\ \eta_5 & \eta_3 \end{vmatrix} & \begin{vmatrix} \eta_6 & \eta_2 \\ \eta_5 & \eta_4 \end{vmatrix} \\ - \begin{vmatrix} \eta_6 & \eta_5 \\ \eta_4 & \eta_3 \end{vmatrix} & \begin{vmatrix} \eta_1 & \eta_5 \\ \eta_5 & \eta_3 \end{vmatrix} & - \begin{vmatrix} \eta_1 & \eta_6 \\ \eta_5 & \eta_4 \end{vmatrix} \\ \begin{vmatrix} \eta_6 & \eta_5 \\ \eta_2 & \eta_4 \end{vmatrix} & - \begin{vmatrix} \eta_1 & \eta_5 \\ \eta_6 & \eta_4 \end{vmatrix} & \begin{vmatrix} \eta_1 & \eta_6 \\ \eta_6 & \eta_2 \end{vmatrix} \end{bmatrix} \qquad \text{(A-8)}$$

It is important to note that in the process of differentiation, the symmetry of the strain matrix is neglected and the nine elements of η are regarded as independent elements. For example, I_2 is given by equation (3.28) as,

$$I_2 = \eta_2\ \eta_3 - \eta_4^{\,2} + \eta_3\ \eta_1 - \eta_5^{\,2} + \eta_1\ \eta_2 - \eta_6^{\,2}$$

In this form $\dfrac{\partial I_2}{\partial \eta_4} = -2\eta_4$ which is wrong. To get the right answer the elements of $\eta_4^{\,2}$ must be considered to be independent. Thus,

$$-\eta_4^{\,2} = -\ \eta_{23}\ \eta_{32}$$

and $\dfrac{\partial I_2}{\partial \eta_{23}} = -\ \eta_{32} = -\ \eta_4$

*If A is any square matric of dimension n, the cofactor matrix of A (denoted by cof A) is the matrix obtained by replacing each element of A by its cofactor, the cofactor of Apq being the product of the determinant of the (n-1) dimensional matrix, obtained by erasing the p column and q row of A, by $(-1)^{p+q}$.

$$\frac{\partial I_2}{\partial \eta_{32}} = - \eta_{23} = - \eta_4$$

and

$$\frac{\partial I_2}{\partial \eta_4} = \frac{\partial I_2}{\partial \eta_{23}} = \frac{\partial I_2}{\partial \eta_{32}} = - \eta_4$$

Combining Eqs. (A-6) and (A-7) yields:

$$\frac{\partial \phi}{\partial \eta} = \lambda I_1 E_3 + 2\mu \eta + (\ell I_1^2 - 2mI_2) E_3 + 2mI_1 \eta + n \text{ cof } \eta \quad \text{(A-9)}$$

or,

$$\frac{\partial \phi}{\partial \eta_1} = \lambda I_1 + 2\mu \eta_1 + \ell I_1^2 - 2m I_2 + 2m I_1 \eta_1 + (\eta_2 \eta_3 - \eta_4^2) n$$

$$\frac{\partial \phi}{\partial \eta_2} = \lambda I_1 + 2\mu \eta_2 + \ell I_1^2 - 2m I_2 + 2m I_1 \eta_2 + (\eta_1 \eta_3 - \eta_5^2) n$$

$$\frac{\partial \phi}{\partial \eta_3} = \lambda I_1 + 2\mu \eta_3 + \ell I_1^2 - 2m I_2 + 2m I_1 \eta_3 + (\eta_1 \eta_2 - \eta_6^2) n$$

$$\frac{\partial \phi}{\partial \eta_4} = 2\mu \eta_4 + 2m I_1 \eta_4 + (\eta_6 \eta_5 - \eta_1 \eta_4) n$$

$$\frac{\partial \phi}{\partial \eta_5} = 2\mu \eta_5 + 2m I_1 \eta_5 + (\eta_6 \eta_4 - \eta_2 \eta_5) n \quad \text{(A-10)}$$

$$\frac{\partial \phi}{\partial \eta_6} = 2\mu \eta_6 + 2m I_1 \eta_6 + (\eta_4 \eta_5 - \eta_6 \eta_3) n$$

The strains in the formulas above can be expressed in terms of b_{ij} and B_{ij} as follows:

$$I_1 = \eta_1 + \eta_2 + \eta_3$$

Substituting for η_1, η_2 and η_3 from Appendix I, yields:

$$I_1 = B + b + 2 (b_{11} B_{11} + b_{22} B_{22} + b_{33} B_{33}) + \frac{B_{11}^2}{2} + \frac{B_{22}^2}{2} + \frac{B_{33}^2}{2} \quad \text{(A-11)}$$

where:

$$B = B_{11} + B_{22} + B_{33}$$

$$b = b_{11} + b_{22} + b_{33}$$

$$I_1^2 = B^2 + 2\,Bb + \text{higher order terms.} \qquad \text{(A-12)}$$

$$I_2 = \eta_2\,\eta_3 + \eta_3\,\eta_1 + \eta_1\,\eta_2 - (\eta_4^2 + \eta_5^2 + \eta_6^2)$$

From Appendix I; η_4, η_5, η_6 have terms of b_{ij} appearing alone. Therefore, the squares of these strains are neglected and I_2 is written as:

$$I_2 = \eta_2\,\eta_3 + \eta_3\,\eta_1 + \eta_1\,\eta_2$$

$$\eta_2\,\eta_3 = b_{22}B_{33} + b_{33}B_{22} + B_{22}B_{33} + \text{higher order terms}$$

$$\eta_3\,\eta_1 = b_{33}B_{11} + b_{11}B_{33} + B_{11}B_{33} + \text{higher order terms} \qquad \text{(A-13)}$$

$$\eta_1\,\eta_2 = b_{11}B_{22} + b_{22}B_{11} + B_{11}B_{22} + \text{higher order terms}$$

Therefore:

$$I_2 = b_{11}(B_{22}+B_{33}) + b_{22}(B_{11}+B_{33}) + b_{33}(B_{22}+B_{11}) + B_{22}B_{33} + B_{11}B_{33} + B_{11}B_{22} \qquad \text{(A-14)}$$

$$\eta_1 I_1 = B\,B_{11} + bB_{11} + b_{11}B$$

$$\eta_2 I_2 = B\,B_{22} + bB_{22} + b_{22}B \qquad \text{(A-15)}$$

$$\eta_3 I_3 = B\,B_{33} + bB_{33} + b_{33}B$$

$$I_1\eta_4 = [B+b+2\,(b_{11}B_{11} + b_{22}B_{22} + b_{33}B_{33}) + \tfrac{1}{2}\,(B_{11}^2 + B_{22}^2 + B_{33}^2)]\,[\frac{b_{23} + b_{32}}{2}\,(1 + B_{22} + B_{33})]$$

$$I_1\ \eta_4 = \frac{B}{2}\ (b_{23} + b_{32})$$

Similarly,

$$I_1\ \eta_5 = \frac{B}{2}\ (b_{13} + b_{31}) \qquad \text{(A-16)}$$

$$I_1\ \eta_6 = \frac{B}{2}\ (b_{12} + b_{21})$$

$$\eta_4^{\,2} = \eta_5^{\,2} = \eta_6^{\,2} = \eta_6\ \eta_5 = \eta_6\ \eta_4 = \eta_4\ \eta_5 = 0 \qquad \text{(A-17)}$$

$$\eta_1\ \eta_4 = \frac{B_{11}}{2}\ (b_{23} + b_{32})$$

$$\eta_2\ \eta_5 = \frac{B_{22}}{2}\ (b_{13} + b_{31}) \qquad \text{(A-18)}$$

$$\eta_6\ \eta_3 = \frac{B_{33}}{2}\ (b_{12} + b_{21})$$

From Eq. (A-10),

$$\frac{\partial \phi}{\partial \eta_1} = \frac{\partial \phi}{\partial \eta_{11}} = \lambda\ I_1 + 2\mu\ \eta_1 + \ell I_1^{\,2} + 2m(I_1\eta_1 - I_2) + n(\eta_2\ \eta_3 - \eta_4^{\,2})$$

Substituting for the strains and strain invariants yields:

$$\frac{\partial \phi}{\partial \eta_1} = \lambda[B + b + 2(b_{11}B_{11} + b_{22}B_{22} + b_{33}B_{33}) + \tfrac{1}{2}(B_{11}^{\,2} + B_{22}^{\,2} + B_{33}^{\,2})]$$

$$+ 2\mu\ [B_{11} + b_{11} + 2b_{11}B_{11} + \frac{B_{11}^{\,2}}{2}] + \ell\ [B^2 + 2bB]$$

$$+ 2m\Big[[BB_{11} + bB_{11} + b_{11}B] - [b_{11}(B_{22} + B_{33}) + b_{22}(B_{11} + B_{33})$$

$$+ b_{33}(B_{22} + B_{11}) + B_{22}B_{33} + B_{11}B_{33} + B_{11}B_{22}]\Big]$$

$$+ n[b_{22}B_{33} + b_{33}B_{22} + B_{22}B_{33}]$$

$$\frac{\partial \phi}{\partial \eta_1} = \lambda \left[B+b+2(b_{11}B_{11} + b_{22}B_{22} + b_{33}B_{33}) + \frac{1}{2}(B_{11}^2 + B_{22}^2 + B_{33}^2)\right] + 2\mu \left[B_{11} + b_{11} + 2b_{11}B_{11} + \frac{B_{11}^2}{2}\right] + \ell[B^2+2bB] + 2m\left[B_{11}^2 + 2b_{11}B_{11} - b_{22}B_{33} - b_{33}B_{22} - B_{22}B_{33}\right] + n\left[b_{22}B_{33} + b_{33}B_{22} + B_{22}B_{33}\right] \quad \text{(A-19)}$$

$\frac{\partial \phi}{\partial \eta_{22}} = \frac{\partial \phi}{\partial \eta_2}$ and $\frac{\partial \phi}{\partial \eta_{33}} = \frac{\partial \phi}{\partial \eta_3}$ are written from $\frac{\partial \phi}{\partial \eta_1}$ by cyclic permutation of the numbers 1, 2, 3.

$$\frac{\partial \phi}{\partial \eta_4} = \frac{\partial \phi}{\partial \eta_{23}} = \frac{\partial \phi}{\partial \eta_{32}} = 2\mu\ \eta_4 + 2mI_1\eta_4 + n(\eta_6\eta_5 - \eta_1\eta_4) + 2\mu\left[\frac{b_{23} + b_{32}}{2}(1+B_{22}+B_{33})\right] + 2m\left[\frac{b_{23} + b_{32}}{2}(B)\right] + n\left[\frac{b_{23} + b_{32}}{2}(-B_{11})\right]$$

$$\frac{\partial \phi}{\partial \eta_4} = \frac{b_{23} + b_{32}}{2}\left[2\mu\ (1+B_{22}+B_{33}) + 2mB - nB_{11}\right]$$

Similarly,

$$\frac{\partial \phi}{\partial \eta_5} = \frac{b_{13} + b_{31}}{2}\left[2\mu(1+B_{11}+B_{33})+2mB - nB_{22}\right] \quad \text{(A-20)}$$

$$\frac{\partial \phi}{\partial \eta_6} = \frac{b_{12} + b_{21}}{2}\left[2\mu(1+B_{11}+B_{22})+2mB - nB_{33}\right]$$

where:

$$\frac{\partial \phi}{\partial \eta_5} = \frac{\partial \phi}{\partial \eta_{13}} = \frac{\partial \phi}{\partial \eta_{31}}$$

$$\frac{\partial \phi}{\partial \eta_6} = \frac{\partial \phi}{\partial \eta_{12}} = \frac{\partial \phi}{\partial \eta_{21}}$$

APPENDIX III

$$\sigma = \frac{\rho}{\rho_o} J \frac{\partial \Phi}{\partial \eta} J^* \tag{A-21}$$

$$\frac{\rho}{\rho_o} = \frac{1}{\text{Det } J} = (1-2I_1 + 4I_2 + 8I_3)^{-\frac{1}{2}} \tag{A-22}$$

The elements of J, (J_{ij}) are given in Appendix I, Eq. (A-2). The elements of J^*, (J^*_{ij}) are given in Appendix I, Eq. (A-1). $\frac{\partial \Phi}{\partial \eta}$ is a symmetric square matrix of dimension 3, and can be written as:

$$\frac{\partial \Phi}{\partial \eta} = \begin{bmatrix} \Phi_{11} & \Phi_{12} & \Phi_{13} \\ \Phi_{21} & \Phi_{22} & \Phi_{23} \\ \Phi_{31} & \Phi_{32} & \Phi_{33} \end{bmatrix}$$

where:

$$\Phi_{ij} = \frac{\partial \Phi}{\partial \eta_{ij}} \quad \text{and} \quad \Phi_{ij} = \Phi_{ji}$$

The elements of (Φ_{ij}) are given in Appendix II, Eqs. (A-19) and (A-20).

Let $N = J \frac{\partial \Phi}{\partial \eta} J^*$ (A-23)

Then N is a symmetric square matrix of dimension 3 whose elements are given by:[71]

$$N_{ir} = \sum_{j=1}^{3} \sum_{k=1}^{3} J_{ij}\ \Phi_{jk}\ J^*_{kr}$$

$$N_{11} = \sum_{j=1}^{3} \sum_{k=1}^{3} J_{1j}\ \Phi_{jk}\ J^*_{k1}$$

$$= \sum_{j=1}^{3} J_{1j}\ \Phi_{j1}\ J^*_{11} + J_{1j}\ \Phi_{j2}\ J^*_{21} + J_{1j}\ \Phi_{j3}\ J^*_{31}$$

$$N_{11} = J_{11}\ \Phi_{11}\ J^*_{11} + J_{11}\ \Phi_{12}\ J^*_{21} + J_{11}\ \Phi_{13}\ J^*_{31}$$

$$+ J_{12}\ \Phi_{21}\ J^*_{11} + J_{12}\ \Phi_{22}\ J^*_{21} + J_{12}\ \Phi_{23}\ J^*_{31}$$

$$+ J_{13}\ \Phi_{31}\ J^*_{11} + J_{13}\ \Phi_{32}\ J^*_{21} + J_{13}\ \Phi_{33}\ J^*_{31}$$

All terms of Φ_{ij}, $i \neq j$ contain terms of b_{rn} or B_{rn}. All terms of J_{ij} or J^*_{ij}, $i \neq j$ contain terms of b_{rn}. All terms of J_{ij} or J^*_{ij}, $i = j$ contain terms of order 1.

Thus, all terms of Φ_{ij}, $i \neq j$ multiplied by J_{rn} or J^*_{rn}, $r \neq n$, are higher order terms. Similarly all terms of Φ_{ij}, $i \neq j$, multiplied by the product $J_{rn}\ J^*_{km}$, $r \neq n$ and $k \neq m$, are higher order terms.

Therefore,

$$N_{11} = J_{11}\ \Phi_{11}\ J^*_{11} + \text{higher order terms}$$

$$= (1+b_{11})^2\ (1+B_{11})^2\ \Phi_{11}$$

$$= (1 + 2\ b_{11} + 2\ B_{11})\ \Phi_{11} + \text{higher order terms}$$

or

$$N_1 = (1 + 2\ b_{11} + 2\ B_{11})\ \Phi_1 \qquad \text{(A-24)}$$

By similar procedure, it can be shown that:

$$N_2 = N_{22} = (1 + 2\, b_{22} + 2\, B_{22})\ \Phi_2$$

$$N_3 = N_{33} = (1 + 2\, b_{33} + 2\, B_{33})\ \Phi_3$$

and

$$N_4 = N_{23} = N_{32} = b_{32}\ \Phi_2 + (1 + B_{22} + B_{33})\ \Phi_4 + b_{23}\ \Phi_3$$

$$N_5 = N_{31} = N_{13} = b_{13}\ \Phi_3 + (1 + B_{33} + B_{11})\ \Phi_5 + b_{31}\ \Phi_1 \qquad \text{(A-25)}$$

$$N_6 = N_{12} = N_{21} = b_{21}\ \Phi_1 + (1 + B_{11} + B_{22})\ \Phi_6 + b_{12}\ \Phi_2$$

$\frac{\rho}{\rho_o}$ can now be approximated as:

$$\frac{\rho}{\rho_o} = 1 - I_1 + \text{higher order terms}$$

$$= 1 - B - b$$

where:

$$B = B_{11} + B_{22} + B_{33}$$

$$b = b_{11} + b_{22} + b_{33}$$

The higher order terms of $\frac{\rho}{\rho_o}$ are neglected because their products with N are all higher order terms.

The stress σ_{11} is now given by:

$$\sigma_1 = \sigma_{11} = \frac{\rho}{\rho_o} N_1$$

$$= (1 + 2\, b_{11} - b + 2B_{11} - B)\ \Phi_1$$

substituting for Φ_1 from (A-19) yields

$$\sigma_1 = \lambda\,[B + b + 2(b_{11}B_{11} + b_{22}B_{22} + b_{33}B_{33}) + \tfrac{1}{2}\,(B_{11}^{\,2} + B_{22}^{\,2} + B_{33}^{\,2})$$

$$+ B\,(2\,b_{11} - b) + (2\,B_{11} - B)\,(B + b)]$$

$$+ 2\mu[B_{11} + b_{11} + 2\,b_{11}B_{11} + \frac{B_{11}^{\,2}}{2} + B_{11}(2\,b_{11} - b)$$

$$+ (2\,B_{11} - B)(B_{11} + b_{11})]$$

$$+ \ell\,[B^2 + 2\,b\,B]$$

$$+ 2m\,[B_{11}^{\,2} + 2\,b_{11}B_{11} - b_{22}B_{33} - b_{33}B_{22} - B_{22}B_{33}]$$

$$+ n\,[b_{22}B_{33} + b_{33}B_{22} + B_{22}B_{33}]$$

Collecting terms of b_{11}, b_{22} and b_{33} yields;

$$\sigma_1 = [\lambda(B + \tfrac{3}{2}\,B_{11}^{\,2} - \frac{B_{22}^{\,2}}{2} - \frac{B_{33}^{\,2}}{2} - 2\,B_{22}B_{33})$$

$$+ 2\mu\,(B_{11} + \tfrac{3}{2}\,B_{11}^{\,2} - B_{11}\,B_{22} - B_{11}\,B_{33})$$

$$+ \ell(B^2) + 2m\,(B_{11}^{\,2} - B_{22}\,B_{33}) + n\,(B_{22}\,B_{33})]$$

$$+ b_{11}\,[\lambda(1+4\,B_{11}) + 2\mu(1 + 4\,B_{11} - B_{22} - B_{33})$$

$$+ \ell(2B) + m\,(4\,B_{11})]$$

$$+ b_{22}\,[\lambda(1-2\,B_{33}) + 2\mu(-B_{11}) + \ell(2B) + m(-2B_{33})$$

$$+ n\,(B_{33})]$$

$$+ b_{33}\,[\lambda(1-2\,B_{22}) + 2\mu\,(-B_{11}) + \ell(2B) + m(-2B_{22})$$

$$+ n\,(B_{22})]$$

(A-26)

Similarly σ_2 and σ_3 are written by cyclic permutation of the numbers 1, 2, 3

$$\begin{aligned}\sigma_2 = {} & [\lambda(B + \tfrac{3}{2} B_{22}^2 - \frac{B_{33}^2}{2} - \frac{B_{11}^2}{2} - 2 B_{33} B_{11}) \\ & + 2\mu (B_{22} + \tfrac{3}{2} B_{22}^2 - B_{22}B_{33} - B_{22}B_{11}) \\ & + \ell(B^2) + 2m (B_{22}^2 - B_{33}B_{11}) + n(B_{33}B_{11})] \\ & + b_{22} [\lambda (1 + 4B_{22}) + 2\mu (1-4 B_{22} - B_{33} - B_{11}) \\ & + 2\ell B + 4mB_{22}] \\ & + b_{33} [\lambda(1-2B_{11}) + 2\mu (-B_{22}) + 2\ell B - 2mB_{11} + nB_{11}] \\ & + b_{11} [\lambda(1-2B_{33}) + 2\mu (-B_{22}) + 2\ell B-2mB_{33} + nB_{33}]\end{aligned} \tag{A-27}$$

$$\begin{aligned}\sigma_3 = {} & [\lambda(B + \tfrac{3}{2} B_{33}^2 - \frac{B_{11}^2}{2} - \frac{B_{22}^2}{2} - 2 B_{11}B_{22}) \\ & + 2\mu (B_{33} + \tfrac{3}{2} B_{33}^2 - B_{33}B_{11} - B_{33}B_{22}) \\ & + \ell B^2 + 2m (B_{33}^2 - B_{11} B_{22}) + n (B_{11} B_{22})] \\ & + b_{33} [\lambda(1+4B_{33}) + 2\mu (1-4B_{33} - B_{11} - B_{22}) \\ & + 2\ell B + 4mB_{33}] \\ & + b_{11} [\lambda(1-2B_{22}) + 2\mu (-B_{33}) + 2\ell B - 2mB_{22} + nB_{22}] \\ & + b_{22} [\lambda(1-B_{11}) + 2\mu (-B_{33}) + 2\ell B - 2mB_{11} + n B_{11}]\end{aligned} \tag{A-28}$$

$$\sigma_4 = \frac{\rho}{\rho_o} (b_{32} \Phi_2 + (1+B_{22} + B_{33}) \Phi_4 + b_{23} \Phi_3)$$

Φ_2, Φ_4, Φ_3 are given in Appendix 2, Eq. (A-19) and (A-20).

Therefore,

$$\frac{\rho}{\rho_o} b_{32}\ \Phi_2 = b_{32}\ \Phi_2 = b_{32}\ [\lambda(B_{11} + B_{22} + B_{33}) + 2\mu\ B_{22}]$$

$$\frac{\rho}{\rho_o} b_{23}\ \Phi_3 = b_{23}\ \Phi_3 = b_{23}\ [\lambda(B_{11} + B_{22} + B_{33}) + 2\mu\ B_{33}]$$

$$\frac{\rho}{\rho_o} (1+B_{22}+B_{33})\ \Phi_4 = (1-B_{11})\ \Phi_4 = \frac{b_{23} + b_{32}}{2} [2\mu(1+B_{22}+B_{33}-B_{11})$$

$$+2m(B_{11} + B_{22} + B_{33})-nB_{11}]$$

Thus:

$$\sigma_4 = \frac{b_{23} + b_{32}}{2} [2\mu(1+B_{22} + B_{33}-B_{11}) + (2m+2\lambda)(B_{11}+B_{22}+B_{33})$$

$$-n\ B_{11}] + 2\mu\ [b_{32}\ B_{22} + b_{23}\ B_{33}]$$

Similarly,

$$\sigma_5 = \frac{b_{13} + b_{31}}{2} [2\mu(1+B_{33} + B_{11} - B_{22})+(2m+2\lambda)(B_{11}+B_{22}+B_{33})$$

$$-n\ B_{22}] + 2\mu[b_{31}B_{11} + b_{13}\ B_{33}] \qquad \text{(A-29)}$$

$$\sigma_6 = \frac{b_{12} + b_{21}}{2} [2\mu(1+B_{11}+B_{22}-B_{33})+(2m+2\lambda)(B_{11}+B_{22}+B_{33})$$

$$-n\ B_{33}] + 2\mu[b_{12}\ B_{22} + b_{21}\ B_{11}]$$